



# TDP1 phosphorylation by CDK1 in mitosis promotes MUS81-dependent repair of trapped Top1-DNA covalent complexes

Srijita Paul Chowdhuri & Benu Brata Das  

## Abstract

Topoisomerase 1 (Top1) controls DNA topology, relieves DNA supercoiling during replication and transcription, and is critical for mitotic progression to the G1 phase. Tyrosyl-DNA phosphodiesterase 1 (TDP1) mediates the removal of trapped Top1-DNA covalent complexes (Top1cc). Here, we identify CDK1-dependent phosphorylation of TDP1 at residue S61 during mitosis. A TDP1 variant defective for S61 phosphorylation (TDP1-S61A) is trapped on the mitotic chromosomes, triggering DNA damage and mitotic defects. Moreover, we show that Top1cc repair in mitosis occurs via a MUS81-dependent DNA repair mechanism. Replication stress induced by camptothecin or aphidicolin leads to TDP1-S61A enrichment at common fragile sites, which over-stimulates MUS81-dependent chromatid breaks, anaphase bridges, and micronuclei, ultimately culminating in the formation of 53BP1 nuclear bodies during G1 phase. Our findings provide new insights into the cell cycle-dependent regulation of TDP1 dynamics for the repair of trapped Top1-DNA covalent complexes during mitosis that prevents genomic instability following replication stress.

**Keywords** Topoisomerase 1; TDP1; MUS81; MiDAS; CDK1

**Subject Categories** Cell Cycle; DNA Replication, Recombination & Repair  
<https://doi.org/10.1038/s44318-024-00169-3>

Received 15 November 2023; Revised 26 June 2024;

Accepted 28 June 2024

Published online: 16 July 2024

## Introduction

To ensure faithful chromosome segregation, mammalian cells need to complete DNA replication in S-phase prior to their entry into mitosis (Shiloh, 2003). Incompletely replicated, or unresolved, chromosomes from the S-phase can often persist into mitosis, where they present a potential threat to the faithful segregation of sister chromatids (Mankouri et al, 2013). Indeed, it is becoming increasingly apparent that the transition from S-phase to M-phase perhaps encounters a less stringent checkpoint, and cells frequently enter mitosis with under-replicated or unrepaired chromosomes following replication stress (RS) (Belotserkovskaya and Jackson,

2014; Blackford and Stucki, 2020; Mankouri et al, 2013; Minocherhomji et al, 2015b; Orthwein et al, 2014). Certain regions of the human genome are intrinsically difficult to replicate, and they are particularly susceptible to RS, like common fragile sites (CFSs), which are prone to form gaps and breaks on metaphase chromosomes. The expression of late replicating CFS on metaphase chromosomes suggests that these sites also fail to complete DNA replication in the S- and G2 phase or suffer breakages that are carried over to mitosis (Chan et al, 2009). Defects in mitotic chromosomal segregation can lead to abnormal structures such as micronuclei or chromatin bridges, which are prevalent in human cancers. Topoisomerase 1 (Top1) has been associated to CFS stability, and Top1 deficiency increases DNA breaks at CFS loci (Arlt and Glover, 2010; Pladevall-Morera et al, 2019).

Top1 is essential for the release of DNA supercoiling during replication and transcription and faithful segregation of chromosomes (Capranico et al, 2017; Champoux, 2001; Pommier et al, 2016). Top1 generates transient and reversible Top1-linked DNA single-strand breaks (SSBs) (Top1 cleavage complexes; Top1cc) during catalysis, which can be preferentially trapped by the anticancer drug camptothecin (CPT) and its clinical derivatives topotecan and irinotecan (Chowdhuri et al, 2023; Pommier, 2006). Abortive Top1ccs are converted to DNA double-strand breaks (DSBs) upon replication and transcription collisions (Pommier, 2006), which triggers cell cycle arrest and cell death (Das et al, 2016). Tyrosyl-DNA Phosphodiesterase 1 (TDP1) typically hydrolyzes the phosphodiester bond between DNA 3'-end and the tyrosyl moiety of Top1 to repair Top1cc (Ashour et al, 2015; Bhattacharjee et al, 2022b; Kawale and Povirk, 2018; Pommier et al, 2014). Accordingly, genetic inactivation of TDP1 causes hypersensitivity to CPT, while homozygous mutation of TDP1 causes the neurodegenerative syndrome, spinocerebellar ataxia with axonal neuropathy (SCAN1) resulting from elevated levels of Top1cc in post-mitotic neurons (Das et al, 2010; Huang et al, 2013; Interthal et al, 2005; Interthal et al, 2001; Katyal et al, 2007; Murai et al, 2012; Pommier et al, 2014; Takashima et al, 2002; Vance and Wilson, 2002). The phosphodiesterase activity of TDP1 also repairs other blocked 3'-DNA lesions, including oxidative DNA damage and ionizing radiations (IR) (Huang et al, 2013; Katyal et al, 2007; McKinnon and Caldecott, 2007; Murai et al, 2012). The N-terminal region of TDP1 spanning 1–148 amino acids is not required for

in vitro catalytic activity of TDP1 (Interthal et al, 2001) however, plays a critical role in subcellular localization, turnover, stability, recruitment of TDP1 at DNA damage sites, and interactions with its repair partners such as PARP1, XRCC1, and Ligase III in response to Top1cc-induced DNA damage (Bhattacharjee et al, 2022a; Bhattacharjee et al, 2022b; Das et al, 2009; Das et al, 2014; El-Khamisy et al, 2005; Hudson et al, 2012; Kawale and Povirk, 2018; Pommier et al, 2014; Rehman et al, 2018).

Top1 undergoes cell cycle-specific phosphorylation that regulates its activity during mitotic transcription to remove supercoiling that allows completion of transcription during prometaphase and reloading of RNAPII at promoters during mitotic exit, facilitating the progression into G1 (Wiegard et al, 2021). Intriguingly, cells deficient for p53 when exposed to CPT undergo mitotic catastrophe (Tse and Schwartz, 2004), suggesting the failure to activate the G2/M checkpoint and the entry of cells with unrepaired Top1cc into mitosis. However, whether TDP1 repairs mitotic Top1cc remains unknown.

Human cells have developed a strategy for “unscheduled” DNA synthesis (termed MiDAS), which is a break-induced repair (BIR) mechanism that operates in early mitosis to rescue under-replicated loci, and involves POLD3, RAD52, and MUS81 as key players (Bhowmick et al, 2023; Bhowmick et al, 2016; Macheret et al, 2020; Malkova and Ira, 2013; Minocherhomji et al, 2015a). MUS81-EME1 is a structure-specific endonuclease that cleaves late replication intermediates at CFSs during early mitosis to trigger DNA repair synthesis that ensures faithful chromosome segregation (Bhowmick et al, 2023; Bhowmick et al, 2016; Calzetta et al, 2020; Di Marco et al, 2017; Minocherhomji et al, 2015a). Several alternative pathways exist in cells to ameliorate the deleterious effects of trapped Top1cc-induced replication stress (Zhang et al, 2022). MUS81 can also resolve 3'-flap structures, generated from Top1cc at the stalled replication (Regairaz et al, 2011; Wu and Wang, 2021). However, it is still unclear how trapped Top1cc on the mitotic chromosome are repaired.

Cyclin-dependent kinase 1 (CDK1) is a serine/threonine kinase that phosphorylates an array of target proteins and play key roles in coordinating DNA repair with cell cycle transitions (Brown et al, 2015; Diril et al, 2012; Holt et al, 2009). Defects in CDK1 activation lead to cell cycle progression beyond metaphase and deleterious late mitotic events. Intriguingly, CDK1-mediated phosphorylation of SLX4 causes folding of the SAP domain, which facilitates its binding with MUS81 and stimulates robust cleavage of DNA replication and recombination structures during mitosis. (Palma et al, 2018; Payliss et al, 2022). Human Top1 also undergoes mitotic phosphorylation by CDK1, although the functional implication of the phosphorylation remains unclear (Hackbarth et al, 2008). However, unscheduled activation of CDK1 leads to mitotic catastrophe in cells deficient for checkpoint after CPT treatment (Szmyd et al, 2019).

Post-translational modifications (PTMs) of TDP1 are critical part of the DNA damage response that accounts for the subcellular localization, turnover, stability, recruitment and modulation of catalytic activity of TDP1 at DNA damage sites (Bhattacharjee et al, 2022a; Bhattacharjee et al, 2022b; Das et al, 2009; Das et al, 2014; Hudson et al, 2012; Kawale and Povirk, 2018; Pommier et al, 2014; Rehman et al, 2018). However, there are no evidence for mitotic regulation of TDP1. Here we report the functional coupling of CDK1 with TDP1 that facilitates phosphorylation of TDP1 at S61

residue in G2/M boundary. TDP1-S61 phosphorylation increased during early mitosis, then declined in telophase to near basal levels in G1. Our results represent the first demonstration of a cell cycle-dependent regulatory phosphorylation of TDP1 at S61 in human cells and its implications in maintaining chromosomal stability.

## Results

### TDP1 is phosphorylated at serine 61 during mitosis

To identify new post-translational modifications of TDP1, we immunoprecipitated ectopic FLAG-TDP1 from cells grown in the presence or absence of CPT and analyzed them by mass spectrometry (MS). This MS analysis of FLAG-TDP1 detected S61 as a phosphorylated residue on TDP1 (Fig. 1A; Appendix Fig. S1A), which was identified as independent of CPT-induced DNA damage. The S61 residue of human TDP1 is phylogenetically conserved across vertebrate species as a proline-directed phosphorylation site (Fig. 1A) and lies within a conserved motif, which is the preferred substrate for Cyclin-dependent kinase 1 (CDK1) (Dephoure et al, 2008). Because CDK1 is a mitotic regulatory kinase, we hypothesized TDP1-S61 phosphorylation as a mitotic event. To that effect, we generated a phospho-specific antibody that recognizes the epitope HKRKI(S\*)PVKFSN (the asterisk denotes phosphorylation) spanning the S61 residue of TDP1 and tested its ability to detect immunoprecipitated ectopic human FLAG-TDP1 complexes from MCF7 cells synchronized to mitosis by thymidine and nocodazole (Noc) treatment as outlined in the protocol (Fig. 1B). Figure 1C shows that the pS61-TDP1 antibody recognizes a single band with a molecular weight similar to that of the FLAG-TDP1 immunoprecipitated from cells synchronized to mitotic phase only (Fig. 1C; panel + Noc). Furthermore, we were able to abolish the pS61-TDP1 signal on TDP1 in mitotic cells by applying broad-spectrum phosphatase ( $\lambda$ -phosphatase) prior to immunoprecipitation (Appendix Fig. S1B). The antibody specificity for phosphorylated S61 residue on TDP1 was validated using FLAG-TDP1 mutant version (S61A) that failed to detect the pS61-TDP1 signal immunoprecipitated from the mitotic cells (Fig. 1C). Knockdown of TDP1 by siRNA abrogated the endogenous pS61-TDP1 signal in MCF7 cells synchronized to mitotic phase (Fig. 1D), confirming the specificity of the antibody for pS61 of TDP1. We further confirmed mitotic phosphorylation of TDP1-S61 by using a pan-anti-MPM2 antibody that recognizes epitopes in proteins phosphorylated during mitosis (Kuang et al, 1989). Notably, the phosphorylation signal on TDP1 was abrogated in the immunoprecipitated FLAG-TDP1<sup>S61A</sup>, indicating S61 as the targeted residue for the mitotic phosphorylation (Appendix Fig. S1C; phosphorylated TDP1).

In order to monitor the temporal kinetics of TDP1 phosphorylation at S61, we pulled down FLAG-TDP1 variants (WT and S61A) ectopically expressing in MCF7 cells synchronized to mitosis with thymidine-nocodazole (Fig. 1B) and monitored the phosphorylation of this site after release from the noc-arrest at indicated time points in early mitotic (0 h), late mitotic (1 h), and G1 (5 h) phases (see FACS profile; Fig. 1E) using anti-pS61-TDP1 (Fig. 1F) and anti-MPM2 antibody (Appendix Fig. S1D). We found that TDP1-S61 phosphorylation peaked upon release from early mitosis before declining in late mitosis to return to near basal levels in G1 (Fig. 1F; Appendix Fig. S1D), which mirrored the CDK1 kinase activity

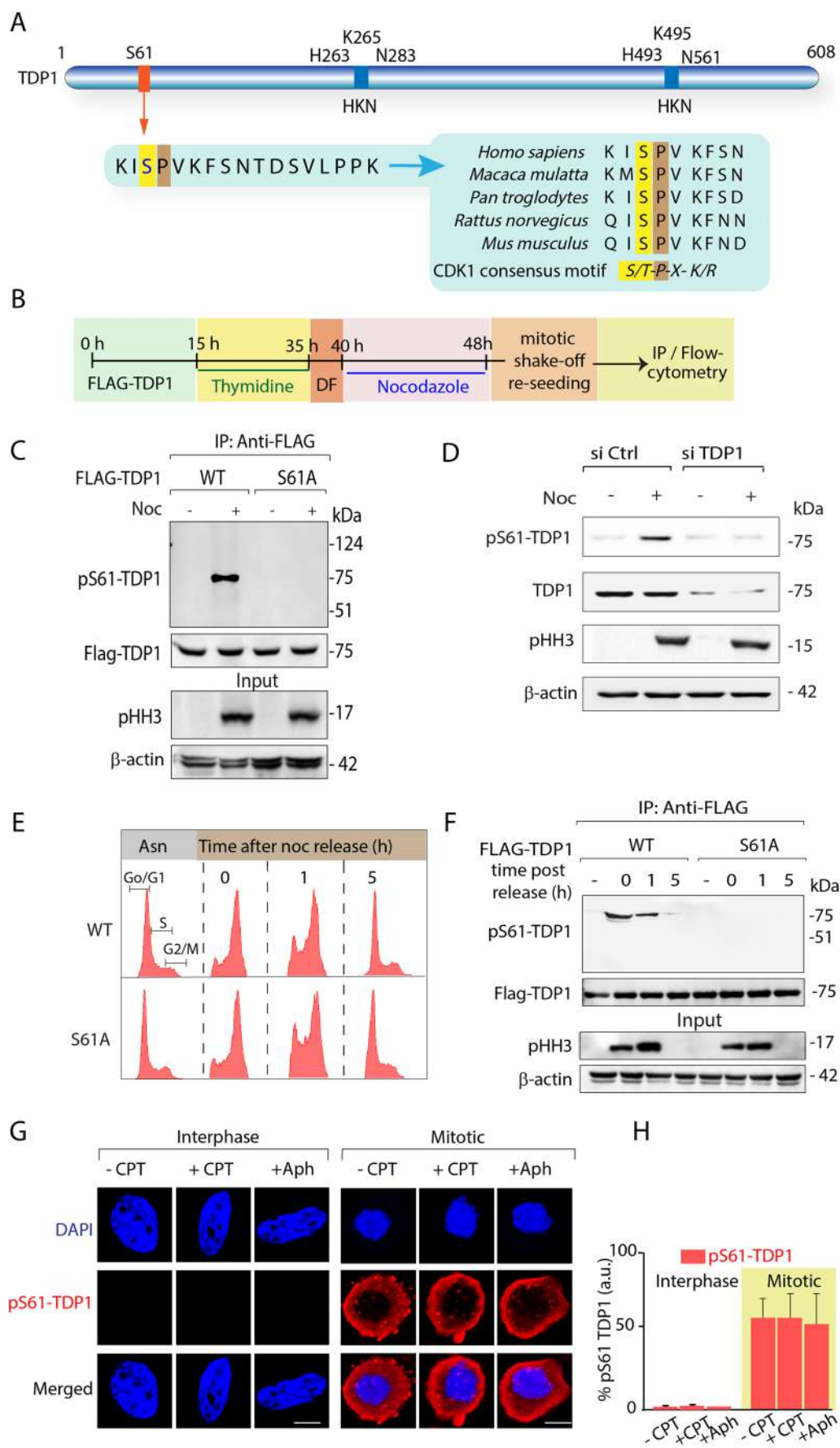


**Figure 1. Human TDP1 is phosphorylated at S61 during early mitosis.**

(A) Schematic representation of human TDP1 showing the serine phosphorylation site (S61) and the catalytic residues (HKN motifs). The sequence alignment of amino acids of TDP1 in the region flanking the S61 phosphorylation site (a conserved CDK1 substrate phosphorylation site S/T-P-X-K/R is highlighted) from human (*Homo sapiens*), monkey (*Macaca mulatta*), chimpanzee (*Pan troglodytes*), rat (*Rattus norvegicus*), mouse (*Mus musculus*) shows the phylogenetic conservation of S61. (B) Schematic representation for the protocol followed for synchronization of MCF7 cells expressing ectopic FLAG-TDP1 variants (WT or S61A) to mitotic phase for immunoprecipitation or PI-RNase based flow cytometry analysis (DF, drug free). (C) Ectopic FLAG-TDP1<sup>WT</sup> or FLAG-TDP1<sup>S61A</sup> in MCF7 cells were left asynchronous or synchronized to mitosis, following immunoprecipitation with anti-FLAG antibody, the immune complexes were analyzed by western blotting. Note: The TDP1-S61 phospho-specific antibody (pS61-TDP1) recognizes a single band with a molecular weight corresponding to TDP1 in the mitotic phase only. The same blot was stripped and reprobed with anti-FLAG antibody (FLAG-TDP1). Aliquots (10%) of the input were probed with phospho-histone H3 at Ser10 (anti-pHH3) to indicate mitotic phase and  $\beta$ -actin as loading control. (D) MCF7 cells were transfected with Si Ctrl or Si TDP1 for 72 h, left asynchronous or synchronized to mitosis with nocodazole treatment, and western blotting was performed using anti-pS61-TDP1 antibody. The level of TDP1 knockdown was confirmed by anti-TDP1 antibody with  $\beta$ -actin as a loading control. (E) Flow cytometry profile of the MCF7 cells expressing ectopic FLAG-TDP1 variants (WT and S61A), synchronized to the mitosis phase, and harvested at indicated time points after release from noc. (F) Following mitotic synchronization, FLAG-TDP1 variants were immunoprecipitated at the indicated time points [0, 1 and 5 h post release in drug-free media from nocodazole (Noc) block] using the anti-FLAG antibody, and immune complexes were blotted with the anti-pS61-TDP1 antibody. The same blot was stripped and reprobed with anti-FLAG antibody. Aliquots (10%) of the input indicate the mitotic marker phospho-histone H3 (anti-pHH3) and  $\beta$ -actin as loading control. (G) Immunolocalization of endogenous pS61-TDP1 (red) in MCF7 cells treated with or without CPT (15 nM, 24 h) or aphidicolin (0.4  $\mu$ M, 24 h) synchronized to interphase or mitosis and detected with anti-pS61-TDP1 antibody. Cells at interphase and mitosis were tallied on the basis of their chromatin morphology, as indicated by DAPI staining (blue). (H) Bar graph showing the intensity of pS61-TDP1 for interphase and mitotic cells following RS with CPT or APH. Intensities from 40 nuclei per stage were expressed as mean  $\pm$  SD.  $n = 3$  biological replicates. a.u. arbitrary unit. Scale bars, 10  $\mu$ m. Source data are available online for this figure.

(Appendix Fig. S1K) (Brown et al, 2015; Diril et al, 2012; Holt et al, 2009). This is congruent with our hypothesis that CDK1 might be the kinase responsible for phosphorylating TDP1 at S61. We further confirmed that FLAG-TDP1<sup>S61A</sup> expression in MCF7 cells did not perturb the cell cycle progression (Fig. 1E).

Next, to follow the subcellular distribution of endogenous pS61-TDP1, we performed immunocytochemistry using the phosphopeptide antibody (pS61-TDP1) in MCF7 cells at interphase or mitosis in the absence or presence of RS induced by CPT or aphidicolin (APH) (Minocherhomji et al, 2015b). Figure 1G–H; Appendix Fig. S1E,F,S1J show that the induction of pS61-TDP1 was detected only in the mitotic cells and was not detected in the interphase cells, consistent with western blotting analysis (Appendix Fig. S1G–I and Fig. 1F; panel +5 h). Furthermore, the subcellular distribution of pS61-TDP1 was shown to be identical regardless of RS generated by CPT or APH (Fig. 1G,H). Notably, pS61-TDP1 localization was excluded from the mitotic chromosomes and showed cytosolic distribution in the M-phase (Fig. 1G and see the field image in Appendix Fig. S1E). Together, we conclude TDP1-S61 is phosphorylated in mitosis, and pS61-TDP1 cellular distribution indicates an inverse correlation with TDP1 enrichment on mitotic chromosomes.

### CDK1 binds with TDP1 to phosphorylate at S61

CDK1 plays a key role in the regulation of the mitotic DNA damage response (Brown et al, 2015; Diril et al, 2012; Holt et al, 2009) and it has been shown to phosphorylate Top1 (Hackbarth et al, 2008). This prompted us to test whether CDK1 interacts with TDP1. Co-immunoprecipitation (co-IP) of ectopically expressed FLAG-TDP1 in MCF7 cells pulled down endogenous CDK1 (Fig. 2A) both in the presence as well as in the absence of CPT, indicating TDP1-CDK1 binding is independent of DNA damage. Further, we co-immunoprecipitated endogenous TDP1 from MCF7 cells and confirmed the association between endogenous TDP1-CDK1 in cells (Fig. 2B). To test whether CDK1 interacts with TDP1, we performed co-IP with FLAG-TDP1 in the presence of the benzonase nuclease (Fig. 2C) (Rehman et al, 2018). We found that

the TDP1-CDK1 association was resistant to benzonase, indicating a protein-protein interaction, not mediated through DNA or RNA (Fig. 2C). We also observed similar levels of endogenous CDK1 in the immune complexes of both FLAG-TDP1 variants (WT and S61A) confirming the dispensable nature of pS61-TDP1 in mediating CDK1 and TDP1 interaction (Fig. 2D). We further established the presence of TDP1 in the CDK1-complex using reverse co-IP in cells ectopically expressing HA-tagged CDK1 (Fig. 2E), confirming the specific association between TDP1 and CDK1. In addition, we co-immunoprecipitated endogenous CDK1 from MCF7 cells and confirmed its association TDP1 in cells (Fig. 2F). Further, the interaction between CDK1 and TDP1 was not abrogated in the presence of the CDK1 inhibitor (RO3306), suggesting CDK1-TDP1 binding is independent of CDK1 catalytic activity (Fig. 2A,E,F).

Next, to determine whether CDK1 is involved in TDP1 phosphorylation at S61, we ectopically expressed and immunoprecipitated FLAG-TDP1<sup>WT</sup> from CDK1 knockdown cells synchronized to the mitotic phase. Figure 2G shows that CDK1 depletion resulted in a marked reduction in pS61-TDP1, suggesting that TDP1 not only physically interacts with CDK1 (Fig. 2A–F) but is also phosphorylated at S61 in vivo by CDK1 during the mitotic phase (Fig. 2G). Further inhibition of CDK1 catalytic activity by treatment with RO3306, resulted in a marked reduction in pS61-TDP1, supporting the role of CDK1 in phosphorylating TDP1 at S61 residue (Fig. 2H). To obtain further evidence for TDP1 phosphorylation at S61 by CDK1, we performed the in vitro kinase assay with recombinant 6X-His-TDP1 protein variants (WT and S61A) as substrates for immune-precipitated HA-CDK1 as the source of the kinase in the presence of ATP. The pS61-TDP1 antibody detected phosphorylation of TDP1<sup>WT</sup> by CDK1, but not of TDP1<sup>S61A</sup> (Fig. 2I), confirming that CDK1 phosphorylates TDP1 in vitro at S61. Under similar conditions, we demonstrated that CDK2 failed to phosphorylate TDP1 at the S61 residue using in vitro kinase assays, confirming CDK1 as the bona fide kinase phosphorylating TDP1 at the S61 residue (Appendix Fig. S2). Taken together, these results confirmed CDK1-TDP1 physically interacts to catalyze TDP1 phosphorylation at S61 during mitosis.



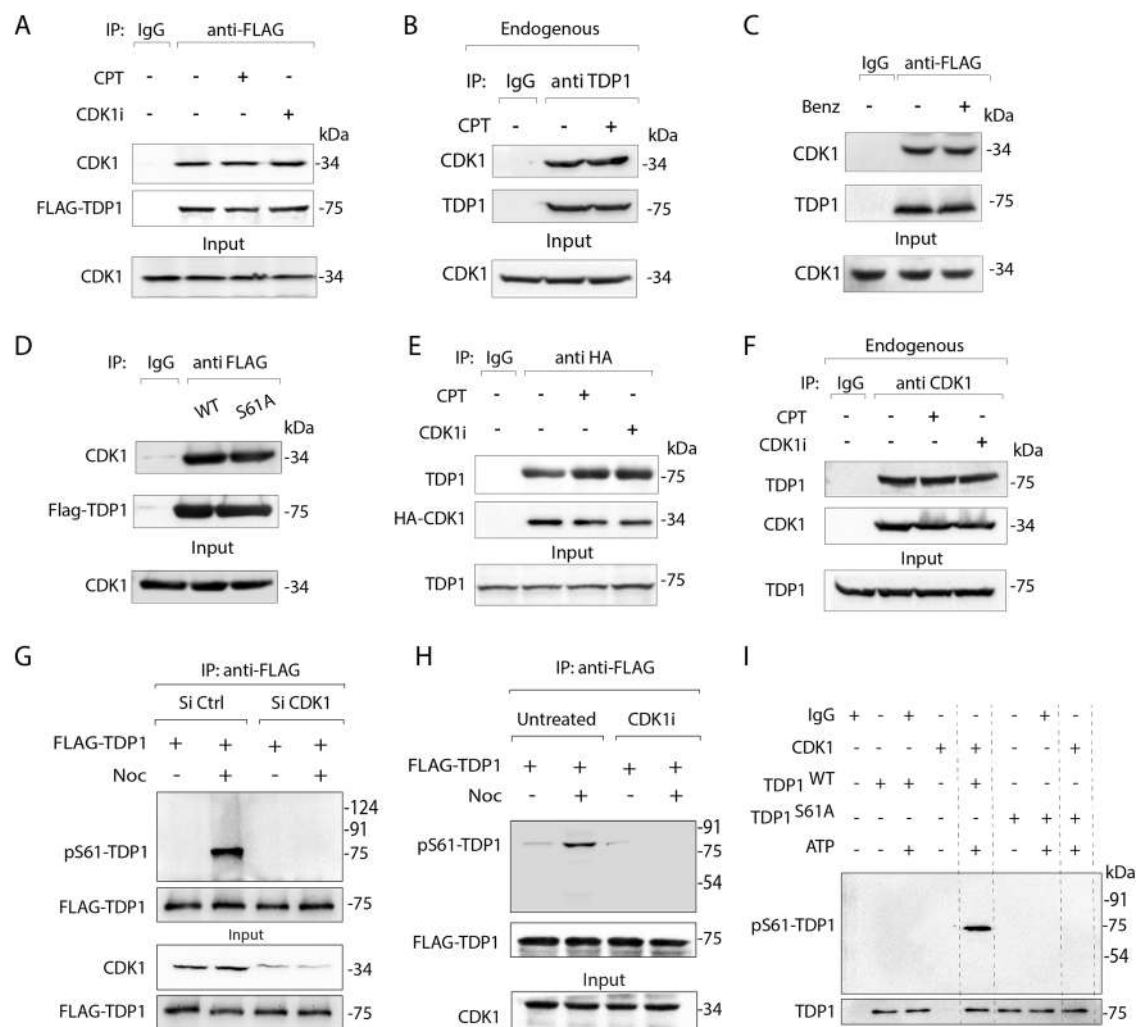


**Figure 2. CDK1 physically interacts with TDP1 to catalyze S61 phosphorylation.**

(A) MCF7 cells ectopically expressing FLAG-TDP1 treated with or without CPT (5  $\mu$ M, 3 h) or CDK1i (9  $\mu$ M, 16 h) were co-immunoprecipitated (co-IP) using anti-FLAG antibody. Immune complexes were blotted with anti-CDK1 antibodies. The same blot was stripped and reprobed with anti-FLAG antibody to show the expression of FLAG-TDP1. Aliquots (10%) of the input show the level of CDK1 prior to immunoprecipitation. (B) Endogenous TDP1 was immunoprecipitated using anti-TDP1 antibody from MCF7 cells treated with or without CPT (5  $\mu$ M, 3 h). Immune complexes were blotted with anti-CDK1 antibody. The same blot was stripped and reprobed with anti-TDP1 antibody to show TDP1 pull-down. Aliquots (10%) of the input show the level of CDK1 prior to immunoprecipitation. (C) Same as (A), except the cell lysates were pretreated with benzonase (nuclease) prior to co-IP as indicated. Note: The TDP1-CDK1 interaction is resistant to benzonase. (D) MCF7 cells ectopically expressing FLAG-TDP1 variants (WT and S61A) were co-immunoprecipitated (co-IP) using anti-FLAG antibody. Immune complexes were blotted with anti-CDK1 antibody. The same blot was stripped and reprobed with anti-FLAG antibody to show the expression of FLAG-TDP1 variants. Aliquots (10%) of the input show the level of CDK1 prior to immunoprecipitation. (E) MCF7 cells ectopically expressing HA-CDK1 were treated with or without CPT (5  $\mu$ M, 3 h) and CDK1i (9  $\mu$ M, 16 h) and immunoprecipitated using anti-HA antibody. The immune complexes were blotted with anti-TDP1 antibody. The same blot was stripped and reprobed with anti-HA antibody. Aliquots (10%) of the input show the level of TDP1 prior to immunoprecipitation. (F) Endogenous CDK1 was co-IPed using anti-CDK1 antibody from MCF7 cells treated with or without CPT (5  $\mu$ M, 3 h) or CDK1i (9  $\mu$ M, 16 h). Immune complexes were blotted with anti-TDP1 antibody. The same blot was stripped and reprobed with anti-CDK1 antibody. Aliquots (10%) of input show TDP1. (G) FLAG-TDP1 was expressed in MCF7 cells transfected with Si CDK1 to knockdown CDK1 or Si Ctrl as indicated. Following nocodazole treatment (200 ng/ml, 8 h), ectopic FLAG-TDP1 was co-IPed using anti-FLAG antibody, and the immune complexes were blotted with pS61-TDP1 antibody. The same blot was stripped and reprobed with anti-FLAG antibody. Aliquots (10%) of the input show the level of CDK1 knockdown and FLAG-TDP1 prior to immunoprecipitation. (H) FLAG-TDP1 was expressed in MCF7 cells left untreated or treated with CDK1 inhibitor (RO3306) as indicated. Following nocodazole treatment (200 ng/ml, 8 h), ectopic FLAG-TDP1 was co-IPed using anti-FLAG antibody, and the immune complexes were blotted with pS61-TDP1 antibody. The same blot was stripped and reprobed with anti-FLAG antibody. Aliquots (10%) of the input show the level of CDK1 prior to immunoprecipitation. (I) In vitro kinase assays with HA-CDK1 immunoprecipitated from MCF7 cells in the presence of ATP. The substrates were recombinant 6xHis-tagged TDP1 variants (WT or S61A). Western blotting against the anti-TDP1 antibody shows the amount of substrate in each reaction. Protein molecular weight markers (kDa) are indicated on the right. Source data are available online for this figure.

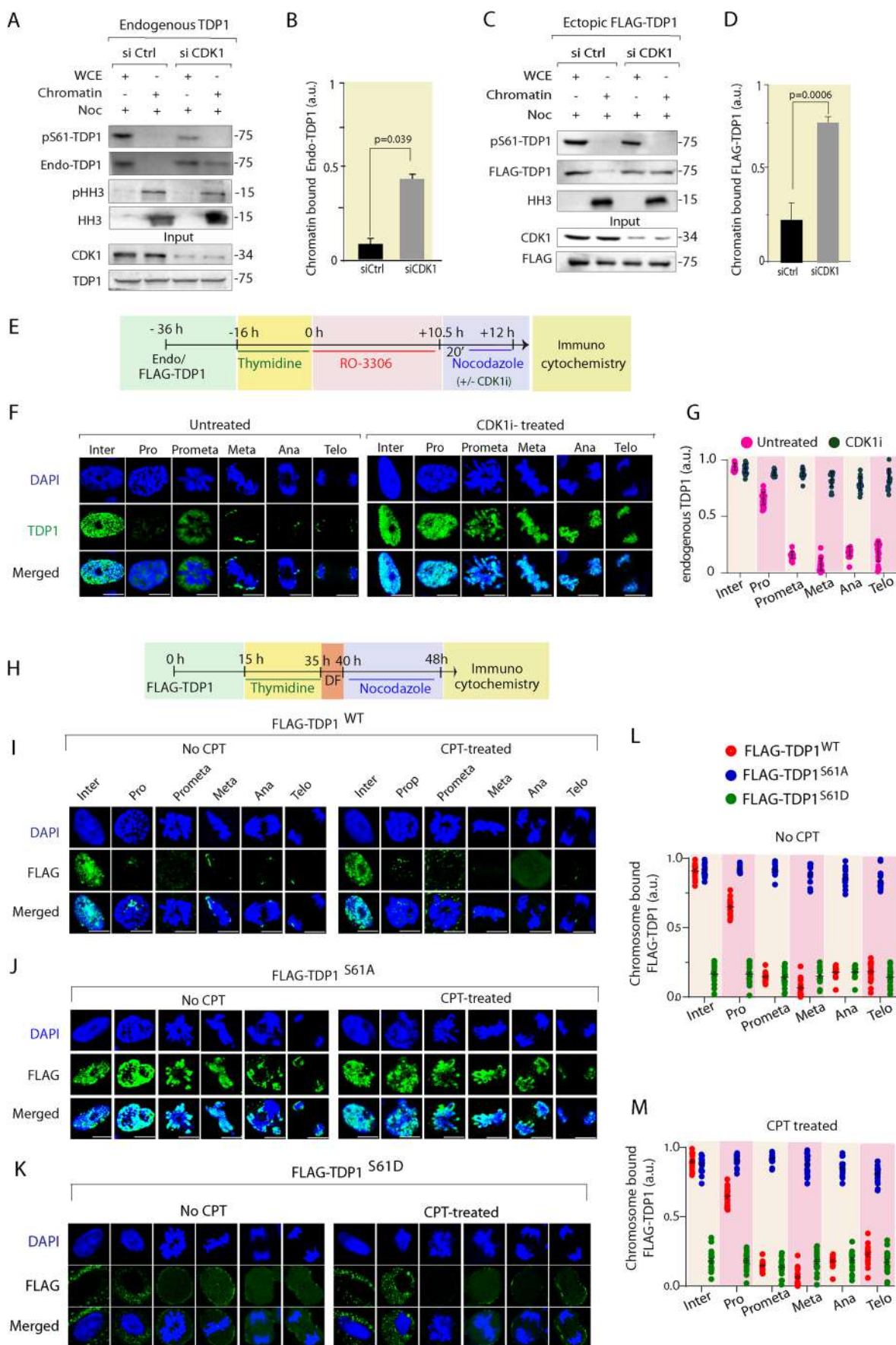


**Figure 3. TDP1 phosphorylation at S61 by CDK1 abrogates chromosomal enrichment of TDP1 during mitosis.**

(A) Chromatin fractions were prepared from Noc synchronized MCF7 cells transfected with Si Ctrl or Si CDK1 and were blotted with pS61-TDP1 and anti-TDP1 antibodies. Aliquots (10%) show levels of endogenous CDK1 and TDP1 in the whole-cell (WCE) lysates prior to chromatin fractionation. (B) Densitometric analysis of chromatin-bound endogenous TDP1 in mitotic cells upon CDK1 knockdown. Data are mean  $\pm$  SD,  $n = 3$  biological replicates. \* $P < 0.05$  (one-way ANOVA). (C) TDP1<sup>-/-</sup> MEFs were co-transfected with FLAG-TDP1<sup>WT</sup> and Si CDK1 or Si Ctrl and were synchronized with Noc. Chromatin fractions from mitotic cells were analyzed by western blotting against the anti-FLAG antibody and the pS61-TDP1 antibody. Aliquots (10%) show levels of endogenous CDK1 and ectopic FLAG-TDP1<sup>WT</sup> in the whole-cell (WCE) lysates prior to chromatin fractionation. (D) Densitometric analysis of chromatin-bound ectopic FLAG-TDP1 in mitotic cells upon CDK1 knockdown. Data are mean  $\pm$  SD,  $n = 3$  biological replicates. \*\*\* $P < 0.001$  (one-way ANOVA). (E) Schematic representation of the protocol followed to study the cell cycle stage-dependent colocalization of endogenous TDP1 with the chromosomes in the presence and absence of CDK1 inhibitor (RO3306) as indicated. (F) MCF7 cells were fixed at different time intervals after release from G2/M arrest as outlined in the protocol and stained with anti-TDP1 antibody to detect endogenous TDP1 (green) and the chromosomes by DAPI (blue). (G) The fluorescence intensity of chromosome-bound endogenous TDP1 was quantified. Staining intensities from 20 to 30 nuclei/stage were expressed as mean  $\pm$  SD. a.u. arbitrary unit. (H) Schematic representation of the protocol followed to study the cell cycle stage-dependent colocalization of FLAG-TDP1 variants (WT, S61A and S61D) with the chromosomes in the presence and absence of CPT as indicated. (I–K) TDP1<sup>-/-</sup> MEFs complemented with FLAG-TDP1<sup>WT</sup> (I) or FLAG-TDP1<sup>S61A</sup> (J) or FLAG-TDP1<sup>S61D</sup> (K) were fixed after release from nocodazole arrest, and FLAG-TDP1 was immunodetected with anti-FLAG antibody (green) in the presence or absence of CPT (15 nM; 24 h) as indicated. Note: FLAG-TDP1<sup>S61A</sup> was readily detected on the different phases of mitotic chromosomes stained with DAPI (blue). (L, M) The fluorescence intensity of the chromosome-bound FLAG-TDP1 variants (WT or S61A or S61D) in the absence of CPT (upper panel) or the presence of CPT (bottom panel) was quantified. Staining intensities from 20 to 30 nuclei per stage were expressed as mean  $\pm$  SD; a.u. arbitrary unit. All the results are expressed as mean  $\pm$  SD for at least three independent experiments ( $n = 3$ ). Scale bars, 10  $\mu$ m. Source data are available online for this figure.

### S61 phosphorylation of TDP1 promotes its dissociation from mitotic chromosomes

To investigate the role of the CDK1-mediated phosphorylation of TDP1 at the S61 residue in its chromosomal recruitment and/or dissociation during mitosis, we knocked down CDK1 by siRNA in MCF7 cells and synchronized the cells to the mitotic phase with nocodazole, followed by chromatin fractionation and western blotting (Wu and Wang, 2021). A 60–70% knockdown of CDK1 was aimed for allowing cells to progress into mitosis because CDK1 deficiency prevents mitotic entry (Diril et al, 2012). We utilized two independent approaches to detect the chromatin-bound fraction of TDP1, either by western blotting with endogenous TDP1 or by analyzing the chromatin-bound fraction of ectopic FLAG-TDP1 expressed in CDK1 knockdown cells synchronized to the mitotic phase. The relative purity of the chromatin-bound fractions was further assessed by analysis of phospho-histone H3 and total histone H3, which were only detectable during mitosis in the chromatin fractions respectively (Fig. 3A). The endogenous pS61-TDP1 was detected in CDK1-proficient cells (siCtrl) that were synchronized to mitotic phase and was markedly reduced following CDK1 knockdown (Fig. 3A,B), which is in agreement with CDK1's role in phosphorylating TDP1 at S61. We also noted that the endogenous pS61-TDP1 signal was only detected in the whole-cell extract (WCE) and was markedly reduced in the chromatin fraction independent of CDK1. We also detected a marked reduction of the endogenous TDP1 in the chromatin-bound fraction (Fig. 3A, *endo-TDP1*), in keeping with the immunolocalization of pS61-TDP1 in the soluble fraction during M-phase (Fig. 1G–H). In contrast, endogenous TDP1 was enriched in the chromatin fraction (~four-fold; Fig. 3B) in CDK1 knockdown cells, a situation mimicking defective TDP1 phosphorylation at S61. Further, we also confirmed the enrichment of ectopic FLAG-TDP1 (~three- to fourfold; Fig. 3C,D) in the chromatin fraction in cells deficient for CDK1 (Fig. 3C) compared to the CDK1-proficient cells by western blotting with anti-FLAG antibodies (Fig. 3C). Therefore, we surmised that TDP1 defective for phosphorylation at S61 is enriched on the mitotic chromosomes.

To further test the effect of CDK1-mediated phosphorylation at S61 on the chromosomal recruitment of endogenous TDP1 during

cell cycle, we used RO3306 to inhibit CDK1 activity and performed confocal immunofluorescence microscopy with anti-TDP1 antibody. MCF7 cells were synchronized following the protocol outlined in Fig. 3E. The cells at the indicated stages of mitosis were selected on the basis of their chromatin morphology, as confirmed by DAPI staining (Wu and Wang, 2021). We noted a similar pattern of colocalization for endogenous TDP1 on chromatin (DAPI) in the interphase cells, which was independent of RO3306 treatment (Fig. 3F, untreated and CDK1i-treated, panels *interphase*). However, TDP1 was not detected on mitotic chromosomes (Fig. 3F untreated, panel *prophase to telophase*). In contrast, treatment with RO3306 resulted in a marked increase in the chromosomal localization of endogenous TDP1 during mitosis (prophase to telophase) when compared to the untreated mitotic cells (Fig. 3F,G). The immunodetection of TDP1 on the chromosomes during mitosis with the CDK1 inhibitor (Fig. 3F) corroborated with chromatin enrichment of TDP1 in CDK1 knockdown cells (Fig. 3A–D). Together, CDK1 inhibition or knockdown during mitosis resulted in the occlusion of TDP1 on the mitotic chromosomes; thereby further strengthening our hypothesis that CDK1-mediated S61 phosphorylation plays a key role in ousting TDP1 from chromosomes during mitosis.

In the next step, we set out to dissect the chromosomal recruitment of the FLAG-TDP1<sup>S61A</sup> mutant during mitosis. To do so, we used TDP1<sup>-/-</sup> MEFs complemented with FLAG-TDP1<sup>WT</sup> (TDP1<sup>-/-</sup>/WT) or phosphomutant FLAG-TDP1<sup>S61A</sup> (TDP1<sup>-/-</sup>/S61A) or phosphomimetic FLAG-TDP1<sup>S61D</sup> (TDP1<sup>-/-</sup>/S61D), synchronized to the mitosis (Fig. 3H) in the presence and absence of a low dose of CPT, which generates replication stress, and protein localization was monitored during interphase and stages of mitosis using confocal immunofluorescence microscopy (Fig. 3I–M). In contrast to interphase cells, we detected a marked reduction of the colocalization of FLAG-TDP1<sup>WT</sup> in the early prophase to telophase of chromosomes (DAPI) (Fig. 3I,L,M). However, the FLAG-TDP1<sup>S61A</sup> was readily detectable on the chromosomes during prophase to telophase independent of replication stress with CPT (Fig. 3J,L,M), suggesting CDK1-mediated S61 phosphorylation of TDP1 promotes its dissociation from mitotic chromosomes. In keeping with pS61-TDP1, the phosphomimetic FLAG-TDP1<sup>S61D</sup> was also delocalized from the chromosomes, emphasizing the role

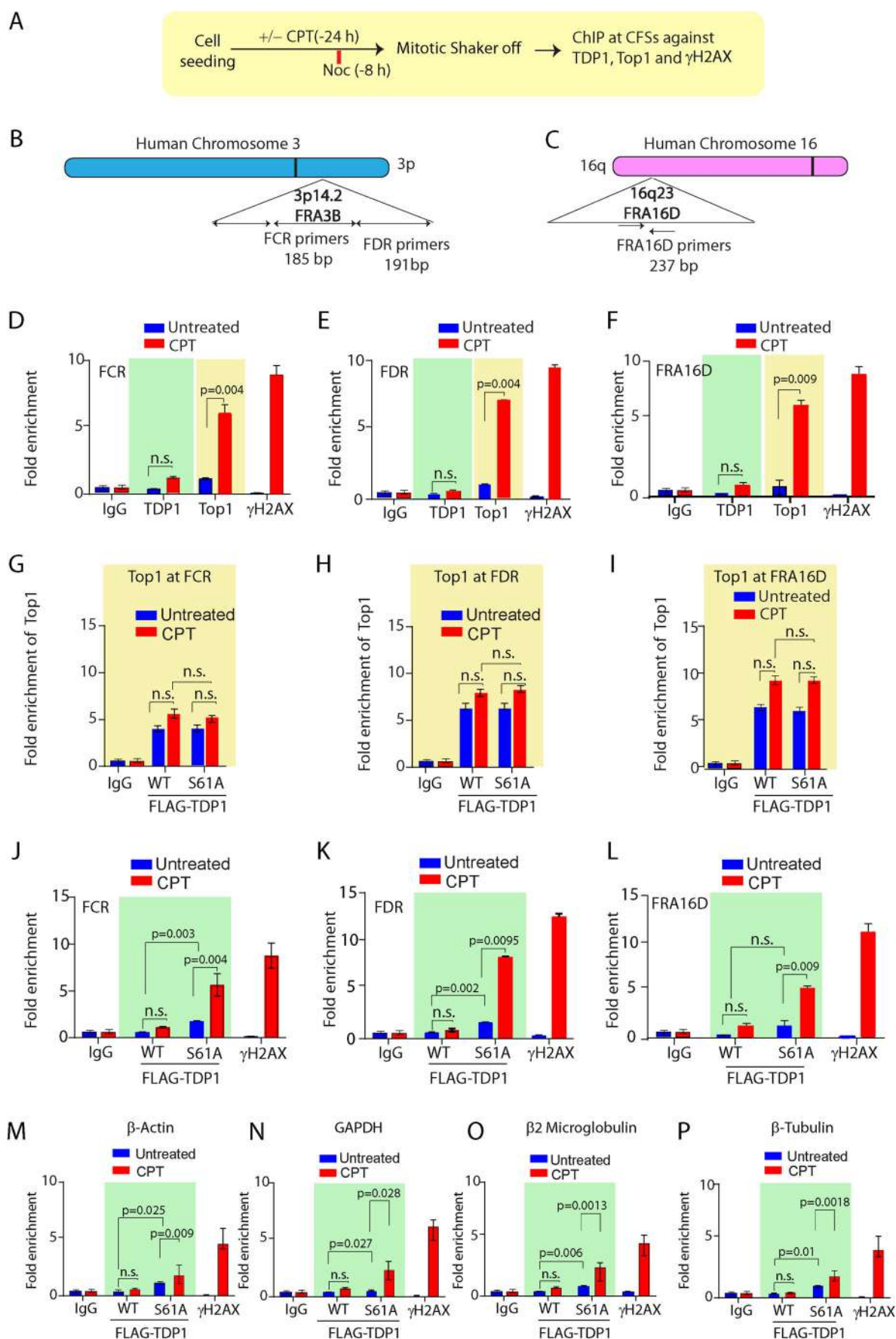




**Figure 4. TDP1<sup>S61A</sup> is enriched at the CFS during mitosis.**

(A) A schematic representation of the protocol for synchronization of MCF7 cells followed by chromatin immunoprecipitation (ChIP) with indicated antibodies at the CFS and non-CFS loci. (B, C) Genomic organization of the FRA3B and FRA16D regions, along with the primer sets of the distal (FDR) and central (FCR) region within the FRA3B locus; FRA16D locus, is designated. (D–F) Endogenous Top1 but not TDP1 preferentially localizes to CFSs upon CPT (15 nM; 24 h) treatment during mitosis. Quantification of cross-linked FRA3B-FCR, FRA3B-FDR and FRA16D loci chromatin-immunoprecipitated from MCF7 cells using the specified antibodies (Top1 and TDP1). The DSB marker  $\gamma$ H2AX antibody was used as a positive control for FRA3B and FRA16D enrichment post CPT treatment. Fold enrichment over IgG was determined and is shown for each primer pair for the ChIP. Data are mean  $\pm$  SD,  $n = 3$  biological replicates. ns, non-significant ( $P > 0.05$ ); \*\* $P \leq 0.01$  (one-way ANOVA). (G–I) Quantification of cross-linked FRA3B-FCR, FRA3B-FDR, and FRA16D loci chromatin-immunoprecipitated from MCF7 cells transfected with FLAG-TDP1 variants (WT or S61A) using the specified antibodies (endogenous Top1). Fold enrichment over IgG was determined and is shown for each primer pair for the ChIP. (J–L) Quantification of cross-linked FRA3B-FCR, FRA3B-FDR, and FRA16D loci chromatin-immunoprecipitated from MCF7 cells ectopically expressing the FLAG-TDP1 variants (WT and S61A) using the specified antibodies with or without CPT treatment (15 nM; 24 h). The DSB marker  $\gamma$ H2AX antibody was used as a positive control for FRA3B and FRA16D enrichment post CPT treatment. Fold enrichment over IgG was determined and is shown for each primer pair for the ChIP. Data are mean  $\pm$  SD,  $n = 3$  biological replicates. ns, non-significant ( $P > 0.05$ ); \*\* $P \leq 0.01$  (one-way ANOVA). (M–P) Quantification of cross-linked  $\beta$ -actin, GAPDH,  $\beta$ 2-microglobulin and  $\beta$ -tubulin loci chromatin-immunoprecipitated from MCF7 cells ectopically expressing the FLAG-TDP1 variants (WT and S61A) using the specified antibodies with or without CPT treatment (15 nM; 24 h). The DSB marker  $\gamma$ H2AX antibody was used as a positive control for  $\beta$ -actin, GAPDH,  $\beta$ 2-microglobulin and  $\beta$ -tubulin enrichment post CPT treatment. Fold enrichment over IgG was determined and is shown for each primer pair for the ChIP. Data are mean  $\pm$  SD,  $n = 3$  biological replicates. n.s. non-significant ( $P > 0.05$ ); \* $P < 0.05$ , \*\* $P < 0.01$ ; (one-way ANOVA). Source data are available online for this figure.

of S61 phosphorylation in ousting TDP1 from the chromosomes (Fig. 3K–M; Appendix Fig. S3A,B).

### TDP1<sup>S61A</sup> is trapped at CFS loci in the G2/M-phase following replication stress and triggers mitotic chromosome breaks

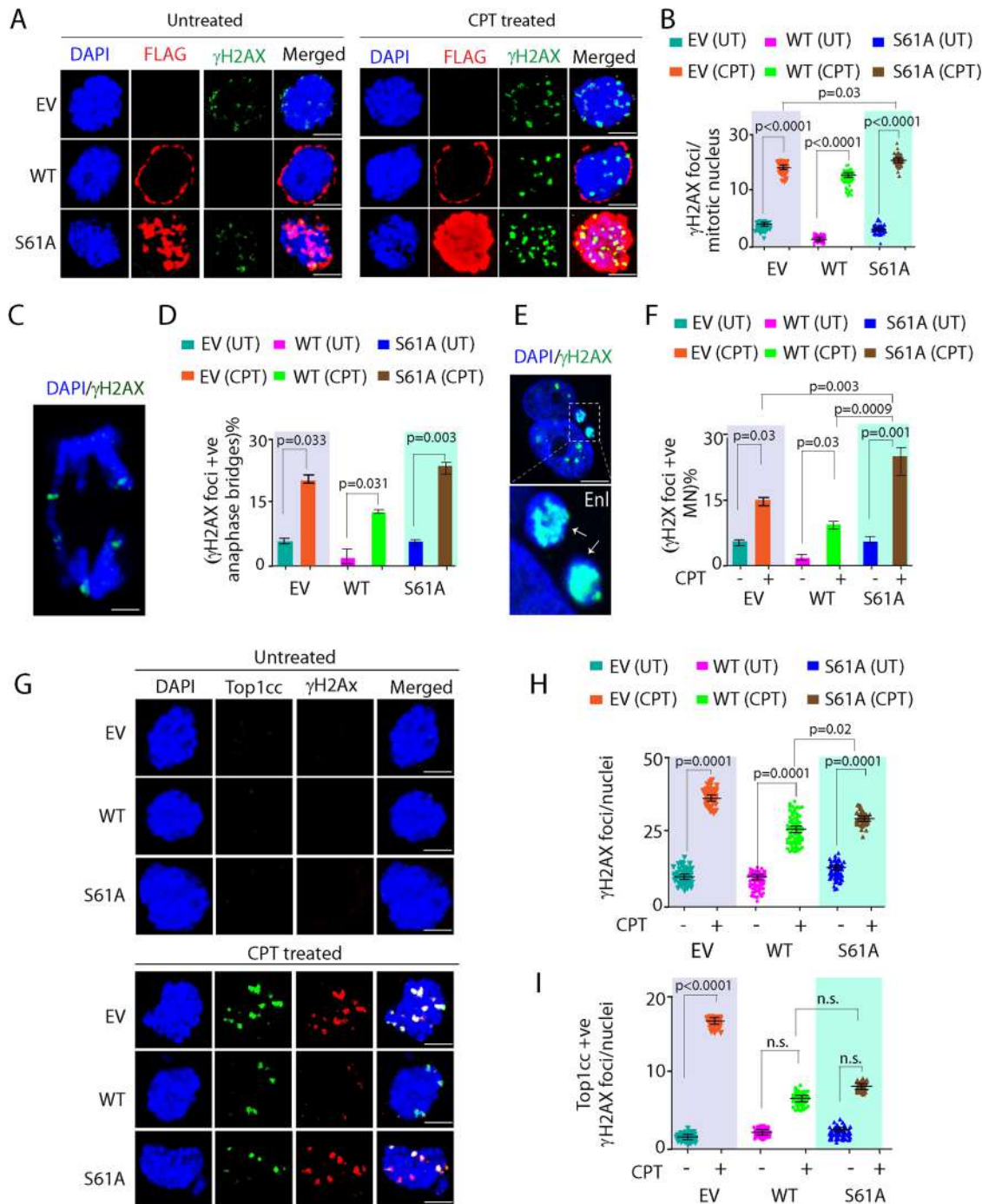
The chromatin-bound fraction of mutant TDP1<sup>S61A</sup> during mitosis (Fig. 3) prompted us to investigate the sites on DNA where TDP1<sup>S61A</sup> becomes trapped on the mitotic chromosomes. Common fragile sites (CFSs) are specific regions of the genome that are susceptible to replication stress and exhibit gaps or breaks on metaphase chromosomes under conditions that partially inhibit DNA replication (Li and Wu, 2020; Minocherhomji et al, 2015b; Özer and Hickson, 2018). We tested the enrichment of endogenous Top1 and TDP1 on mitotic chromosomes at three different CFS loci: FRA3B-FDR and FCR regions, and FRA16D (Fig. 4D–F), located on chromosomes 3 and 16, respectively (Fig. 4A–C), using chromatin immunoprecipitation (ChIP) followed by quantitative polymerase chain reaction (qPCR) analysis (Ghosh et al, 2019). To induce mild RS that causes CFS instability, the MCF7 cells were treated with a low dose of CPT or APH for 24 h, then synchronized to mitosis (Fig. 4A; Appendix Fig. 4SA). We noted a significant increase in endogenous Top1 enrichment but not TDP1 at the fragile sites which is consistent with the S61 phosphorylation dependent chromatin dissociation of TDP1 during mitosis following CPT treatment (Fig. 4D–F), in accordance to the role of Top1 in CFS breakage (Arlt and Glover, 2010; Sbrana et al, 1998; Tuduri et al, 2009). Subsequent enrichment of  $\gamma$ H2AX confirmed CPT-induced DNA break sites at the CFSs (Fig. 4D–F,J–L).

In addition, we confirmed using ChIP assays (Fig. 4G–I) that ectopic expression of the FLAG-TDP1 variants (FLAG-TDP1<sup>WT</sup> and FLAG-TDP1<sup>S61A</sup>) in MCF7 cells had no effect on the Top1 enrichment at the CFSs, which suggests that CPT-induced Top1cc trapping on mitotic chromosomes is independent of TDP1-S61 phosphorylation. We detected FLAG-TDP1<sup>S61A</sup> enrichment at CFSs that was markedly increased after CPT treatment (Fig. 4J–L). In addition, replication stress induced with APH similarly enriched TDP1<sup>S61A</sup> at the CFSs together with  $\gamma$ H2AX (Appendix Fig. S4B–D). We noted that both replication stress with CPT (Fig. 4J–L) and APH (Appendix Fig. S4B–D) treatment markedly increased the

enrichment of TDP1<sup>S61A</sup> in all the CFSs, suggesting the S61 phosphorylation defective TDP1 are additionally trapped on the CFSs of mitotic chromosomes. However, we also detected CPT-induced enriched FLAG-TDP1-S61A at the four tested non-CFS, including  $\beta$ -actin (Fig. 4M), GAPDH (Fig. 4N),  $\beta$ 2-microglobulin (Fig. 4O), and  $\beta$ -tubulin (Fig. 4P), albeit to a significantly lesser extent (Appendix Fig. S4F) compared to the CFSs, which are intrinsically more susceptible to RS. APH treatment also causes TDP1<sup>S61A</sup> enrichment at  $\beta$ -actin (Appendix Fig. S4E) to significantly lesser extent than CFSs (Appendix Fig. S4B–D).

We subsequently hypothesized that TDP1<sup>S61A</sup> trapping on mitotic chromosomes instigates additional DNA damage. To test this assumption, we used TDP1<sup>-/-WT</sup> or TDP1<sup>-/-S61A</sup> MEFs, arrested in mitosis and treated with CPT during mitotic progression, and analyzed  $\gamma$ H2AX levels using immunocytochemistry (Fig. 5A–F). Indeed, we detected a significant increase in  $\gamma$ H2AX levels in mitotic cells expressing TDP1<sup>-/-S61A</sup> MEFs compared to TDP1<sup>-/-WT</sup> (Fig. 5A) that was markedly increased after RS induced with CPT (Fig. 5B), suggesting TDP1<sup>S61A</sup> trapping induces accumulation of DSBs. Further, CPT treatment also resulted in  $\gamma$ H2AX-positive anaphase bridges and micronuclei, suggesting chromosomal DNA breaks during mitosis in TDP1<sup>-/-S61A</sup> MEFs (Fig. 5C–F).

We subsequently tested whether CPT-induced DNA damage during late S/G2 phase persists into mitosis, by co-staining with Top1cc and  $\gamma$ H2AX antibodies in the TDP1<sup>-/-WT</sup> or TDP1<sup>-/-S61A</sup> or TDP1<sup>-/-</sup> MEFs complemented empty vector (TDP1<sup>-/-EV</sup>) MEFs. CPT treatment in late S/G2 (Appendix Fig. S5B–D) phase led to marked accumulation of mitotic DNA breaks both in TDP1<sup>-/-EV</sup> or TDP1<sup>-/-S61A</sup> MEFs, while the CPT-induced  $\gamma$ H2AX and Top1cc levels were significantly reduced in early S-phase (Appendix Fig. S5A,S5C,D) both in the TDP1<sup>-/-WT</sup> or TDP1<sup>-/-S61A</sup> MEFs, suggesting that S61 of TDP1 is dispensable for Top1cc repair during S-phase. Though, we noted a substantial increase in CPT-induced  $\gamma$ H2AX in TDP1<sup>-/-S61A</sup> MEFs compared to TDP1<sup>-/-WT</sup> MEFs (Fig. 5G–H); however, this effect was not due to increased accumulation of Top1cc (Fig. 5G,I; Appendix Fig. S5E,F). Because TDP1 is excluded from the mitotic chromosomes (Figs. 3 and 4), therefore, it is suggestive that mitotic DNA breaks in TDP1<sup>-/-S61A</sup> MEFs are dependent on MUS81 activity, which might be required for the clearance of the trapped TDP1<sup>S61A</sup> (Wu and Wang, 2021).



### Mitotic Top1ccs are repaired by MUS81-dependent mitotic DNA synthesis (MiDAS) independent of TDP1

Trapped Top1ccs, are broadly repaired by phosphodiesterase pathway that includes TDP1 (Huang et al, 2013; Interthal et al, 2001; Kawale and Povirk, 2018; Pommier et al, 2014); while alternative endonuclease pathways that include MUS81-EME1, XPF-ERCC1 have been implicated in the repair of trapped Top1cc (Chowdhuri and Das, 2021; Liu et al, 2002; Wu and Wang, 2021; Zhang et al, 2022). During early mitosis the nuclease activity of the

structure-specific MUS81-EME1 endonuclease complex promotes a RAD52- and POLD3-mediated DNA repair synthesis (MiDAS), which serves to minimize chromosome breaks under conditions of replication stress (Bhowmick et al, 2016; Groelly et al, 2022). To test the repair of pre-mitotic trapped Top1cc-linked DNA breaks by MiDAS, we looked into BrdU or EDU incorporation on prophase DNA to mark the newly replicating cells. We ensured that the TDP1<sup>-/-</sup>/WT or TDP1<sup>-/-</sup>/S61A or TDP1<sup>-/-</sup>/EV MEFs had no inherent replication defect (Appendix Fig. S6A,B). The TDP1<sup>-/-</sup>/WT or TDP1<sup>-/-</sup>/S61A or TDP1<sup>-/-</sup>/EV MEFs were synchronized to mitosis,

**Figure 5. TDP1<sup>S61A</sup> trapping generates mitotic DNA breaks independent of Top1ccs.**

(A) TDP1<sup>-/-</sup> MEFs complemented with FLAG-TDP1 variants (TDP1<sup>-/-</sup>/WT; TDP1<sup>-/-</sup>/S61A) or Empty vector (TDP1<sup>-/-</sup>/EV) were synchronized in mitosis and treated with or without CPT (10 μM, 1 h), released in presence of nocodazole followed by immunocytochemistry with anti-FLAG (red) to detect FLAG-TDP1 and anti-γH2AX (green) antibody. Cells were counterstained with DAPI to visualize mitotic nuclei (blue). (B) Quantification for the number of γH2AX foci per mitotic nucleus calculated for 50 nuclei. Data are mean ± SD, *n* = 3 biological replicates. \**P* ≤ 0.05; \*\*\*\**P* ≤ 0.0001 (one-way ANOVA). (C) Representative merged image showing anaphase nucleus (blue) with γH2AX (green) foci on bridges resulting from CPT treatment in TDP1<sup>-/-</sup>/S61A MEFs. The enlarged view of the anaphase bridge has been shown. (D) Quantification of γH2AX-positive anaphase bridges in TDP1<sup>-/-</sup>/EV; TDP1<sup>-/-</sup>/WT and TDP1<sup>-/-</sup>/S61A MEFs. Data are mean ± SD, *n* = 3 biological replicates. \**P* ≤ 0.05; \*\**P* ≤ 0.01 (one-way ANOVA). (E) Representative merged image showing G1 primary nucleus (PN) with micronuclei (MN) harboring γH2AX (green) foci resulting from CPT treatment in mitosis. The enlarged view of the MN with γH2AX in TDP1<sup>-/-</sup>/S61A MEFs has been shown. (F) Quantification of the number of γH2AX-positive G1-MN in TDP1<sup>-/-</sup>/EV; TDP1<sup>-/-</sup>/WT, and TDP1<sup>-/-</sup>/S61A MEFs as indicated. Data are mean ± SD, *n* = 3 biological replicates. \**P* ≤ 0.05; \*\**P* ≤ 0.01; \*\*\**P* ≤ 0.001 (one-way ANOVA). (G) TDP1<sup>-/-</sup>/EV; TDP1<sup>-/-</sup>/WT, and TDP1<sup>-/-</sup>/S61A MEFs were treated with CPT (15 nM; 9 h) in late S-phase as indicated to generate replication stress, synchronized in G2/M-phase followed by immunocytochemistry with anti-γH2AX (red) and anti-Top1cc (green) antibody. Cells were counterstained with DAPI to visualize mitotic nuclei (blue). (H, I) Quantifications for the number γH2AX foci (H) and Top1cc-positive γH2AX foci (I) per mitotic nucleus of TDP1<sup>-/-</sup>/EV; TDP1<sup>-/-</sup>/WT and TDP1<sup>-/-</sup>/S61A MEFs treated with CPT in late S calculated for 50 cells. Data are mean ± SD, *n* = 3 biological replicates. ns non-significant (*P* > 0.05); \**P* ≤ 0.05; \*\*\*\**P* ≤ 0.0001 (one-way ANOVA). Scale bars, 10 μm. Source data are available online for this figure.

while BrdU incorporation was used to monitor MiDAS. We could detect BrdU foci on mitotic chromosomes that implicate DNA synthesis was occurring in early mitosis (Fig. 6A–D). Also, to exclusively capture DNA synthesis in mitosis, we inhibited S/G2 replication with hydroxyurea, as previously described (Macheret et al, 2020) and analyzed BrdU incorporation by immunofluorescence microscopy. We detected no BrdU or γH2AX foci in untreated cells (Fig. 6A, panel “No treatment”) and these were markedly increased after CPT treatment (Fig. 6B, panel “CPT”). Under similar conditions, APH treatment shows a marked reduction in BrdU foci formation compared to cells treated with CPT (Fig. 6C, panel “APH”) (Groelly et al, 2022). It is possible that MiDAS is engaged in the repair of CPT-induced Top1cc during mitosis because pS61-TDP1 is excluded (Fig. 1G,H) from mitotic chromosomes and we see the colocalization of CPT-induced BrdU and γH2AX foci (Fig. 6A–D). Notably, TDP1<sup>-/-</sup>/S61A MEFs showed a marked increase in the colocalization of BrdU and γH2AX foci upon CPT treatment (Fig. 6B) compared to TDP1<sup>-/-</sup>/WT MEFs, suggesting that trapping of TDP1<sup>S61A</sup> on mitotic chromosomes hyperactivates MiDAS. Intriguingly, we detected a significant reduction of both BrdU and γH2AX foci in the TDP1<sup>-/-</sup>/WT, TDP1<sup>-/-</sup>/S61A or TDP1<sup>-/-</sup>/EV MEFs after co-treatment with APH and CPT (Fig. 6D), suggesting replication conflicts as a potential source of these Top1cc-induced DNA breaks (Fig. 6E,F). Our study further suggests that mitotic Top1ccs are repaired primarily by MUS81-dependent endonuclease pathways.

### TDP1<sup>S61</sup> trapping amplifies mitotic DNA breaks by elevating MUS81 association with chromatin

Because MUS81 has been implicated in the cleavage of stalled Top1cc at the replication forks (Wu and Wang, 2021), and is an important factor in MiDAS (Bhowmick et al, 2016), we tested the recruitment of MUS81 at the CPT-induced mitotic Top1cc. We utilized two independent approaches to detect the chromatin-bound fraction of MUS81 in TDP1<sup>-/-</sup>/WT or TDP1<sup>-/-</sup>/S61A MEFs synchronized to the mitotic phase: (i) chromatin fractionation and western blotting, and (ii) immunofluorescence staining of mitotic chromatin-bound MUS81 foci after CPT treatment. Figure 6G,H shows that CPT-induced MUS81 loading on the chromatin fraction was markedly increased in TDP1<sup>-/-</sup>/S61A MEFs compared to TDP1<sup>-/-</sup>/WT MEFs which is consistent with the marked increase

of TDP1<sup>S61A</sup> in the chromatin-bound fraction (Fig. 6H, left panel). Accordingly, MUS81 knockdown enriched TDP1<sup>S61A</sup> at the FDR loci (Appendix Fig. S6C), which is consistent with the role of MUS81 in the clearance of trapped TDP1<sup>S61A</sup>. Therefore, TDP1<sup>S61A</sup> trapping resulted in the overloading of MUS81 on the mitotic chromosomes.

Next, we tested if MUS81 overloading triggers uncontrolled MUS81-mediated increase in DSB levels during MiDAS. CPT-induced DSBs were analyzed using γH2AX and BrdU or EdU; we already show that the number of γH2AX foci significantly increased in TDP1<sup>-/-</sup>/S61A MEFs during MiDAS, compared to TDP1<sup>-/-</sup>/WT MEFs after CPT treatment (Fig. 6B). Notably, siRNA-mediated knockdown of MUS81 significantly reduced CPT-induced γH2AX and BrdU or EdU foci in all independent cell types (TDP1<sup>-/-</sup>/WT, TDP1<sup>-/-</sup>/S61A, and TDP1<sup>-/-</sup>/EV MEFs), indicating that the extensive DNA breakage of CPT-induced collapsed replication forks in mitotic cells is dependent on MUS81 but independent of TDP1 activity (Fig. 6I–L; Appendix Fig. S6D–I). Accordingly, MUS81 knockdown resulted in a significant reduction both in the EdU foci and γH2AX foci (Appendix Fig. S6D–I), suggesting the role of MUS81-mediated MiDAS in the clearance of trapped Top1ccs as well as TDP1<sup>S61A</sup>. Because TDP1<sup>S61A</sup> trapping accumulates mitotic DNA breaks, we tested the co-occupancy of TDP1<sup>S61A</sup> and MUS81 at the CFS loci in MCF7 human cells. We also performed ChIP for endogenous MUS81 at CFSs in MCF7 cells expressing ectopic FLAG-TDP1<sup>WT</sup> or FLAG-TDP1<sup>S61A</sup>, which confirmed the co-enrichment of endogenous MUS81 together with TDP1<sup>S61A</sup> at the CFSs, which was markedly increased after CPT treatment (Fig. 6M–P). Because both Top1cc and TDP1<sup>S61A</sup> are enriched at CFSs after CPT treatment and cause a concomitant increase in DNA breaks (Figs. 4, 5, and 6A–F), our data suggest that MUS81 endonuclease generates DNA breaks at trapped Top1cc and TDP1<sup>S61A</sup> sites on the mitotic chromosomes (Fig. 6M–P).

### Mitotic phosphorylation of TDP1 at serine 61 prevents genome instability

To test whether trapping of the TDP1<sup>S61A</sup> on the mitotic chromosomes can lead to defective mitotic progression and accumulation of chromosomal aberrations (Wu and Wang, 2021), we analyzed the frequency of micronuclei (MN), bulky anaphase bridges (AB), chromatid breaks (CB), and cohesion defects (CD) in



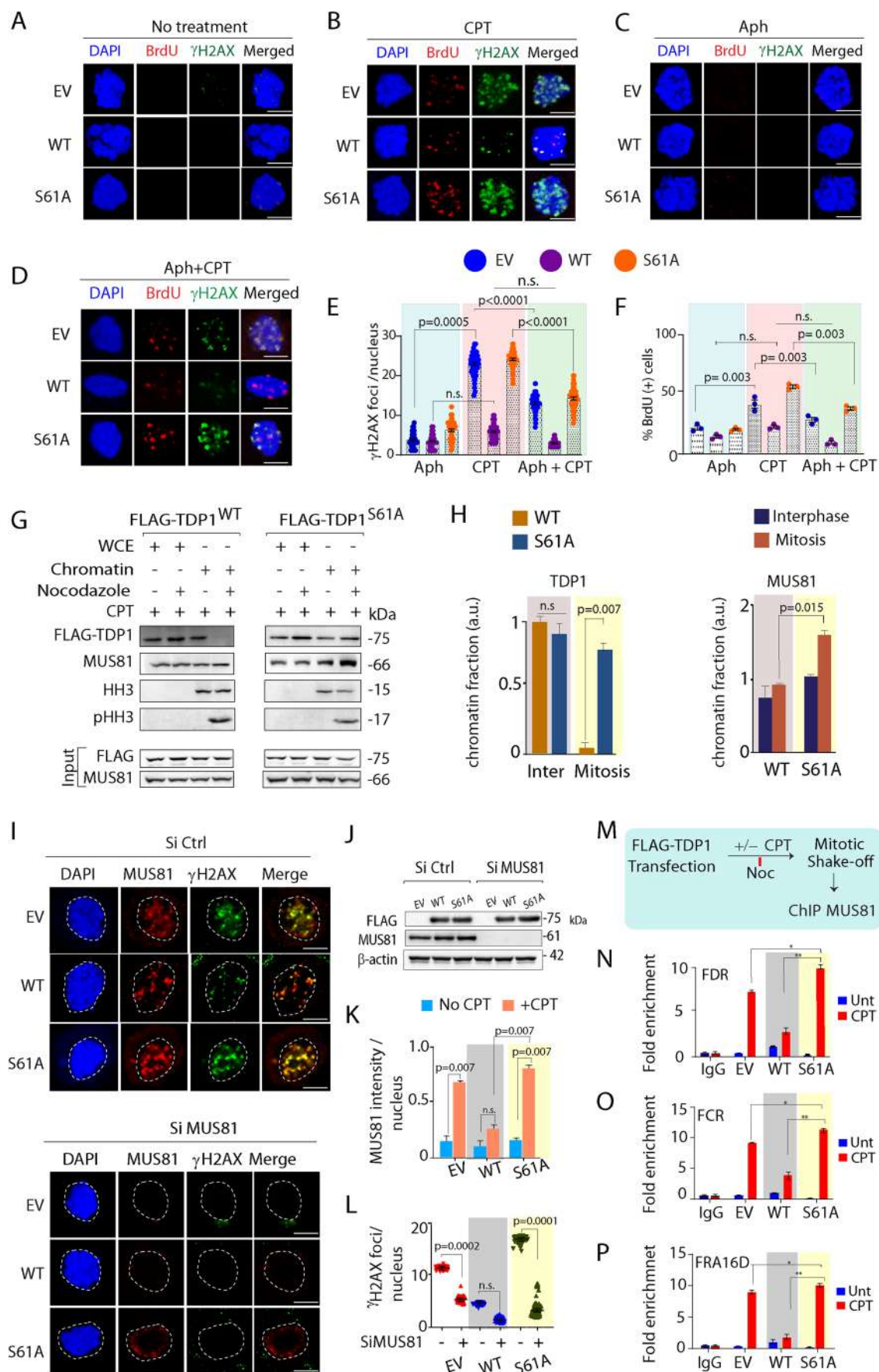




# Figure 6. TDP1<sup>S61</sup> trapping amplifies mitotic DNA breaks by elevating MUS81 chromatin enrichment.

(A–D) TDP1<sup>-/-</sup> MEFs complemented with EV or FLAG-TDP1 variants (TDP1<sup>-/-</sup>/WT and TDP1<sup>-/-</sup>/S61A) were treated with or without CPT (15 nM; 24 h) or Aph (0.4 μM, 24 h) alone or in combination (CPT + APH 24 h) and enriched at M-phase. Representative images show break-induced repair with newly synthesized mitotic DNA marked by BrdU foci (red). The γH2AX foci, signifying the DNA strand breaks, are shown in green. Cells were counterstained with DAPI to visualize nuclei (blue). (E, F) Quantification of γH2AX foci per nucleus and percentage of BrdU-positive mitotic nucleus obtained from immunofluorescence by confocal microscopy were calculated for 20–25 cells. Data are mean ± SD, *n* = 3 biological replicates. ns, non-significant (*P* > 0.05); \*\*\**P* ≤ 0.001; \*\*\*\**P* ≤ 0.0001 (one-way ANOVA). (G) Chromatin fractions were prepared from TDP1<sup>-/-</sup>/WT and TDP1<sup>-/-</sup>/S61A MEFs after CPT treatment (15 nM; 24 h) and analyzed by western blotting to detect FLAG-TDP1 variants and MUS81 with anti-FLAG and anti-MUS81 antibodies, respectively. Anti-HH3 and anti-pHH3 were used as chromosomal and mitotic markers. Protein levels of MUS81, FLAG-TDP1<sup>WT</sup>, and FLAG-TDP1<sup>S61A</sup> were analyzed in whole-cell lysates (WCE) to ensure equal levels of protein before chromatin fractionation. (H) Quantification showing the relative chromosomal enrichment of FLAG-TDP1 variants (WT or S61A) in interphases (Asn) and mitotic (M) chromosomes (left panel). Quantification showing the relative enrichment of MUS81 on mitotic chromosomes in interphases (Asn) and mitosis (M) for indicated cells treated with CPT (15 nM; 24 h) (right panel) *n* = 3 biological replicates. Data are mean ± SD, *n* = 3 biological replicates. ns, non-significant (*P* > 0.05); \**P* ≤ 0.05; \*\**P* ≤ 0.01 (one-way ANOVA). (I) Representative images of immunofluorescence microscopy showing induction of CPT (15 nM, 24 h)-induced γH2AX (green) and MUS81 (red) foci during mitosis in TDP1<sup>-/-</sup>/EV, TDP1<sup>-/-</sup>/WT, and TDP1<sup>-/-</sup>/S61A MEFs, co-transfected either with Si Ctrl or Si MUS81 to knockdown MUS81. Cells were counterstained with DAPI to visualize mitotic nuclei (blue). Note: Colocalization of CPT-induced γH2AX and MUS81 foci in merged images indicates MUS81 overloading amplifies mitotic DNA breaks in TDP1<sup>-/-</sup>/S61A MEFs. (J) Representative western blot analysis for the immunofluorescence microscopy in (I) to detect the levels of MUS81 and FLAG-TDP1 in TDP1<sup>-/-</sup>/EV, TDP1<sup>-/-</sup>/WT, and TDP1<sup>-/-</sup>/S61A MEFs, co-transfected either with Si Ctrl or Si MUS81 to knockdown MUS81. β-actin has been used as loading control. (K) Quantifications of MUS81 foci on the mitotic chromosomes scored for 50 nuclei (each category) as depicted by the corresponding bar diagram. Data are mean ± SD, *n* = 3 biological replicates. ns, non-significant (*P* > 0.05); \*\**P* ≤ 0.01 (one-way ANOVA). (L) Quantifications for CPT-induced γH2AX foci on mitotic nuclei in indicated cells (*n* = 50 cells from three biological replicates; mean ± SD). Note: siRNA knockdown of MUS81 significantly reduced CPT-induced γH2AX. ns, non-significant (*P* > 0.05); \*\*\*\**P* ≤ 0.0001 (one-way ANOVA). (M) A schematic representation for the protocol followed for the ChIP of endogenous MUS81 at the CFS loci in mitosis following CPT (15 nM, 24 h) treatment. (N–P) Quantification of cross-linked FRA3B-FCR, FRA3B-FDR, and FRA16D loci chromatin-immunoprecipitated from MCF7 cells transfected with empty vector (EV) or FLAG-TDP1 variants (WT or S61A) using the specified antibodies. Fold enrichment over IgG was determined and is shown for each primer pair for the ChIP. Data are mean ± SD, *n* = 3 biological replicates. \**P* ≤ 0.1; \*\**P* ≤ 0.01 (one-way ANOVA). Scale bars, 10 μm. Source data are available online for this figure.

TDP1<sup>-/-</sup>/WT, TDP1<sup>-/-</sup>/S61A, and TDP1<sup>-/-</sup>/EV MEFs when exposed to a CPT (Fig. 7A–E). We found that CPT treatment markedly increased micronuclei, and chromatid breaks in the TDP1<sup>-/-</sup>/S61A MEFs compared to the TDP1<sup>-/-</sup>/WT or TDP1<sup>-/-</sup>/EV MEFs (Fig. 7A–E), suggesting TDP1<sup>S61A</sup> trapping triggers mitotic defects. Notably, TDP1<sup>-/-</sup>/S61A MEFs showed a reduction in the CPT-induced chromatin breaks CB and CD when subjected to knockdown of MUS81 (Fig. 7C).

Next, to test whether the TDP1<sup>S61A</sup> trapping on the mitotic chromosomes can lead to the accumulation of 53BP1 nuclear bodies in the subsequent G1 phase (Fig. 7F,G), we used TDP1<sup>-/-</sup>/WT, TDP1<sup>-/-</sup>/S61A, and TDP1<sup>-/-</sup>/EV MEFs exposed to a low dose of CPT followed by synchronization to the next G1 phase of the cell cycle. Immunostaining of 53BP1 detected a marked increase in G1-phase 53BP1 nuclear bodies in the TDP1<sup>-/-</sup>/S61A MEFs as compared to TDP1<sup>-/-</sup>/WT or TDP1<sup>-/-</sup>/EV MEFs, suggesting TDP1<sup>S61A</sup> trapping in mitotic chromosomes propagates DNA breaks into 53BP1 bodies in G1 phase (Fig. 7F,G).

Next, we performed neutral comet assays to compare CPT-induced DSBs in TDP1<sup>-/-</sup>/WT, TDP1<sup>-/-</sup>/S61A, and TDP1<sup>-/-</sup>/EV MEFs synchronized to mitosis (Cortés-Gutiérrez et al, 2012). Figure 7H shows that TDP1<sup>-/-</sup>/S61A MEFs accumulated higher levels of CPT-induced DNA breaks (~fivefold) than TDP1<sup>-/-</sup>/WT MEFs, which is due to TDP1<sup>S61A</sup> trapping (Fig. 6B). Notably, MUS81 knockdown resulted in a significant decrease in mean comet length (Fig. 7H, siMUS81), indicating MUS81 deficiency reduces CPT-induced DNA breaks. Taken together our results provide evidence for the role of S61 phosphorylation of TDP1 during mitosis in the maintenance of genomic stability.

## MUS81 knockdown partly reverses TDP1<sup>-/-</sup>/S61A MEFs against CPT-induced replication stress

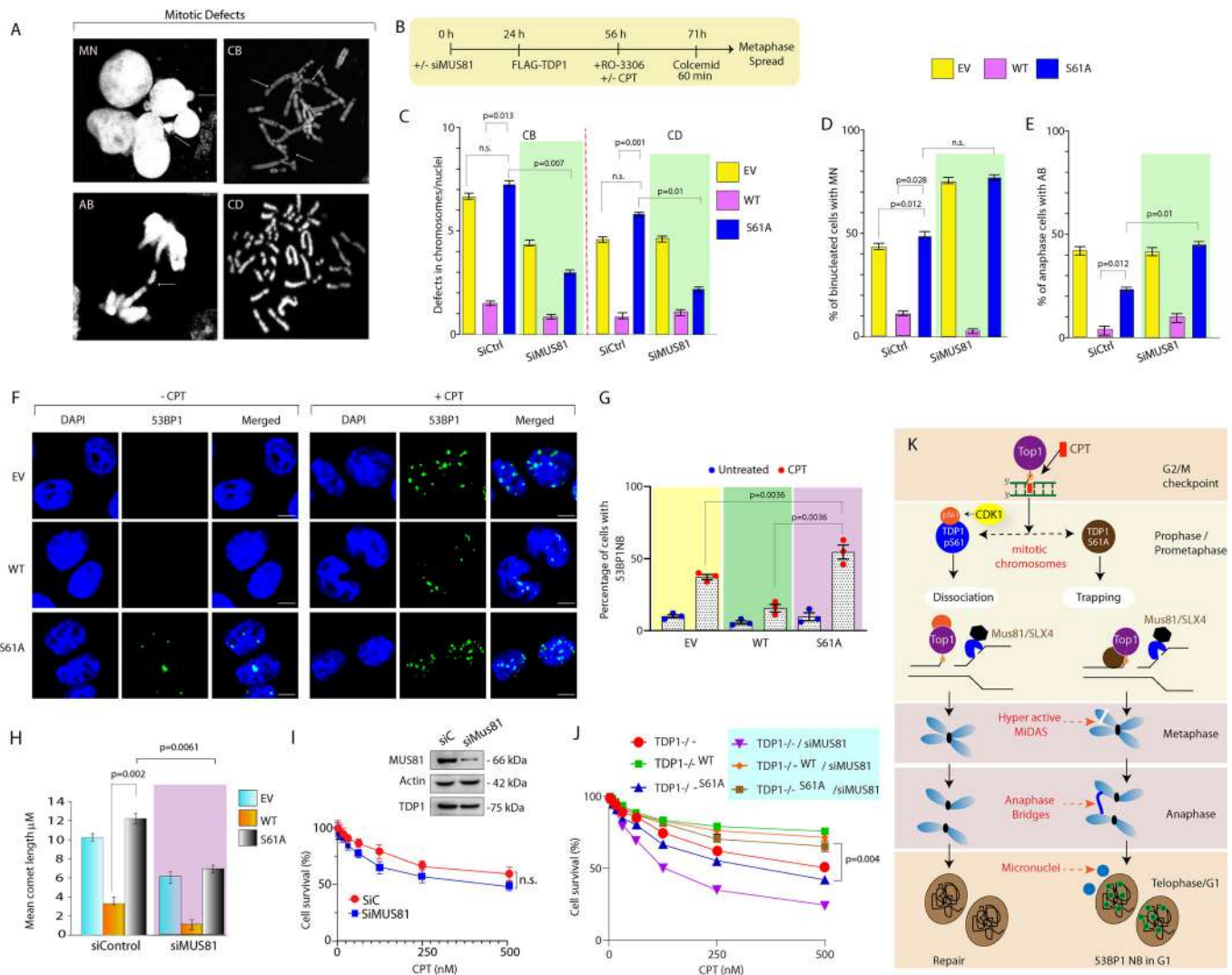
BIR is a mutagenic mechanism that involves extensive DNA resection and mutagenic DNA synthesis and, if uncontrolled

loading of MUS81, can lead to RS-mediated cell death (Kramara et al, 2018; Malkova and Ira, 2013). MCF7 cells knockdown for MUS81 had no significant effect on CPT-induced cell survival when compared to wild-type counterpart (Fig. 7I). However, we noted MUS81 depletion, on the other hand, made TDP1<sup>-/-</sup> MEFs much more susceptible to CPT, suggesting that the TDP1-dependent pathway and the endonuclease pathways operate in the repair of trapped Top1ccs (Fig. 7J) as shown previously (Marini et al, 2023). The hypersensitivity to CPT in TDP1<sup>-/-</sup> MEFs caused by MUS81 depletion could be rescued by complementation with FLAG-TDP1<sup>WT</sup>, further substantiating the role of TDP1 in Top1cc repair (Fig. 7J).

Because excessive DNA breaks and enhanced BIR in TDP1<sup>-/-</sup>/S61A MEFs cells are dependent on MUS81 overloading (Fig. 6G,H), we investigated whether knocking down of MUS81 can rescue TDP1<sup>-/-</sup>/S61A MEFs viability in response to CPT treatment. MUS81 knockdown partly restored TDP1<sup>-/-</sup>/S61A MEFs survival to CPT (Fig. 7J). The rescue of the effects of TDP1<sup>S61A</sup> trapping in MEFs by knockdown of MUS81 was small but reproducible in independent experiments (Fig. 7C,J). Although uncontrolled BIR causes cell death, it is plausible that regulated BIR is required for TDP1<sup>-/-</sup>/S61A MEFs to survive CPT-induced DNA damage. Alternatively, MUS81's role in processing additional replication intermediates in resuming the collapsed replication forks may be needed for TDP1<sup>-/-</sup>/S61A MEFs survival in response to CPT (Fig. 7J), as it is required for TDP1<sup>+/+</sup> MEFs expressing TDP1<sup>S61A</sup>, which further validates that excessive loading of MUS81 on the chromatin due to TDP1<sup>S61A</sup> trapping leads to a marked increase in end resection causing chromosomal defects and cell death (Appendix Fig. S7).

## Discussion

In this study, we establish that principal mitotic kinase CDK1 can regulate TDP1 through phosphorylation of serine 61 during



mitosis, promoting its dissociation from mitotic chromosomes, which is crucial for genome stability. TDP1 defective for S61 phosphorylation (TDP1<sup>S61A</sup>) is trapped on the mitotic chromosomes, triggering DNA damage and mitotic defects. We detected that TDP1<sup>S61A</sup> is enriched at CFS loci, which are of late replicating origin, are intrinsically susceptible to RS, and also accumulate Top1ccs. Our study provides additional evidence that MUS81-dependent MiDAS is partly responsible for the clearance of mitotic Top1ccs. It is interesting to note that the significant spike in CPT-induced mitotic DNA breaks in TDP1<sup>-/-</sup>/S61A cells is not caused by the Top1cc elevation but due to uncontrolled MUS81 loading and excessive DNA breakage, which causes elevated MiDAS, 53BP1 nuclear bodies in G1 phase, chromosome abnormalities, and cell mortality that could be partly reversed by MUS81 depletion.

CDK1 is essential for mitotic progression and regulates mitotic DNA damage response, checkpoint activation, and mitotic catastrophe via phosphorylation of DDR proteins (Brown et al, 2015; Diril et al, 2012; Holt et al, 2009). The mechanistic implications of CDK1-mediated TDP1 phosphorylation at S61 (Fig. 2) appear to aid TDP1 temporal dynamics during mitosis

(Fig. 3). TDP1-S61 phosphorylation increased during early mitosis, then declined in late mitosis to near baseline levels in G1 (Fig. 1F), which is paralleled by CDK1 kinase activity (Appendix Fig. S1K). The mitotic chromosomes are innately refractory to pS61-TDP1 recruitment (Fig. 1G,H). Defects in TDP1-S61 phosphorylation either by CDK1 inhibition (Fig. 3E-G) or by knockdown of CDK1 (Fig. 3A-D) markedly increased (~fourfold) TDP1 in the chromatin-bound fraction during M-phase irrespective of replication stress. Accordingly, immunodetection evidenced a marked increase in retention of TDP1<sup>S61A</sup> on the chromosomes during prophase to telophase chromosomes (Fig. 3J,L,M), confirming CDK1-mediated S61 phosphorylation dissociates TDP1 from mitotic chromosomes. Intriguingly, we observed that replication stress with CPT or APH markedly increased the enrichment of TDP1<sup>S61A</sup> (Fig. 4; Appendix Fig. S4) on the mitotic chromosomes, exhibiting induction of CPT-induced DNA breaks and  $\gamma$ H2AX on metaphase chromosomes (Fig. 5). Our results fit well with previous observations that the DDR proteins, which are the substrates of mitotic kinases, promote the dissociation of RNF8, 53BP1, Claspin, and XRCC4 at DSB-flanking chromatin sites in M-phase (Giunta

**Figure 7. MUS81 knockdown protects TDP1<sup>-/-S61A</sup> MEFs against CPT-induced replication stress.**

(A) Representative confocal microscopic images showing the mitotic defects observed in TDP1<sup>-/-</sup> MEFs complemented with FLAG-TDP1<sup>S61A</sup> following CPT treatment (15 nM; 24 h). MN micronuclei, AB anaphase bridges, CB chromatid breaks, CD cohesion defect. (B) Schematic representation of the protocol followed for the scoring of mitotic defects on metaphase chromosomes in TDP1<sup>-/-</sup> MEFs complemented with FLAG-TDP1 variants (TDP1<sup>-/-WT</sup> and TDP1<sup>-/-S61A</sup>) or Empty vector (TDP1<sup>-/-EV</sup>), co-transfected either with Si Ctrl or Si MUS81 to knockdown MUS81. The indicated cells were synchronized in the mitotic phase following CPT treatment before metaphase spread. (C) The percentage of mitotic defects was scored for 150 metaphase spreads (each category), as depicted by the corresponding bar diagram quantification as indicated. Data are mean  $\pm$  SD,  $n = 3$  biological replicates. ns, non-significant ( $P > 0.05$ ), \* $P \leq 0.05$ ; \*\* $P \leq 0.01$  (one-way ANOVA). (D) Bar graphs showing the percentage of binucleated cells with MN in TDP1<sup>-/-</sup> MEFs complemented with FLAG-TDP1 variants (TDP1<sup>-/-WT</sup> and TDP1<sup>-/-S61A</sup>) or Empty vector (TDP1<sup>-/-EV</sup>), co-transfected either with Si Ctrl or Si MUS81 to knockdown MUS81. Data are mean  $\pm$  SD,  $n = 3$  biological replicates. ns non-significant ( $P > 0.05$ ), \* $P \leq 0.05$  (one-way ANOVA). (E) Bar graphs showing the percentage of anaphase cells with AB in TDP1<sup>-/-</sup> MEFs complemented with FLAG-TDP1 variants (TDP1<sup>-/-WT</sup> and TDP1<sup>-/-S61A</sup>) or Empty vector (TDP1<sup>-/-EV</sup>), co-transfected either with Si Ctrl or Si MUS81 to knockdown MUS81. Data are mean  $\pm$  SD,  $n = 3$  biological replicates. \* $P \leq 0.05$ ; (one-way ANOVA). (F) Representative images of immunofluorescence microscopy show the induction of CPT-induced 53BP1 nuclear bodies in the G1 phase. TDP1<sup>-/-</sup> MEFs complemented with FLAG-TDP1 variants (WT and S61A) were treated with CPT (15 nM, 24 h) followed by G2/M arrest with 200 ng/mL nocodazole during the last 8 h of CPT treatment. Mitotic cells were harvested by shake-off and re-seeded in drug-free medium. Five hours after release, cells were fixed and stained with the anti-53BP1 antibody (green) and DAPI (blue) as nuclear stain. Scale bars, 10  $\mu$ m. (G) Quantifications showing the percentage of cells detected with CPT-induced 53BP1 nuclear bodies in G1 phase calculated for 45–50 cells in indicated cell types. Data are mean  $\pm$  SD,  $n = 3$  biological replicates. \*\* $P \leq 0.01$ ; (one-way ANOVA). (H) Quantification of CPT-induced DNA strand breaks measured by neutral comet assays in TDP1<sup>-/-</sup> MEFs complemented with FLAG-TDP1 variants (WT and S61A) or Empty vector (EV), co-transfected either with Si Ctrl or Si MUS81 to knockdown MUS81 arrested in mitotic phase with 200 ng/mL nocodazole added during the last 8 h of CPT treatment. CPT-induced comet tail lengths were calculated for 50 cells. Data are mean  $\pm$  SD,  $n = 3$  biological replicates. \*\* $P \leq 0.01$  (one-way ANOVA). (I) Survival of MCF7 cells transfected either with Si Ctrl or Si MUS81 to knockdown MUS81 in the presence of CPT. Percentage survival was normalized for the CPT-untreated cells  $\pm$  SEM.  $n = 3$  biological replicates. n.s. non-significant ( $P > 0.05$ ). Inset: western blots showing the levels of MUS81 knockdown and the corresponding TDP1 levels in the MCF7 cells. Actin was used as a loading control. (J) Survival of TDP1<sup>-/-</sup> MEF cells complemented with FLAG-TDP1 variants (WT or S61A), co-transfected with expressing Si Ctrl or Si MUS81 to knockdown MUS81 and in the presence of CPT. Percent survival was normalized to the CPT-untreated cells  $\pm$  SEM.  $n = 3$  biological replicates. Asterisks denote statistically significant differences \*\* $P \leq 0.01$  (t test). (K) Model depicting how TDP1<sup>S61A</sup> trapping on mitotic chromosomes leads to hyperactivation of mitotic DNA synthesis (MiDAS), causing excessive MUS81-Eme1 endonuclease-mediated DNA resection and breaks on the mitotic DNA. These breaks manifest as bulky anaphase bridges followed by chromosomal segregation defects leading to the formation of micronuclei and the accumulation of 53BP1 nuclear bodies in G1 daughter cells. CDK1-mediated phosphorylation of TDP1 at the S61 residue promotes its exclusion from the mitotic chromosome to safeguard genomic stability. Source data are available online for this figure.

et al, 2010; Terasawa et al, 2014). RS-induced activation of CDK1-dependent phosphorylation of human 53BP1 during mitosis can eventually lead to the deactivation of 53BP1 (Belotserkovskaya and Jackson, 2014; Giunta et al, 2010; Orthwein et al, 2014). Similarly, CDK1-dependent phosphorylation of MDC1 disrupts MDC1 and  $\gamma$ H2AX interaction, presumably to avoid checkpoint activation during mitosis (Yu et al, 2012).

RS causes cells to fail to complete replication before the S-G2 transition, allowing them to progress through the cell cycle with under-replicated DNA. These late-cell cycle stage DNA synthesis loci, which include CFSs, are among the most difficult in the human genome to replicate. Intriguingly, it is apparent that Top1 is critical for controlling the topological state of DNA during mitosis at the CFS loci (Fig. 4) (Arlt and Glover, 2010). Thus it becomes imperative that the trapped Top1ccs need clearance in mitosis for the re-establishment of the interphase transcriptome during mitotic exit (Wiegard et al, 2021). MiDAS occurs at CFSs and telomeres upon RS induced by APH and at other collapsed replication forks induced by CPT (Arlt and Glover, 2010; Chan et al, 2009; Li and Wu, 2020; Minocherhomji et al, 2015b; Özer and Hickson, 2018; Pladevall-Morera et al, 2019). Therefore, we favor the interpretation that CPT-induced DNA breaks in the condensed mitotic chromosomes are refractory to the canonical TDP1-dependent DNA repair pathways and have to rely on the nuclease activity of the structure-specific endonuclease MUS81-EME1 (Figs. 6 and 7), which has been implicated in the cleavage of stalled Top1cc at the replication forks (Regairaz et al, 2011; Wu and Wang, 2021), promotes a RAD52-mediated break-induced replication process using POLD3 at mitotic break sites (Bhowmick et al, 2023; Bhowmick et al, 2016), to minimize chromosome mis-segregation under conditions of RS. CPT-induced retention of TDP1<sup>S61A</sup> on mitotic chromosomes may cause replication obstacles that require MUS81 processing to prevent transcription replication collisions (Chappidi et al, 2020; Marini et al, 2023; Matos et al, 2020). In yeast,

TDP1 and RAD52 act in the same epistasis group for the repair of trapped Top1cc (Pouliot et al, 2001). Although HR is indicated as a high-fidelity repair mechanism, MiDAS is a mutagenic error-prone mechanism that leads to chromosome rearrangements and chromosomal instabilities (Wu and Wang, 2021).

Despite the N-terminal region of TDP1 spanning 1–148 aa is not required for in vitro catalytic activity (Interthal et al, 2001), the inability of TDP1<sup>S61A</sup> to repair mitotic Top1ccs can be attributed to the paucity of the SSBR partners associated with TDP1 like XRCC1, PNKP, Ligase III, and Pol $\beta$  on the mitotic chromosomes following RS. It is interesting to note that TDP1 requires a cohort of downstream repair factors for the repair of Top1ccs (Pommier et al, 2014). The functional coupling between PARP1 and TDP1 accelerates CPT-Top1cc repair (Das et al, 2014). However, PARP1/2 gene deletion had no significant effect on RS-induced MiDAS (Richards et al, 2023), demonstrating that PARP1/2-dependent activity is not essential for BIR in mitosis, and supporting our hypothesis that RS-induced mitotic Top1cc is repaired independently of TDP1. Accordingly, TDP1<sup>-/-S61A</sup> MEFs exhibited a remarkable increase in the mitotic DSBs, which were not restricted to Top1ccs generated by CPT treatment (Fig. 5). Another possibility could be due to the lack of promiscuity of TDP1 towards DNA damage substrates and a general proclivity towards a limited cohort of 3' or 5'-DNA adducts (Pommier et al, 2014). As a result, we detected an elevated enrichment of MUS81 on mitotic DNA following RS, which could be readily associated with unrestrained MiDAS in TDP1<sup>-/-S61A</sup> cells (Fig. 6). Following MUS81 knockdown in these cells, there was a significant reduction in DSBs and MiDAS (Fig. 6J–M; Fig. S6D–I), allowing for a partial restoration in cell viability (Fig. 7H), suggesting the role of MUS81 endonuclease in DNA break formation for both trapped Top1cc and TDP1<sup>S61A</sup> from the mitotic chromosomes. Concurrent to the deleterious effects of MUS81 overloading and unrestrained MiDAS



in TDP1<sup>S61A</sup> expressing cells was associated with several mitotic defects like chromatid breaks, bulky anaphase bridge formation, micronuclei formation, and also the accumulation of 53BP1 nuclear bodies in the G1 daughter cells suggestive of chromosomal instability which again could be partly salvaged by MUS81 depletion (Figs. 6 and 7; Appendix Fig. S6D–I).

In conclusion, our findings show that TDP1 undergoes a unique post-translational alteration during mitosis. It demonstrates the biological importance of TDP1 phosphorylation at S61 and offers a new TDP1 post-translational regulatory mechanism (Fig. 7I). It is worth noting that melanoma and oral cavity cancer variations associated with serine-to-leucine (S61L) SNPs in TDP1 are critical to the physiological importance of S61 phosphorylation (<https://portal.gdc.cancer.gov/genes>). Because MiDAS is elevated in cells challenged with RS and is especially prevalent in aneuploid cancer cells with oncogene activation, inhibition of CDK1 may provide a therapeutic intervention in cancers with elevated TDP1 expression, which is known to cause chromosomal instability (Duffy et al, 2016).

## Methods

### Reagents and tools table

Reagent or resource	Source	Identifier
<b>Antibodies</b>		
Rabbit polyclonal anti-phospho-Histone H3 (Ser10)	Millipore	Cat# 06-570; RRID: AB_310177
Mouse anti-MPM2 monoclonal antibody	Millipore	Cat# 05-368; RRID: AB_309698
Mouse monoclonal anti-phospho-Histone H2A.X (Ser139) Antibody, clone JBW301	Millipore	Cat# 05-636; RRID: AB_309864
Mouse monoclonal Anti-MUS81 antibody	Abcam	Cat# ab14387; RRID: AB_301167 [MTA30 2G10/3] Cat# sc-53382; RRID: AB_2147138
Rabbit polyclonal anti-histone H3 antibody	Millipore	Cat# 06-755; RRID: AB_2118461
Mouse monoclonal anti-FLAG antibody (M2)	Sigma-Aldrich	Cat# F3165; RRID: AB_259529
Rabbit polyclonal anti-FLAG antibody	Sigma-Aldrich	Cat# F7425; RRID: AB_439687
Mouse monoclonal anti-CDK1 antibody	Cell Signaling technologies	Cat# 9116; RRID: AB_2074795
Mouse anti-actin monoclonal, unconjugated, Clone actn05 (c4) antibody	Novus	Cat# NB 600-535; RRID: AB_521546
Mouse anti-53BP1 monoclonal, unconjugated, Clone BP13 antibody	Millipore	Cat# 05-726 RRID: AB_309940
Mouse anti-Top1cc monoclonal antibody	Millipore	Cat# MABE1084 RRID: AB_2756354
Mouse anti-Top1 (C21) monoclonal antibody	Santa Cruz	Cat# sc-32736 RRID: AB_628382
Mouse anti-BrdU monoclonal antibody (MoBU-1), conjugated Alexa Fluor™ 488	Thermo Fisher Scientific	Cat# B35130 RRID: AB_2536434
Rabbit serine 61-TDP1 (S61-TDP1)	Custom made	N/A
Rabbit phospho serine 61-TDP1 (pS61-TDP1)	Custom made	N/A
Goat anti-rabbit IgG (H + L) secondary antibody, HRP	Thermo Fisher Scientific	Cat# 31460, RRID:AB_228341

Reagent or resource	Source	Identifier
Goat anti-mouse mouse IgG-h&I polyclonal, HRP-conjugated antibody	Novus	Cat# NB 7539, RRID:AB_524788
Goat anti-mouse IgG (H + L) secondary antibody, Alexa Fluor 488-10 nm colloidal gold	Thermo Fisher Scientific	Cat# A-31561, RRID:AB_2536175
Goat anti-rabbit IgG (H + L) highly cross-adsorbed antibody, Alexa Fluor 568-conjugated	Thermo Fisher Scientific	Cat# A-11036, RRID:AB_10563566
Goat anti-mouse IgG (H + L) cross-adsorbed secondary antibody, Alexa Fluor 488	Thermo Fisher Scientific	Cat# A-11001, RRID:AB_2534069
Goat anti-mouse IgG (H + L) cross-adsorbed Secondary antibody, Alexa Fluor 568	Thermo Fisher Scientific	Cat# A-11004, RRID:AB_2534072
<b>Bacterial and virus strains</b>		
<i>E. coli</i> BL21 DE3	Thermo Fisher Scientific	Cat# EC0114
<i>E. coli</i> DH5a	Thermo Fisher Scientific	Cat# 18265017
<b>Chemicals, peptides, and recombinant proteins</b>		
Camptothecin (CPT)	Sigma-Aldrich	Cat# C9911
Aphidicolin (Aph)	Calbiochem	Cat# 178273
RO3306	Sigma-Aldrich	Cat# SML0569
Hydroxyurea	Sigma-Aldrich	Cat# H8627
Thymidine	Sigma-Aldrich	Cat#1895
Nocodazole	Sigma-Aldrich	Cat# M1404
BrdU	Thermo Fisher Scientific	Cat#00-013
ProLong™ Gold Antifade Mountant with DAPI	Thermo Fisher Scientific	Cat# P36935
Lipofectamine 2000	Thermo Fisher Scientific	Cat# 11668027
X-tremeGENE™ HP DNA Transfection Reagent	Sigma-Aldrich	Cat# 6366244001
DNase	Sigma-Aldrich	Cat# AMPD1
Tris-HCl	Himedia	Cat# MB030
NaCl	SRL	Cat# 33205
Sodium lauryl sulphate extrapure AR, ACS, 99%	SRL	Cat# 54468
NP-40	Sigma-Aldrich	Cat# 492016
Albumin bovine (pH 6–7) fraction V for molecular biology (bovine serum albumin, BSA), 98%	SRL	Cat# 85171
Sodium deoxycholate	Sigma-Aldrich	Cat# D6750
Phosphatase inhibitor	Sigma-Aldrich	Cat# 524636
Dithiothreitol (DTT)	Sigma-Aldrich	Cat# 11583786001
Magnesium chloride	SRL	Cat# 31196
Protein A/G beads	Santa Cruz	Cat# sc-2003
Glycine	Sigma-Aldrich	Cat# 50046250 G
Paraformaldehyde	Sigma-Aldrich	Cat# P6148
BSA	Sigma-Aldrich	Cat# A5611
Potassium chloride extrapure AR, 99.5%	SRL	Cat# 38630
EDTA	SRL	Cat# 43272
DMSO	Sigma-Aldrich	Cat# 276855
DMEM—Dulbecco's Modified Eagle Medium	Thermo Fisher Scientific	Cat# 10569044
Fetal bovine serum	Gibco (By Life Technologies)	Cat# 10270106
Trypsin-EDTA (0.05%)	Sigma-Aldrich	Cat# 25300054
cComplete Mini, EDTA-free (protease inhibitor cocktail)	Sigma-Aldrich	Cat# 4693159001
Proteinase K	Sigma-Aldrich	Cat# P2308



Reagent or resource	Source	Identifier
<b>Critical commercial assays</b>		
Reverse transcription kit	Applied Biosystems	Cat# 4368814
QuikChange II XL site-directed mutagenesis kit	Agilent Technologies	Cat# 200521
<b>Deposited data</b>		
Raw Imaging day	This paper; Mendeley data	
<b>Experimental models: cell lines</b>		
TDP1 <sup>+/+</sup> and <sup>-/-</sup> MEFs	Dr Cornelius F Boerkoel (Centre for Molecular Medicine and Therapeutics, University of British Columbia, Vancouver, British Columbia, Canada)	N/A
MCF7	Developmental Therapeutics Program (NCI, NIH)	N/A
<b>Oligonucleotides</b>		
TDP1 siRNA AAGGAGCAGCAAUGAGCCC	This paper	N/A
CDK1 siRNA duplex 1: (RNA) – CCU AGU ACU GCA AUU CGG GAA AUU U duplex 2: (RNA) – GGA CAA UCA GAU UAA GAA GAU GUA G	This paper	N/A
MUS81 siRNA CAGCCUGGUGAUCGAUA	This paper	N/A
Primers for human TDP1 (forward: GACGTGGACTGGCTCGTAAA; reverse: GAGCCTTAGCCTCTCTCGCTTATC)	This paper	N/A
Primers for human actin (forward GACCCAGATCATGTTTGAGACC; reverse: CATCACGATGCCAGTGGTAC)	PMID: 31723605	N/A
Primers for CFS loci FCR forward 5'-TGTTGGAATGTTAACTCTAT CCCAT-3'; FCR; reverse 5'-ATATCTCATCAAGACCGCT G- CA-3'; FDR; forward 5'-CAATGGCTTAAGCAGACATG GT-3'; FDR; reverse 5'-AGTGAATGGCATGGCTGGA ATG-3'; FRA16D; forward 5'-TCCTGTGGAAGGGATATTTA-3'; FRA16D; reverse 5'-CCCCTCATATTCTGCTTCTA-3';	PMID: 26354865	N/A
<b>Recombinant DNA</b>		
pCMV-Tag2B-TDP1 WT (FLAG-TDP1 <sup>WT</sup> )	PMID: 29718323	N/A
pCMV-Tag2B-TDP1-S61A (FLAG-TDP1 <sup>S61A</sup> )	This paper	N/A
pCMV-Tag2B-TDP1 S61D (FLAG-TDP1 <sup>S61D</sup> )	This paper	N/A
pET15b-His-TDP1 WT (His-TDP1 <sup>WT</sup> )	PMID: 29718323	N/A
pET28A-His-TDP1-S61A (His-TDP1 <sup>S61A</sup> )	This paper	N/A
pET28A-His-TDP1 S61D (His-TDP1 <sup>S61D</sup> )	This paper	N/A
pCDNA3-HA-CDK1 WT (HA-CDK1 <sup>WT</sup> )	Gift from Dr. Sohrab Dalal (ACTREC)	N/A
<b>Software and algorithms</b>		
ImageJ	ImageJ	<a href="https://imagej.nih.gov/ij/">https://imagej.nih.gov/ij/</a> , RRID:SCR_003070

Reagent or resource	Source	Identifier
LAS AF	Leica	<a href="https://www.leica-microsystems.com/products/microscope-software/p/leica-las-x-ls/">https://www.leica-microsystems.com/products/microscope-software/p/leica-las-x-ls/</a> RRID:SCR_013673
Origin	Origin	<a href="http://www.originlab.com/index.aspx?go=PRODUCTS/Origin">http://www.originlab.com/index.aspx?go=PRODUCTS/Origin</a> RRID:SCR_014212
GraphPad Prism	GraphPad Software, Inc	<a href="https://www.graphpad.com/443/">https://www.graphpad.com/443/</a> , RRID:SCR_002798

## Mass spectrometry

The mass spectrometry proteomics data have been deposited to the ProteomeXchange Consortium via the PRIDE partner repository with the dataset identifier [PXD053309](https://www.ebi.ac.uk/PRIDE/archive/PXD053309).

## Cell culture, treatment, and transfections

Cell cultures were maintained at 37 °C under 5% CO<sub>2</sub> in Dulbecco's modified Eagle's medium containing 10% fetal bovine serum (Life Technologies, Rockville, MD, USA). The human embryonic kidney origin (HEK293) and human breast cancer (MCF7) cell lines were obtained from the Developmental Therapeutics Program (NCI, NIH/ USA). TDP1<sup>+/+</sup> and TDP1<sup>-/-</sup> primary mouse embryonic fibroblast (MEF) cells were a kind gift from Dr Cornelius F Boerkoel (University of British Columbia, Vancouver, British Columbia, Canada). Cells were treated with the indicated concentrations of different drugs as detailed in the schematic representations in Figures. Plasmid DNAs and Si RNAs were transfected with Lipofectamine 2000 (Invitrogen) according to the manufacturer's protocol. TDP1<sup>+/+</sup> and TDP1<sup>-/-</sup> MEF cells were transfected with the FLAG-TDP1 constructs using X-tremeGENE HP DNA transfection reagent (Roche) according to the manufacturer's protocol.

## Cell extracts, immunoblotting, and immunoprecipitation

Preparation of whole-cell extracts, immunoprecipitation, and immunoblotting were carried out as described previously (Rehman et al, 2018). Briefly, cells were lysed in a lysis buffer (10 mM Tris-HCl (pH 8), 150 mM NaCl, 0.1% SDS, 1% NP-40, 0.5% Na-deoxycholate supplemented with complete protease inhibitor cocktail) (Roche Diagnostics, Indianapolis, IN) and phosphatase inhibitors (Phosphatase Inhibitor Cocktail 1 from Sigma). After thorough mixing and incubation at 4 °C for 2 h, lysates were centrifuged at 12,000 × g at 4 °C for 20 min. Supernatants were collected, aliquoted, and stored at -80 °C. For immunoprecipitation, cells were lysed in a lysis buffer (50 mM Tris-HCl (pH 7.4), 300 mM NaCl, 0.4% NP-40, 10 mM MgCl<sub>2</sub>, 0.5 mM dithiothreitol supplemented with protease and phosphatase inhibitors). Supernatants of cell lysates were obtained by centrifugation at 15,000 × g at 4 °C for 20 min and precleared with 50 µl of protein A/G-PLUS agarose beads (Santa Cruz, CA, USA). About 5 mg of precleared lysate was incubated overnight at 4 °C with indicated antibodies (2–5 µg/ml) and 50 µl of protein A/G-PLUS agarose beads. Isolated immunocomplexes were recovered by centrifugation, washed thrice

with lysis buffer, and were subjected to electrophoresis on 10% Tris–glycine gels and immunoblot analysis. Immunoblottings were carried out following standard procedures, and immunoreactivity was detected using ECL chemiluminescence reaction (Amersham) under ChemiDoc™ MP System (Bio-Rad, USA). Densitometric analyses of immunoblots were performed using ImageJ software.

### Mass spectrometry analysis of TDP1

Ectopic FLAG-TDP1<sup>WT</sup> complexes were immunoprecipitated with anti-FLAG antibody as described above (Rehman et al, 2018). To induce DNA damage cells expressing FLAG-TDP1 were treated with CPT (5  $\mu$ M/3 h) prior to anti-FLAG immunoprecipitation and were subjected to tryptic digestion at 37 °C, overnight, followed by lyophilization, reconstitution, and fractionation applying strong cation exchange (SCX) liquid chromatography (LC) and mass spectrometry analysis as previously described (Rehman et al, 2018).

### siRNA transfection

Transfections were performed as described previously (Rehman et al, 2018). In brief, cells ( $1.5 \times 10^5$ ) were transfected with control siRNA or 100 nM CDK1, MUS81 or TDP1 siRNA (GE Dharmacon, siRNA-SMARTpool) using lipofectamine 2000 (Invitrogen) according to the manufacturer's protocol. Time course experiments revealed a maximum suppression of CDK1, MUS81 or TDP1 protein expression at day 3 after transfection, as analyzed by western blotting.

### Expression constructs and site-directed mutagenesis

Human FLAG-tagged full-length TDP1 (FLAG-TDP1<sup>WT</sup>) and His-tagged-TDP1 constructs were described previously (Das et al, 2009; Das et al, 2014). The HA-CDK1 construct were a kind gift from Dr. Sorab Dalal (Tata Memorial Centre Advanced Centre for Treatment, Research and Education in Cancer, India). The point mutations: TDP1<sup>S61A</sup> and in TDP1<sup>S61D</sup> FLAG as well as His-TDP1<sup>S61A</sup> and His-TDP1<sup>S61D</sup> were created using the “QuickChange” protocol (Stratagene, La Jolla, CA, USA). All PCR-generated constructs were confirmed by DNA sequencing.

### Immunocytochemistry and confocal microscopy

Immunofluorescence staining and confocal microscopy were performed as described previously (Das et al, 2009; Das et al, 2014). Briefly, cells were grown and drug treated on chamber slides (Thermo Scientific™ Nunc™ Lab-Tek™ II Chamber slides) followed by fixation with 4% paraformaldehyde for 10 min at room temperature and permeabilisation with absolute ethanol overnight. Primary antibodies against phosphopeptide-TDP1 (pS61), control immunopeptide TDP1, FLAG,  $\gamma$ H2AX, Top1, MUS81, BrdU and Top1cc were detected using anti-rabbit or anti-mouse IgG secondary antibodies labeled with Alexa 488/568 (Invitrogen). Primary and secondary antibodies were used at 1:300 and 1:500 dilutions respectively. Cells were mounted in antifade solution with 4',6-diamidino-2-phenylindole (DAPI) (Vector Laboratories, Burlingame, CA, USA) and examined under Leica TCS SP8 confocal laser-scanning microscope (Germany) with a 63 $\times$ /1.4 NA oil objective. Images were collected and processed using the Leica software and sized in Adobe Photoshop 7.0. The

intensity per nucleus for the different proteins of interest were determined with Adobe Photoshop 7.0 by measuring the fluorescence intensities normalized to the number of cell count (Das et al, 2009; Das et al, 2014).

### $\lambda$ -phosphatase assay

To validate the phosphorylation at TDP1-S61 residue induced by nocodazole treatment (200 ng/ml) FLAG-TDP1<sup>WT</sup> lysates were pretreated with lambda protein phosphatase ( $\lambda$ -phosphatase; New England Biolabs) prior to immunoprecipitation. For this, cell lysates were supplemented with benzamidine (1.25  $\mu$ l/ml) and N-Ethylmaleimide (10 mM) and mixed with  $\lambda$ -phosphatase in a 30  $\mu$ l volume of 1 $\times$  NEB buffer for PMP (New England Biolabs) supplemented with 1 mM MnCl<sub>2</sub>. Reactions were incubated at 30 °C for 30 min and stopped by adding 5 $\times$  Laemmli sample buffer followed by immunoprecipitation with anti-FLAG antibody. Samples were analyzed by western blotting along with mock-treated samples.

### In vitro kinase assays

Recombinant His-TDP1 (WT, S61A or S61D) proteins (1 $\mu$ g) as indicated were incubated with immunoprecipitated HA-CDK1<sup>WT</sup> kinase or immunoprecipitated endogenous CDK2, 0.05 mM ATP and in 1X kinase assay buffer (25 mM Tris-HCl (pH 7.5), 5 mM beta-glycerophosphate, 2 mM dithiothreitol (DTT), 0.1 mM Na<sub>3</sub>VO<sub>4</sub>, 10 mM MgCl<sub>2</sub>) buffer for 30 min at 37 °C as described previously (Das et al, 2009). Reactions were stopped by adding 2 $\times$  Laemmli sample buffer and heating at 95 °C for 5 min. Samples were loaded onto a 10% SDS-PAGE gel and run at 25 mA for 2 h. Phosphorylation reaction products were separated by SDS-PAGE, transferred onto PVDF membrane and analyzed by western blotting using anti-pS61-TDP1 and anti-TDP1 antibodies.

### Flow cytometry-based cell cycle analysis

For cell cycle profile analysis, cell samples are harvested by scraping or trypsinisation followed by pelleting the cells at 1500 rpm. The cell pellets were washed with 1 $\times$  PBS before fixation with 70% ethanol. On the day of the flow cytometry, the cell suspension in 70% ethanol was pelleted and washed using 1 $\times$  PBS. Next, the flow cytometry samples each containing  $\sim 1 \times 10^6$  cells in suspension are prepared. The samples are centrifuged, and the supernatant is decanted, leaving a pellet of cells in each sample tube. In total, 0.5 mL of FxCycle™ PI/RNase Staining Solution stain is added to each flow cytometry sample, mixed well. The samples are incubated for 15–30 min at room temperature, protected from light. The samples are analyzed the samples without washing, using 488-nm, 532-nm, or similar excitation, and collect emission using a 585/42 bandpass filter or equivalent following the manufacturer's protocol.

### Cell fractionation and isolation of chromatin-bound protein

For cell fractionation and isolation of chromatin-bound proteins (Wu and Wang, 2021), cells were washed with 1 $\times$  PBS followed by washing with hypotonic buffer containing 20 mM HEPES, pH 7.5, 20 mM NaCl, 5 mM MgCl<sub>2</sub> and suspended in hypotonic buffer

(10 ml). Post 10 min incubation on ice, cells were lysed to free nuclei by 45 strokes of a Dounce homogenizer and were centrifuged at  $1500 \times g$  at  $4^\circ\text{C}$  for 5 min to isolate the supernatant from the nuclear pellet. This whole-cell lysate was used as the input fraction for western blotting. Nuclei were further suspended in extraction buffer containing 50 mM HEPES, pH 7.5, 100 mM KCl, 0.25% Triton X-100, 2.5 mM  $\text{MgCl}_2$ , 1 mM dithiothreitol, aprotinin (1  $\mu\text{M}$ ), leupeptin (50  $\mu\text{M}$ ), 4-(2-aminoethyl)-benzenesulfonylfluoride/HCl (1 mM) and NaF (10 mM) followed by centrifugation at  $600 \times g$  at  $4^\circ\text{C}$  for 3 min. Nuclei were further suspended thrice in extraction buffer for complete lysis of the nuclear envelope and full extraction. Supernatants were pooled to yield nucleosolic proteins and the residual pellet contained all DNA and structure-bound proteins (chromatin fraction).

### Chromatin immunoprecipitation (ChIP)

Cells were cultured overnight at a density of  $1 \times 10^7$  per 100 mm petri dish and subjected to transfections or treatments for mitotic synchronization as indicated in the experimental protocol outlines. Chromatin and proteins were cross-linked by incubating cells in 1% formaldehyde for 15 min at room temperature, and the reaction was stopped by 10 min incubation with 125 mM glycine. Cells were collected and washed sequentially with solution A (10 mM HEPES [pH 7.5], 10 mM EDTA, 0.5 mM EGTA, 0.75% Triton X-100) and solution B (10 mM HEPES [pH 7.5], 200 mM NaCl, 1 mM EDTA, 0.5 mM EGTA). The cell pellets were resuspended in 1 ml lysis buffer (25 mM Tris-HCl [pH 7.5], 150 mM NaCl, 0.1% SDS, 1% Triton X-100, 0.5% deoxycholate freshly supplemented with protease inhibitor cocktail (Roche) and sonicated on ice by 10 s pulses at 25% of maximal power on a sonicator. After centrifugation at 13,000 rpm for 15 min to remove any debris, the supernatant was precleared with protein-G-sepharose/salmon sperm DNA beads at  $4^\circ\text{C}$  for 1 h. For each immunoprecipitation, 600  $\mu\text{l}$  of the precleared chromatin was incubated overnight at  $4^\circ\text{C}$  with 6 mg of antibodies specific for TDP1, FLAG, Top1, MUS81, and  $\gamma\text{H2AX}$ . A reaction containing an equivalent amount of Goat/rabbit IgG was included as the background control. In total, 10% of the precleared chromatin was taken as input control. Antibody-chromatin complexes were pulled down by adding 50  $\mu\text{l}$  of protein-G-sepharose/salmon sperm DNA beads and incubated for 4 h at  $4^\circ\text{C}$ . The beads were washed for 10 min each with the lysis buffer followed by high-salt wash buffer (0.1% SDS, 1% Triton X-100, 2 mM EDTA, 20 mM Tris-HCl [pH 8.1], 500 mM NaCl), LiCl wash buffer (250 mM LiCl, 1% NP-40, 1% deoxycholate, 1 mM EDTA, 10 mM Tris-HCl [pH 8.0]), and TE buffer (10 mM Tris-HCl [pH 8.0], 1 mM EDTA). Finally, DNA was eluted with elution buffer (1% SDS, 100 mM  $\text{NaHCO}_3$ ). Elutes were incubated at  $65^\circ\text{C}$  for overnight with the addition of 5 M NaCl to a final concentration of 200 mM to reverse the formaldehyde cross-linking and digested at  $55^\circ\text{C}$  for 3 h with proteinase K at a final concentration of 50 mg/ml. Following phenol/chloroform extraction and ethanol precipitation, sheared DNA fragments served as templates in semi-quantitative and real-time PCR analysis.

### Metaphase spread

For metaphase spreads, cells were transfected as per experimental requirements treated with or without low dose of CPT (15 nM for

24 h) and later incubated with 1 g/ml colcemid for the last 4 h. Cells were then harvested and treated with hypotonic solution (75 mM KCl) for 12 min, washed with chilled fixative (methanol/acetic acid 3:1), and left overnight at  $4^\circ\text{C}$ . Cells were later dropped onto a chilled glass slide, air-dried and stained with 5% aqueous Giemsa. For each case, 150 metaphase plates were scored for defects.

### Analysis of micronuclei

TDP1<sup>+/+</sup> or TDP1<sup>-/-</sup> MEFs transfected with EV or FLAG-TDP1 variants (WT or S61A) and/or Si MUS81 were grown on chamber slides for analysis of micronuclei as described previously (Di Marco et al, 2017). Cell culture medium was supplemented 16 h before fixation with 2  $\mu\text{g/ml}$  cytochalasin B (Sigma-Aldrich) to block cells in cytokinesis. Cells were fixed with 4% formaldehyde for 10 min and mounted with Vectashield mounting medium containing DAPI. Slides were analyzed by confocal fluorescent microscope. For quantification, only DAPI-stained binucleated cells were counted, and distinct micronuclei in the vicinity of these cells were considered as positive. At least 50 binucleated cells were scored in each experiment.

### Analysis of bulky anaphase bridges

Bulky anaphase bridges were detected as described previously (Boleslavskaya and Oravetzova, 2022). Briefly, TDP1<sup>+/+</sup> or TDP1<sup>-/-</sup> MEFs transfected with EV or FLAG-TDP1 variants (WT or S61A) and/or Si MUS81 were grown on chamber slides were synchronized with 9  $\mu\text{M}$  RO3306 for 16 h, followed by three washes with  $1 \times$  PBS for 5 min at RT and subsequent incubation in DMEM medium for a total time of 2 h at  $37^\circ\text{C}$ . Cells were fixed with 4% (v/v) paraformaldehyde in PBS for 15 min at RT, followed by staining with DAPI (1  $\mu\text{g/ml}$ ). Cell images were acquired in a confocal microscope using a  $63 \times / 1.4$  NA objective with oil immersion. The percentage of anaphase cells with bulky bridges was determined using ImageJ. At least 25 anaphase cells were scored per condition in each experiment.

### Detection of mitotic BrdU foci (mitotic DNA synthesis)

For detection of mitotic BrdU foci in MEFs, cells were transfected with empty vector (EV) or FLAG-TDP1 variants (WT or S61A) as detailed in experimental protocol, synchronized at the G1/S transition with 1.5 mM thymidine (Sigma-Aldrich) for 16 h, washed three times with PBS, released in fresh medium containing 6  $\mu\text{M}$  RO3306 (Sigma-Aldrich) for 10.5 h (in the absence of aphidicolin) or for 17.5 h (in the presence of low dosage of CPT (15 nM) alone or combined with aphidicolin (1  $\mu\text{M}$ )) and treated as indicated. Cells were then washed three times with warm medium and released in medium containing 100 ng/mL nocodazole (Sigma-Aldrich) and  $1 \times$  BrdU (Thermo Fisher) for 60–90 min before being processed following a protocol described earlier. To suppress replication in S-phase cells that could potentially contaminate the mitotic shake-off 2 mM HU (Sigma-Aldrich) was added during the final 3 h as described previously (Groelly et al, 2022). Briefly, cells were fixed after removal of BrdU-containing medium with 4% paraformaldehyde for 10 min. The cells were washed and incubated with methanol for 15 min at  $-20^\circ\text{C}$ . Fixed cells were stored in 70% ethanol at  $4^\circ\text{C}$  for up to a week. At the time of antibody staining, ethanol was removed, and cells were

washed twice with PBS and incubated for 1 h with 8% BSA in PBS to block nonspecific binding. After a 5-min PBS wash, the cells were incubated for 3 h with anti- $\gamma$ -H2AX antibody diluted in 3% BSA in PBS. Slides were washed twice with PBS and then incubated with anti-rabbit antibody conjugated with Alexa Fluor 568 for 2 h. After a PBS wash, the cells were again fixed with 4% paraformaldehyde for 5 min, followed by 10-min incubation with 1.5 M HCl at 37°C to denature the DNA. Cells were washed again, incubated with 0.5% Tween 20 in PBS for 5 min, and incubated with NGS for 20 min. Anti-BrdU (conjugated to alexa 488) was diluted in blocking buffer and incubated for 2 h in a humid environment. Microscopy was done on Leica TCS SP8 confocal laser-scanning microscope (Germany) with 63 $\times$ /1.4 NA oil objective. Leica software was used for image processing which was later sized in Adobe Photoshop 7.0. The  $\gamma$ H2AX or BrdU foci/intensity per nucleus was measured by the fluorescence intensities normalized to the number of cell counts in Adobe Photoshop 7.0. Cells analyzed for  $\gamma$ H2AX without nucleotide were fixed with 4% paraformaldehyde and stored in 70% ethanol at 4°C. Antibody staining was done according to the protocol outlined above until the secondary antibody; after which cells were washed and incubated with. Preparations were mounted and imaged as described above. The  $\gamma$ H2AX fluorescence intensity was measured as the average pixel intensity (Adobe Photoshop 7.0) of 25 cells from each sample.

### EdU labeling and detection in mitotic cells

Asynchronously growing TDP1<sup>-/-</sup> MEFs were transfected with Si MUS81 followed by transfection with EV or FLAG-TDP1 variants (WT or S61A) after 24 h. Cells were synchronized in late G2 phase of the cell cycle by incubation with 9  $\mu$ M RO3306 for 16 h along with 15 nM CPT. Cells were then washed three times with warm medium and released in medium containing 100 ng/mL nocodazole (Sigma-Aldrich) and 20  $\mu$ M 5-ethynyl-2'-deoxyuridine (EdU) for 60–90 min before being processed following a protocol described earlier. To suppress replication in S-phase cells that could potentially contaminate the mitotic shake-off 2 mM HU (Sigma-Aldrich) was added during the final 3 h as described previously (Groelly et al, 2022). This was followed by EdU detection using Click-IT Plus EdU Alexa fluor 488 Imaging Kit (Thermo Fisher Scientific). Chromosomes were stained using DAPI (Vectashield; Vector Labs). Images were captured using a Leica SP8 inverted confocal laser-scanning microscope (63 $\times$ /1.40 OIL) objective.

### Neutral COMET assays

To compare the levels of DNA damage in TDP1<sup>+/+</sup> or TDP1<sup>-/-</sup> MEFs transfected with the different TDP1 variants (WT or S61A) and/or Si MUS81, samples were subjected to neutral comet assays according to the manufacturer's instructions (Trevigen, Gaithersburg, MD) as described previously (Das et al, 2009; Das et al, 2010; Das et al, 2014). Briefly, after treatment with 15 nM CPT and mitotic arrest by nocodazole treatment, cells were collected and mixed with low melting agarose. Slides were immersed in lysis solution at 4°C for 1 h. After a rinse with deionized water, slides were immersed in a 4°C electrophoresis solution (50 mM NaOH, 1 mM EDTA, and 1% dimethyl sulfoxide) for 1 h. Electrophoresis was carried out at a constant voltage of 25 V for 30 min at 4°C. After electrophoresis, slides were neutralized in 0.4 M Tris-HCl

(pH 7.5), dehydrated in ice-cold 70% ethanol for 5 min, and air-dried. DNA was stained with ethidium bromide (EtBr) purchased from Sigma (USA). The relative length and intensity of EtBr-stained DNA, tails to heads, is proportional to the amount of DNA damage present in the individual nucleus. Comet length was measured using the TriTek Comet Score software (TriTek Corp, Sumerduck, VA) and was scored for at least 50 cells. Distributions of comet lengths were compared using ANOVA.

### Cell survival assays

MCF7 cells (1–2  $\times$  10<sup>3</sup>) were transfected with control or MUS81 siRNA (100 nM) as described above and seeded in 96-well plates. After 24 h, cells were treated with CPT at the indicated concentrations and kept further for 48 h. In a related experiment the TDP1<sup>+/+</sup> and TDP1<sup>-/-</sup> MEFs ectopically expressing FLAG-TDP1 variants (WT or S61A) and/or Si MUS81 and treated with varying doses of CPT for 72 h. In all independent cases the transient knockdown was performed 24 h prior to the DNA transfections and cell survival was then assessed by 3-(4,5-dimethylthiazol-2-yl)-2,5-diphenyltetrazolium bromide (MTT) purchased from Sigma, USA as described previously (Rehman et al, 2018). Plates were analyzed on Molecular Devices SpectraMax M2 Microplate Reader at 570 nm. The percent inhibition of viability for each concentration of CPT was calculated with respect to the control. Data are represented mean values  $\pm$  SD for three independent experiments.

### Data availability

The mass spectrometry proteomics data have been submitted to the ProteomeXchange Consortium via the PRIDE partner repository under the dataset number [PXD053309](https://doi.org/10.1038/s44318-024-00169-3). The raw data for each figure and the numerical data for this study are provided with the manuscript. Correspondence and material requests should be directed to Dr. Benu Brata Das, [pcbhd@iacs.res.in](mailto:pcbhd@iacs.res.in). This article includes expanded view data, reagent table and appendices.

The source data of this paper are collected in the following database record: [biostudies:S-SCDT-10\\_1038-S44318-024-00169-3](https://biostudies.org/studies/S-SCDT-10_1038-S44318-024-00169-3).

Expanded view data, supplementary information, appendices are available for this paper at <https://doi.org/10.1038/s44318-024-00169-3>.

### Peer review information

A peer review file is available at <https://doi.org/10.1038/s44318-024-00169-3>

### References

- Arlt MF, Glover TW (2010) Inhibition of topoisomerase I prevents chromosome breakage at common fragile sites. *DNA Repair* 9:678–689
- Ashour ME, Atteya R, El-Khamisy SF (2015) Topoisomerase-mediated chromosomal break repair: an emerging player in many games. *Nat Rev Cancer* 15:137–151
- Belotserkovskaya R, Jackson SP (2014) Keeping 53BP1 out of focus in mitosis. *Cell Res* 24:781–782



- Bhattacharjee S, Rehman I, Basu S, Nandy S, Richardson JM, Das BB (2022a) Interplay between symmetric arginine dimethylation and ubiquitylation regulates TDP1 proteostasis for the repair of topoisomerase I-DNA adducts. *Cell Rep* 39:110940
- Bhattacharjee S, Rehman I, Nandy S, Das BB (2022b) Post-translational regulation of Tyrosyl-DNA phosphodiesterase (TDP1 and TDP2) for the repair of the trapped topoisomerase-DNA covalent complex. *DNA Repair* 111:103277
- Bhowmick R, Hickson ID, Liu Y (2023) Completing genome replication outside of S phase. *Mol Cell* 83:3596–3607
- Bhowmick R, Minocherhomji S, Hickson ID (2016) RAD52 facilitates mitotic DNA synthesis following replication stress. *Mol Cell* 64:1117–1126
- Blackford AN, Stucki M (2020) How cells respond to DNA breaks in mitosis. *Trends Biochem Sci* 45:321–331
- Boleslavskaya B, Oravetzova A (2022) DDX17 helicase promotes resolution of R-loop-mediated transcription-replication conflicts in human cells. *Nucleic Acids Res* 50:12274–12290
- Brown NR, Korolchuk S, Martin MP, Stanley WA, Moukhametzianov R, Noble MEM, Endicott JA (2015) CDK1 structures reveal conserved and unique features of the essential cell cycle CDK. *Nat Commun* 6:6769
- Calzetta NL, González Besteiro MA, Gottifredi V (2020) Mus81-Eme1-dependent aberrant processing of DNA replication intermediates in mitosis impairs genome integrity. *Sci Adv* 6:eabc8257
- Capranico G, Marinello J, Chillemi G (2017) Type I DNA topoisomerases. *J Med Chem* 60:2169–2192
- Champoux JJ (2001) DNA topoisomerases: structure, function, and mechanism. *Annu Rev Biochem* 70:369–413
- Chan KL, Palma-Pallag T, Ying S, Hickson ID (2009) Replication stress induces sister-chromatid bridging at fragile site loci in mitosis. *Nat Cell Biol* 11:753–760
- Chappidi N, Nascakova Z, Boleslavskaya B, Zellweger R, Isik E, Andrs M, Menon S, Dobrovolna J, Balbo Pogliano C, Matos J, Porro A, Lopes M, Janscak P (2020) Fork cleavage-religation cycle and active transcription mediate replication restart after fork stalling at co-transcriptional R-Loops. *Mol Cell* 77:528–541.e528
- Chowdhuri SP, Das BB (2021) Top1-PARP1 association and beyond: from DNA topology to break repair. *NAR Cancer* 3:zcab003
- Chowdhuri SP, Dhiman S, Das SK, Meena N, Das S, Kumar A (2023) Novel Pyrido[2,1':2,3]imidazo[4,5-c]quinoline derivative selectively poisons *Leishmania donovani* bisubunit topoisomerase 1 to inhibit the antimony-resistant *Leishmania* infection in vivo. *J Med Chem* 66:3411–3430
- Cortés-Gutiérrez EI, Hernández-Garza F, García-Pérez JO, Dávila-Rodríguez MI, Aguado-Barrera ME, Cerda-Flores RM (2012) Evaluation of DNA single and double strand breaks in women with cervical neoplasia based on alkaline and neutral comet assay techniques. *J Biomed Biotechnol* 2012:385245
- Das BB, Antony S, Gupta S, Dexheimer TS, Redon CE, Garfield S, Shiloh Y, Pommier Y (2009) Optimal function of the DNA repair enzyme TDP1 requires its phosphorylation by ATM and/or DNA-PK. *EMBO J* 28:3667–3680
- Das BB, Dexheimer TS, Maddali K, Pommier Y (2010) Role of tyrosyl-DNA phosphodiesterase (TDP1) in mitochondria. *Proc Natl Acad Sci USA* 107:19790–19795
- Das BB, Huang S-N, Murai J, Rehman I, Amé J-C, Sengupta S, Das SK, Majumdar P, Zhang H, Biard D, Majumder HK, Schreiber V, Pommier Y (2014) PARP1-TDP1 coupling for the repair of topoisomerase I-induced DNA damage. *Nucleic Acids Res* 42:4435–4449
- Das SK, Rehman I, Ghosh A, Sengupta S, Majumdar P, Jana B, Das BB (2016) Poly(ADP-ribose) polymers regulate DNA topoisomerase I (Top1) nuclear dynamics and camptothecin sensitivity in living cells. *Nucleic Acids Res* 44:8363–8375
- Dephoure N, Zhou C, Villén J, Beausoleil SA, Bakalarski CE, Elledge SJ, Gygi SP (2008) A quantitative atlas of mitotic phosphorylation. *Proc Natl Acad Sci USA* 105:10762–10767
- Di Marco S, Hasanova Z, Kanagaraj R, Chappidi N, Altmannova V, Menon S, Sedlackova H, Langhoff J, Surendranath K, Hühn D (2017) RECQ5 helicase cooperates with MUS81 endonuclease in processing stalled replication forks at common fragile sites during mitosis. *Mol cell* 66:658–671.e658
- Diril MK, Ratnacaram CK, Padmakumar VC, Du T, Wasser M, Coppola V, Tassarollo L, Kaldis P (2012) Cyclin-dependent kinase 1 (Cdk1) is essential for cell division and suppression of DNA re-replication but not for liver regeneration. *Proc Natl Acad Sci USA* 109:3826–3831
- Duffy S, Fam HK, Wang YK, Styles EB, Kim JH, Ang JS, Singh T, Larionov V, Shah SP, Andrews B, Boerkoel CF, Hieter P (2016) Overexpression screens identify conserved dosage chromosome instability genes in yeast and human cancer. *Proc Natl Acad Sci USA* 113:9967–9976
- El-Khamisy SF, Saifi GM, Weinfeld M, Johansson F, Helleday T, Lupski JR, Caldecott KW (2005) Defective DNA single-strand break repair in spinocerebellar ataxia with axonal neuropathy-1. *Nature* 434:108–113
- Ghosh A, Bhattacharjee S, Chowdhuri SP, Mallick A, Rehman I, Basu S, Das BB (2019) SCAN1-TDP1 trapping on mitochondrial DNA promotes mitochondrial dysfunction and mitophagy. *Sci Adv* 5:eaax9778
- Giunta S, Belotserkovskaya R, Jackson SP (2010) DNA damage signaling in response to double-strand breaks during mitosis. *J Cell Biol* 190:197–207
- Groelly FJ, Dagg RA, Petropoulos M, Rossetti GG, Prasad B, Panagopoulos A, Paulsen T, Karamichali A, Jones SE, Ochs F, Dionellis VS, Puig Lombardi E, Miossec MJ, Lockstone H, Legube G, Blackford AN, Altmeyer M, Halazonetis TD, Tarsounas M (2022) Mitotic DNA synthesis is caused by transcription-replication conflicts in BRCA2-deficient cells. *Mol Cell* 82:3382–3397.e3387
- Hackbarth JS, Galvez-Peralta M, Dai NT, Loegering DA, Peterson KL, Meng XW, Karnitz LM, Kaufmann SH (2008) Mitotic phosphorylation stimulates DNA relaxation activity of human topoisomerase I. *J Biol Chem* 283:16711–16722
- Holt LJ, Tuch BB, Villén J, Johnson AD, Gygi SP, Morgan DO (2009) Global analysis of Cdk1 substrate phosphorylation sites provides insights into evolution. *Science* 325:1682–1686
- Huang SY, Murai J, Dalla Rosa I, Dexheimer TS, Naumova A, Gmeiner WH, Pommier Y (2013) TDP1 repairs nuclear and mitochondrial DNA damage induced by chain-terminating anticancer and antiviral nucleoside analogs. *Nucleic Acids Res* 41:7793–7803
- Hudson JJ, Chiang SC, Wells OS, Rookyard C, El-Khamisy SF (2012) SUMO modification of the neuroprotective protein TDP1 facilitates chromosomal single-strand break repair. *Nat Commun* 3:733
- Interthal H, Chen HJ, Kehl-Fie TE, Zotzmann J, Leppard JB, Champoux JJ (2005) SCAN1 mutant Tdp1 accumulates the enzyme-DNA intermediate and causes camptothecin hypersensitivity. *EMBO J* 24:2224–2233
- Interthal H, Pouliot JJ, Champoux JJ (2001) The tyrosyl-DNA phosphodiesterase Tdp1 is a member of the phospholipase D superfamily. *Proc Natl Acad Sci USA* 98:12009–12014
- Katyal S, el-Khamisy SF, Russell HR, Li Y, Ju L, Caldecott KW, McKinnon PJ (2007) TDP1 facilitates chromosomal single-strand break repair in neurons and is neuroprotective in vivo. *EMBO J* 26:4720–4731
- Kawale AS, Povirk LF (2018) Tyrosyl-DNA phosphodiesterases: rescuing the genome from the risks of relaxation. *Nucleic Acids Res* 46:520–537
- Kramara J, Osia B, Malkova A (2018) Break-induced replication: the where, the why, and the how. *Trends Genet* 34:518–531
- Kuang J, Zhao J, Wright DA, Saunders GF, Rao PN (1989) Mitosis-specific monoclonal antibody MPM-2 inhibits *Xenopus* oocyte maturation and depletes maturation-promoting activity. *Proc Natl Acad Sci USA* 86:4982–4986
- Li S, Wu X (2020) Common fragile sites: protection and repair. *Cell Biosci* 10:29
- Liu C, Pouliot JJ, Nash HA (2002) Repair of topoisomerase I covalent complexes in the absence of the tyrosyl-DNA phosphodiesterase Tdp1. *Proc Natl Acad Sci USA* 99:14970–14975

- Macheret M, Bhowmick R, Sobkowiak K, Padayachy L, Mailler J, Hickson ID, Halazonetis TD (2020) High-resolution mapping of mitotic DNA synthesis regions and common fragile sites in the human genome through direct sequencing. *Cell Res* 30:997–1008
- Malkova A, Ira G (2013) Break-induced replication: functions and molecular mechanism. *Curr Opin Genet Dev* 23:271–279
- Mankouri HW, Huttner D, Hickson ID (2013) How unfinished business from S-phase affects mitosis and beyond. *EMBO J* 32:2661–2671
- Marini V, Nikulenkov F, Samadder P, Juul S, Knudsen BR, Krejci L (2023) MUS81 cleaves TOP1-derived lesions and other DNA-protein cross-links. *BMC Biol* 21:110
- Matos DA, Zhang JM, Ouyang J, Nguyen HD, Genois MM, Zou L (2020) ATR protects the genome against R loops through a MUS81-triggered feedback loop. *Mol Cell* 77:514–527.e514
- McKinnon PJ, Caldecott KW (2007) DNA strand break repair and human genetic disease. *Annu Rev Genomics Hum Genet* 8:37–55
- Minocherhomji S, Ying S, Bjerregaard VA, Bursomanno S, Aleliunaite A, Wu W, Mankouri HW, Shen H, Liu Y, Hickson ID (2015a) Replication stress activates DNA repair synthesis in mitosis. *Nature* 528:286–290
- Minocherhomji S, Ying S, Bjerregaard VA, Bursomanno S, Aleliunaite A, Wu W, Mankouri HW, Shen H, Liu Y, Hickson ID (2015b) Replication stress activates DNA repair synthesis in mitosis. *Nature* 528:286–290
- Murai J, Huang SY, Das BB, Dexheimer TS, Takeda S, Pommier Y (2012) Tyrosyl-DNA phosphodiesterase 1 (TDP1) repairs DNA damage induced by topoisomerases I and II and base alkylation in vertebrate cells. *J Biol Chem* 287:12848–12857
- Orthwein A, Fradet-Turcotte A, Noordermeer SM, Canny MD, Brun CM, Strecker J, Escibano-Diaz C, Durocher D (2014) Mitosis inhibits DNA double-strand break repair to guard against telomere fusions. *Science* 344:189–193
- Özer Ö, Hickson ID (2018) Pathways for maintenance of telomeres and common fragile sites during DNA replication stress. *Open Biol* 8:180018
- Palma A, Pugliese GM, Murfuni I, Marabitti V, Malacaria E, Rinalducci S, Minoprio A, Sanchez M, Mazzei F, Zolla L, Franchitto A, Pichierri P (2018) Phosphorylation by CK2 regulates MUS81/EME1 in mitosis and after replication stress. *Nucleic Acids Res* 46:5109–5124
- Payliss BJ, Tse YWE, Reichheld SE, Lemak A, Yun HY, Houliston S, Patel A, Arrowsmith CH, Sharpe S, Wyatt HDM (2022) Phosphorylation of the DNA repair scaffold SLX4 drives folding of the SAP domain and activation of the MUS81-EME1 endonuclease. *Cell Rep* 41:111537
- Pladevall-Morera D, Munk S, Ingham A, Garribba L, Albers E, Liu Y, Olsen JV, Lopez-Contreras AJ (2019) Proteomic characterization of chromosomal common fragile site (CFS)-associated proteins uncovers ATRX as a regulator of CFS stability. *Nucleic Acids Res* 47:8004–8018
- Pommier Y (2006) Topoisomerase I inhibitors: camptothecins and beyond. *Nat Rev Cancer* 6:789–802
- Pommier Y, Huang SY, Gao R, Das BB, Murai J, Marchand C (2014) Tyrosyl-DNA-phosphodiesterases (TDP1 and TDP2). *DNA Repair* 19:114–129
- Pommier Y, Sun Y, Huang SN, Nitiss JL (2016) Roles of eukaryotic topoisomerases in transcription, replication and genomic stability. *Nat Rev Mol Cell Biol* 17:703–721
- Pouliot JJ, Robertson CA, Nash HA (2001) Pathways for repair of topoisomerase I covalent complexes in *Saccharomyces cerevisiae*. *Genes Cells* 6:677–687
- Regairaz M, Zhang YW, Fu H, Agama KK, Tata N, Agrawal S, Aladjem MI, Pommier Y (2011) Mus81-mediated DNA cleavage resolves replication forks stalled by topoisomerase I-DNA complexes. *J Cell Biol* 195:739–749
- Rehman I, Basu SM, Das SK, Bhattacharjee S, Ghosh A, Pommier Y, Das BB (2018) PRMT5-mediated arginine methylation of TDP1 for the repair of topoisomerase I covalent complexes. *Nucleic Acids Res* 46:5601–5617
- Richards F, Llorca-Cardenosa MJ, Langton J, Buch-Larsen SC, Shamkhi NF, Sharma AB, Nielsen ML, Lakin ND (2023) Regulation of Rad52-dependent replication fork recovery through serine ADP-ribosylation of PolD3. *Nat Commun* 14:4310
- Sbrana I, Zavattari P, Barale R, Musio A (1998) Common fragile sites on human chromosomes represent transcriptionally active regions: evidence from camptothecin. *Hum Genet* 102:409–414
- Shiloh Y (2003) ATM and related protein kinases: safeguarding genome integrity. *Nat Rev Cancer* 3:155–168
- Szmyd R, Niska-Blakie J, Diril MK, Renck Nunes P, Tzelepis K, Lacroix A, van Hul N, Deng L-W, Matos J, Dreesen O, Bisteau X, Kaldis P (2019) Premature activation of Cdk1 leads to mitotic events in S phase and embryonic lethality. *Oncogene* 38:998–1018
- Takashima H, Boerkoel CF, John J, Saifi GM, Salih MA, Armstrong D, Mao Y, Quiocho FA, Roa BB, Nakagawa M, Stockton DW, Lupski JR (2002) Mutation of TDP1, encoding a topoisomerase I-dependent DNA damage repair enzyme, in spinocerebellar ataxia with axonal neuropathy. *Nat Genet* 32:267–272
- Terasawa M, Shinohara A, Shinohara M (2014) Canonical non-homologous end joining in mitosis induces genome instability and is suppressed by M-phase-specific phosphorylation of XRCC4. *PLoS Genet* 10:e1004563
- Tse AN, Schwartz GK (2004) Potentiation of cytotoxicity of topoisomerase I poison by concurrent and sequential treatment with the checkpoint inhibitor UCN-01 involves disparate mechanisms resulting in either p53-independent clonogenic suppression or p53-dependent mitotic catastrophe. *Cancer Res* 64:6635–6644
- Tuduri S, Crabbé L, Conti C, Tourrière H, Holtgreve-Grez H, Jauch A, Pantesco V, De Vos J, Thomas A, Theillet C, Pommier Y, Tazi J, Coquelle A, Pasero P (2009) Topoisomerase I suppresses genomic instability by preventing interference between replication and transcription. *Nat Cell Biol* 11:1315–1324
- Vance JR, Wilson TE (2002) Yeast Tdp1 and Rad1-Rad10 function as redundant pathways for repairing Top1 replicative damage. *Proc Natl Acad Sci USA* 99:13669–13674
- Wiegand A, Kuzin V, Cameron DP, Grosser J, Ceribelli M, Mehmood R, Ballarino R, Valant F, Grochowski R, Karabogdan I, Crosetto N, Lindqvist A, Bizard AH, Kouzine F, Natsume T, Baranello L (2021) Topoisomerase 1 activity during mitotic transcription favors the transition from mitosis to G1. *Mol Cell* 81:5007–5024.e5009
- Wu X, Wang B (2021) Abraxas suppresses DNA end resection and limits break-induced replication by controlling SLX4/MUS81 chromatin loading in response to TOP1 inhibitor-induced DNA damage. *Nat Commun* 12:4373
- Yu B, Dalton WB, Yang VW (2012) CDK1 regulates mediator of DNA damage checkpoint 1 during mitotic DNA damage. *Cancer Res* 72:5448–5453
- Zhang H, Xiong Y, Su D, Wang C, Srivastava M, Tang M, Feng X, Huang M, Chen Z, Chen J (2022) TDP1-independent pathways in the process and repair of TOP1-induced DNA damage. *Nat Commun* 13:4240

## Acknowledgements

BBD team is supported by SERB core research grant (CRG/2022/001322), BRNS grant (54/14/10/2022-BRNS/11014) and ICMR grant (2021-11299/CMB/ADHOC-BMS) and IACS intramural funds. SPC is the recipient of the IACS senior research fellowship, India.

## Author contributions

**Srijita Paul Chowdhuri:** Resources; Data curation; Formal analysis; Validation; Investigation; Visualization; Methodology; Writing—original draft; Project administration. **Benu Brata Das:** Conceptualization; Resources; Formal analysis; Supervision; Funding acquisition; Writing—original draft; Project administration; Writing—review and editing.

Source data underlying figure panels in this paper may have individual authorship assigned. Where available, figure panel/source data authorship is listed in the following database record: [biostudies:S-SCDT-10\\_1038-S44318-024-00169-3](https://www.ebi.ac.uk/biostudies/studies/S-SCDT-10_1038-S44318-024-00169-3).

### Disclosure and competing interests statement

The authors declare no competing interests.

**Open Access** This article is licensed under a Creative Commons Attribution 4.0 International License, which permits use, sharing, adaptation, distribution and reproduction in any medium or format, as long as you give appropriate credit to the original author(s) and the source, provide a link to the Creative Commons licence, and indicate if changes were made. The images or other third party material in this article are included in the article's Creative Commons licence,

unless indicated otherwise in a credit line to the material. If material is not included in the article's Creative Commons licence and your intended use is not permitted by statutory regulation or exceeds the permitted use, you will need to obtain permission directly from the copyright holder. To view a copy of this licence, visit <http://creativecommons.org/licenses/by/4.0/>. Creative Commons Public Domain Dedication waiver <http://creativecommons.org/public-domain/zero/1.0/> applies to the data associated with this article, unless otherwise stated in a credit line to the data, but does not extend to the graphical or creative elements of illustrations, charts, or figures. This waiver removes legal barriers to the re-use and mining of research data. According to standard scholarly practice, it is recommended to provide appropriate citation and attribution whenever technically possible.

© The Author(s) 2024

## MOLECULAR BIOLOGY

## SCAN1-TDP1 trapping on mitochondrial DNA promotes mitochondrial dysfunction and mitophagy

Arijit Ghosh<sup>1</sup>, Sangheeta Bhattacharjee<sup>1</sup>, Srijita Paul Chowdhuri<sup>1</sup>, Abhik Mallick<sup>2</sup>, Ishita Rehman<sup>1</sup>, Sudipta Basu<sup>3</sup>, Benu Brata Das<sup>1\*</sup>

A homozygous mutation of human tyrosyl-DNA phosphodiesterase 1 (TDP1) causes the neurodegenerative syndrome, spinocerebellar ataxia with axonal neuropathy (SCAN1). TDP1 hydrolyzes the phosphodiester bond between DNA 3'-end and a tyrosyl moiety within trapped topoisomerase I (Top1)-DNA covalent complexes (Top1cc). TDP1 is critical for mitochondrial DNA (mtDNA) repair; however, the role of mitochondria remains largely unknown for the etiology of SCAN1. We demonstrate that mitochondria in cells expressing SCAN1-TDP1 (TDP1<sup>H493R</sup>) are selectively trapped on mtDNA in the regulatory non-coding region and promoter sequences. Trapped TDP1<sup>H493R</sup>-mtDNA complexes were markedly increased in the presence of the Top1 poison (mito-SN38) when targeted selectively into mitochondria in nanoparticles. TDP1<sup>H493R</sup>-trapping accumulates mtDNA damage and triggers Drp1-mediated mitochondrial fission, which blocks mitobiogenesis. TDP1<sup>H493R</sup> prompts PTEN-induced kinase 1-dependent mitophagy to eliminate dysfunctional mitochondria. SCAN1-TDP1 in mitochondria creates a pathological state that allows neurons to turn on mitophagy to rescue fit mitochondria as a mechanism of survival.

## INTRODUCTION

Spinocerebellar ataxia with axonal neuropathy (SCAN1) is an autosomal recessive neurodegenerative disorder that is linked with a homozygous point mutation (H493R) in human tyrosyl-DNA phosphodiesterase 1 (TDP1) (1). TDP1 is primarily involved in the repair of DNA strand breaks linked with abortive topoisomerase I (Top1) activity (2–8). Cells derived from patients with SCAN1 are hypersensitive to camptothecin that selectively traps Top1-DNA covalent complexes (Top1cc) (5, 9–12). Patients with SCAN1 develop progressive cerebellar ataxia and peripheral neuropathy, which becomes noticeable at late childhood (13 to 15 years), indicating a slow onset of neurodegeneration (1). However, three independently developed TDP1 knockout mouse models revealed no obvious behavioral phenotypes related to patients with SCAN1 (8, 13, 14). Nevertheless, in one of these mouse models, loss of TDP1 resulted in gradual age-related cerebellar atrophy (8). This suggests that the SCAN1 phenotype is a complex phenomenon and has a multifactorial mechanism that has not been elucidated.

TDP1 hydrolyzes the phosphodiester bond between the Top1-tyrosyl moiety and the DNA 3'-end that involves a two-step mechanism: The first nucleophilic attack is initiated by catalytic H263 on the phosphate bond linking the DNA and the tyrosyl-containing peptide. The C-terminal domain of TDP1 harboring H493 residue acts as a general acid and donates a proton to the apical tyrosine-containing peptide-leaving group. This results in the generation of a TDP1-DNA covalent intermediate (step 1). The H493 acts as a general base catalyst and activates a water molecule that subsequently hydrolyzes the phosphoenzyme intermediate (step 2) (3, 4). The SCAN1 point mutation (H493R) retains partial TDP1

activity and results in defective turnover owing to the formation of TDP1<sup>H493R</sup>-DNA complexes (8, 10, 14); therefore, SCAN1 cells do not provide a true knockout model of TDP1 (14). The nuclear encoded TDP1 is transported to the mitochondria for mitochondrial DNA (mtDNA) repair (15–18), and the ability of TDP1 to resolve 3'-phosphotyrosyl linkages is not limited to the removal of nuclear Top1-DNA adducts (3–5) but is also required for the excision of mitochondrial Top1 (Top1mt)-DNA covalent complexes (Top1mtcc) that are exclusively formed in the mitochondria (18). TDP1 can also hydrolyze a broad spectrum of 3'-DNA blocking lesions that are formed during oxidative DNA damage (4, 9, 15, 19–22), including 3'-phosphoglycolate and 3'-deoxyribose phosphate ends (19, 21). Accordingly, TDP1-deficient cells are defective in repairing mtDNA damage associated with trapped Top1mtcc or 3'-DNA lesions related to oxidative damage and chain-terminating anticancer or antiviral nucleosides (15, 18, 23, 24). Post-translational modifications by phosphorylation, (ADP)-ribosylation, SUMOylation, arginine methylation, and ubiquitylation are common regulators for the recruitment, turnover, and modulation of enzymatic activity and stability of TDP1 (12, 25–29).

Vertebrate mtDNA constitutes approximately 5% of the total cellular DNA content where several thousand copies of mtDNA are distributed across hundreds of mitochondria as covalently closed circular DNA (16.5 kb) encoding critical components of the mitochondrial adenosine 5'-triphosphate (ATP) production machinery (30, 31). Mitochondrial network dynamics uses the process of fission or fusion as a complex physiological adaptation to coordinate the segregation or unification of two physically distinct mitochondria, which is essential for regulating mitochondrial morphology, biogenesis, and stress response mechanisms (32, 33). In the context of mtDNA copy number maintenance, the mitochondrial network undergoes fusion to complement the mtDNA lesion by transfer of nucleoids (34). In contrast, mitochondrial fission predominates under conditions of nonrepaired mtDNA lesions, which results in mitochondrial dysfunction (35, 36). To preserve mitochondrial homeostasis, increased mitochondrial fission ensues the degradation of dysfunctional

<sup>1</sup>Laboratory of Molecular Biology, School of Biological Sciences, Indian Association for the Cultivation of Science, 2A & B, Raja S. C. Mullick Road, Jadavpur, Kolkata 700032, India. <sup>2</sup>Department of Chemistry, Indian Institute of Science Education and Research (IISER) Pune, Dr. Homi Bhabha Road, Pashan, Pune, Maharashtra 411008, India. <sup>3</sup>Discipline of Chemistry, Indian Institute of Technology (IIT) Gandhinagar, Palaj, Gandhinagar, Gujarat 382355, India.

\*Corresponding author. Email: pcbbd@iacs.res.in



mitochondria by autophagy (lysosome-dependent degradation), specifically termed as mitophagy (32, 36–39).

Unlike chromosomal DNA, mtDNA is more vulnerable to oxidative DNA damage, as they are profoundly exposed to reactive oxygen species (ROS) generated from the electron transport chain (40–42). Moreover, the mitochondria are completely dependent on the nucleus for mtDNA repair and integrity (42). Marked elevation of mtDNA damage has been attributed to the progression of several neurodegenerative disorders, including Alzheimer's disease, Parkinson's disease, Huntington's disease, myopathies and diabetes, aging, and age-related disorders (30, 43). Thus, efficient repair of mtDNA in postmitotic cells like neurons is critical for normal brain functioning. However, the role of mitochondria in the pathoetiology of the SCAN1 phenotype has not been elucidated.

This study provides the first evidence for connecting mitochondrial dysfunction with etiology of SCAN1. We show that cells expressing SCAN1-TDP1 are trapped on the mtDNA, which is escalated in the presence of mitochondria-targeted Top1 poison (mito-SN38). We show that trapping TDP1<sup>H493R</sup> on mtDNA increases the mitochondrial fission rate and abrogates mitobiogenesis. Last, we show that increased mitochondrial degradation may allow identification of dysfunctional daughter mitochondria expressing TDP1<sup>H493R</sup> and their subsequent removal through mitophagy, which may serve as a mechanism to restore fit mitochondria for cell survival.

## RESULTS

### Mitochondria harboring SCAN1 mutant TDP1 (H493R) are hypersensitive to mitochondria-targeted Top1 poison

To investigate the role of SCAN1 mutant TDP1 in mitochondria, we stably complemented TDP1 knockout (TDP1<sup>-/-</sup>) mouse embryonic fibroblasts (MEFs) with lentiviral constructs harboring FLAG-tagged human SCAN1 mutant TDP1<sup>H493R</sup>. The presence of the exogenous FLAG-TDP1 variants in the mitochondria of TDP1<sup>-/-</sup> MEFs (TDP1<sup>-/-/WT</sup> or TDP1<sup>-/-/H493R</sup>) was confirmed by cell fractionation and Western blotting, and the relative purity of the mitochondrial fraction was further assessed by analysis of mitochondrial cytochrome c oxidase (COX IV) protein (Fig. 1A), which is consistent with previous reports showing the import of exogenous TDP1 into the mitochondria (15–18).

The active metabolite of irinotecan (SN38) stabilizes Top1-cleavage complexes (Top1cc). Irinotecan is a widely used anticancer drug (44). We engineered mitochondrial targeting cationic nanoparticles containing irinotecan (mito-SN38) (45) to selectively trap Top1mt on the mtDNA (Top1mtcc). To test the intracellular delivery of mito-SN38 into the mitochondria, we performed live-cell confocal microscopy in cells treated with mito-SN38 (intrinsically green fluorescent) by costaining with the mitochondrion-specific dye MitoTracker red. Colocalization of mito-SN38 with MitoTracker red (Fig. 1B; see merged image) within 30 min of drug exposure confirmed the accumulation of the mito-SN38 nanoparticle exclusively inside the mitochondria. The correlation between the pixel intensities along a line in the two channels (Fig. 1B) substantiated the colocalization. We further validated the activity of mito-SN38 in the mitochondria by directly measuring *in vivo* trapping of Top1mtcc in isolated mitochondria using ICE (immunocomplex of enzyme) assays (Fig. 1, C and D) (46, 47). Under similar conditions, mito-SN38 failed to trap nuclear Top1 (fig. S1A).

Mitochondrial ICE assays detected covalently trapped Top1mt linked to mtDNA (Top1mtcc) without mito-SN38 in TDP1<sup>-/-</sup> MEFs ( $P < 0.01$ ; Fig. 1C), which was markedly increased (~7-fold) after mito-SN38 treatment. TDP1-proficient MEFs (TDP1<sup>+/+</sup> or TDP1<sup>-/-/WT</sup>) show reduced (~3-fold) Top1mtcc compared to TDP1-deficient cells, consistent with the role of TDP1 in excision of trapped Top1mtcc (Fig. 1D) in the mitochondria. Although TDP1<sup>-/-/H493R</sup> MEFs partially rescued (~1.5-fold) mito-SN38-induced Top1mtcc compared to TDP1<sup>-/-</sup> ( $P < 0.01$ ; Fig. 1D), SCAN1-TDP1 was significantly defective in unhooking trapped Top1mtcc in the mitochondria compared to TDP1<sup>-/-/WT</sup> or TDP1<sup>+/+</sup> cells (Fig. 1D).

We further performed survival assays to test the impact of mito-SN38 (Fig. 1E). We noted a substantial increase in mito-SN38-induced cell death in TDP1<sup>-/-/H493R</sup> MEFs compared to TDP1<sup>-/-</sup> MEFs (Fig. 1E); however, this effect was not due to increased accumulation of Top1mtcc (Fig. 1D). Under similar conditions, TDP1<sup>-/-</sup> MEFs complemented with wild-type human TDP1 (TDP1<sup>-/-/WT</sup>) or TDP1<sup>+/+</sup> MEFs rescued the mito-SN38-mediated hypersensitivity (Fig. 1D). Consistent with TDP1<sup>-/-/H493R</sup> cells, the SCAN1 patient-derived lymphoblastoid cell lines (BAB1662), harboring TDP1 (H493R) mutation, were also hypersensitive to mito-SN38 compared to its wild-type counterpart (BAB1668) (Fig. 1F). Together, these results suggest that defective TDP1 activity is detrimental to the mitochondria challenged with a Top1 poison.

### TDP1<sup>H493R</sup> trapping accumulates mtDNA damage

Because SCAN1 patient-derived lymphoblastoid cells and TDP1<sup>-/-/H493R</sup> MEFs are hypersensitive to mito-SN38 (Fig. 1, E and F), we tested whether the additional mito-SN38-mediated toxicity was due to trapping of TDP1<sup>H493R</sup> in the isolated mitochondria using ICE assays. In the absence of mito-SN38, we detected a significant increase (~1.5- to 2-fold) in TDP1<sup>H493R</sup>-mtDNA complexes ( $P < 0.1$ ; Fig. 2A), which increased (~4- to 5-fold) after mito-SN38 treatment in TDP1<sup>-/-/H493R</sup> MEFs compared to TDP1<sup>-/-</sup> MEFs ( $P < 0.001$ ; Fig. 2A). Similarly, we also detected mito-SN38-induced (~4- to 5-fold) increase in trapping of TDP1<sup>H493R</sup> ( $P < 0.001$ ; Fig. 2A, right) in human SCAN1 cells (BAB1662), confirming that defective SCAN1-TDP1 activity generates TDP1<sup>H493R</sup>-mtDNA lesions.

To gain further insight into the sites on mtDNA where TDP1<sup>H493R</sup> becomes trapped, we performed chromatin immunoprecipitation (ChIP) followed by mtDNA-specific quantitative polymerase chain reaction (qPCR) analysis (18, 48). TDP1 is primarily involved in hydrolysis of trapped Top1cc complexes (Fig. 2B); therefore, we tested the enrichment of TDP1<sup>H493R</sup> in specific mtDNA segments associated with Top1mtcc binding sites (46). Figure 2B shows that specific trapping of TDP1<sup>H493R</sup> corresponds to the nucleotide residues 15420, 15690, and 16060 as well as the heavy and light strand promoter (HSP/LSP) along the regulatory noncoding region of mtDNA (mtNCR). Under similar conditions, mito-SN38-induced TDP1<sup>H493R</sup> enrichment within the coding sequences of the mtDNA was not detected (fig. S1B). Therefore, mito-SN38 recruits TDP1 at sites corresponding to Top1mtcc binding sites on mtDNA (46, 48), generating secondary TDP1-mtDNA cross-links in SCAN1 cells ( $P < 0.001$ ; Fig. 2B).

We next tested whether TDP1<sup>H493R</sup> trapping instigates mtDNA damage using long-range PCR, a well-established method to evaluate mtDNA damage (15). Top1ccs reverse within minutes after washing out the drug (44); we therefore analyzed the subsequent mtDNA repair by incubating the cells in drug-free medium for an additional 12 hours. Figure 2D shows that mitochondria harboring

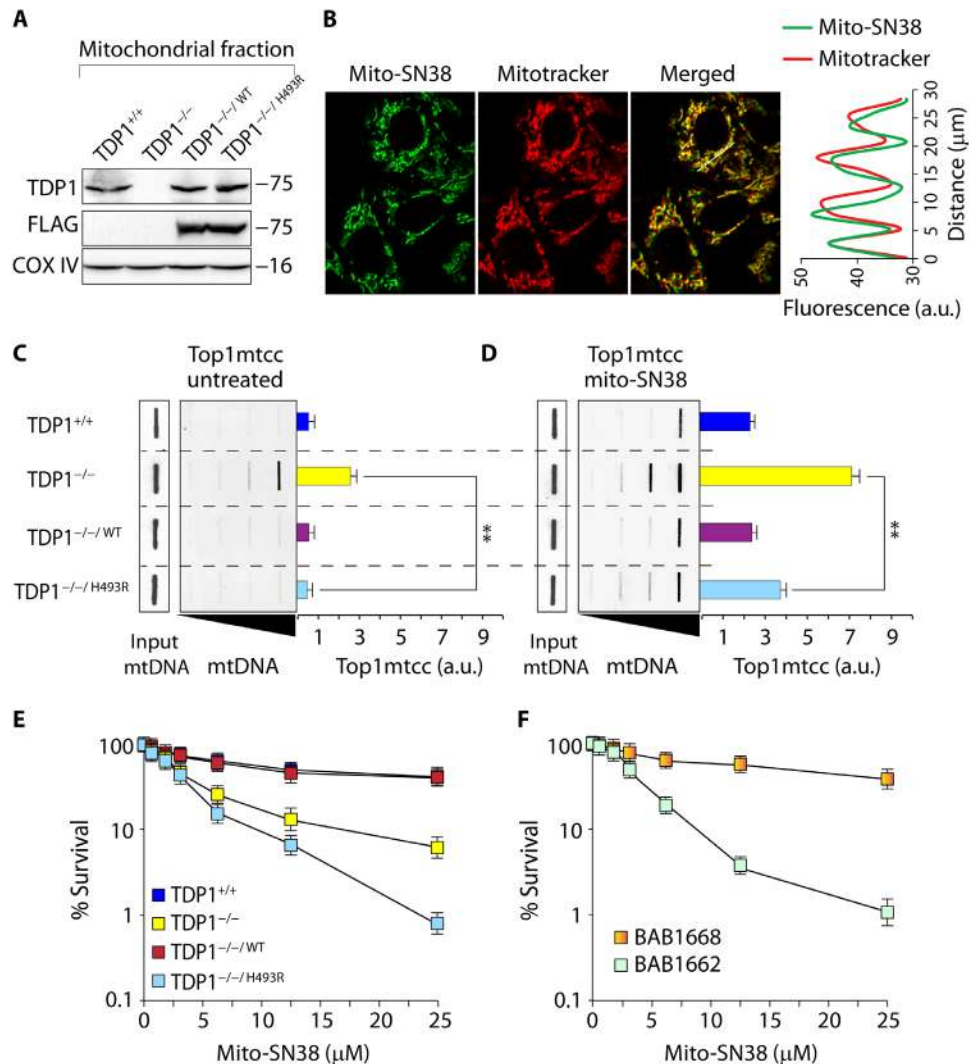


**Fig. 1. Mito-SN38 containing nanoparticle poisons Top1mt (Top1mtcc).** (A) Western blot analysis of mitochondrial lysates extracted from the indicated MEFs. TDP1<sup>-/-</sup>WT and TDP1<sup>-/-</sup>H493R; TDP1<sup>-/-</sup> complemented with exogenous FLAG-tagged human wild-type or SCAN1 mutant (H493R) TDP1, respectively. Blots were probed with anti-TDP1, anti-FLAG, and anti-COX IV antibodies. COX IV served as a positive mitochondrial marker. (B) Representative confocal images showing accumulation of mitochondria-targeted cationic nanoparticle containing Top1 poison irinotecan (mito-SN38; intrinsic green fluorescence) inside the mitochondria (labeled with Mitotracker red). MEFs were incubated with mito-SN38 (5 μM for 20 min), and the fluorescence patterns were recorded under live-cell microscopy. Colocalization is shown in the merged image. Quantitation of the pixel intensity of fluorescence along the indicated white line in the merged image (right). The white line was drawn arbitrarily along the region of interest (ROI). a.u., arbitrary units. (C and D) Poisoning of Top1mt (Top1mtcc) in the indicated MEFs expressing TDP1 variants; either untreated (C) or treated with mito-SN38 (5 μM for 3 hours) (D). Top1mtcc was detected by ICE (immunocomplex of enzyme) bioassay. MtDNA at increasing concentrations (0.5, 1, 2, and 4 μg) was immunoblotted with an anti-Top1mt-specific antibody. The mtDNA input was probed with anti-dsDNA (double-stranded DNA) antibody. Densitometry analysis of trapped Top1mtcc band intensity was quantified and expressed as fold increase relative to mtDNA input (error bars represent means ± SEM). Asterisks denote statistically significant differences (\*\**P* < 0.01, *t* test). (E and F) Cell survival curves of indicated MEF variants (E) and a SCAN1 patient-derived lymphoblastoid cell line (BAB1662) and its wild-type counterpart (BAB1668) (F). Mito-SN38-induced cytotoxicity (%) was calculated with respect to the untreated control. Each point corresponds to the mean ± SD of at least three experiments. Error bars represent SDs (*n* = 3).

defective TDP1 (H493R) display rapid depletion of mtDNA (~2-fold) and were significantly deficient in recovery of mtDNA even after 12 hours of repair in drug-free medium (~4-fold) compared to TDP1-deficient (TDP1<sup>-/-</sup>) or TDP1-proficient MEFs (TDP1<sup>-/-</sup>WT or TDP1<sup>+/+</sup>) (*P* < 0.001; Fig. 2, D and E). Similarly, SCAN1 patient-derived lymphoblastoid cells show a marked depletion (~3- to 4-fold) and impaired recovery of mtDNA (~6- to 7-fold) even after 12 hours of culture in drug-free medium (*P* < 0.001; Fig. 2, D and E), suggesting that mito-SN38-induced hypersensitivity in

TDP1<sup>-/-</sup>H493R cells is primarily attributed to toxic mtDNA lesions linked to TDP1<sup>H493R</sup>.

### Mitochondrial network harboring TDP1<sup>H493R</sup> undergoes fission upon mito-SN38 treatment

Mitochondrial dynamics is critical in regulating morphology and function (32). Therefore, to investigate the role of TDP1<sup>H493R</sup> on the dynamics of the mitochondrial network, i.e., the fission and fusion rates, we used a fluorescence recovery after photobleaching (FRAP)

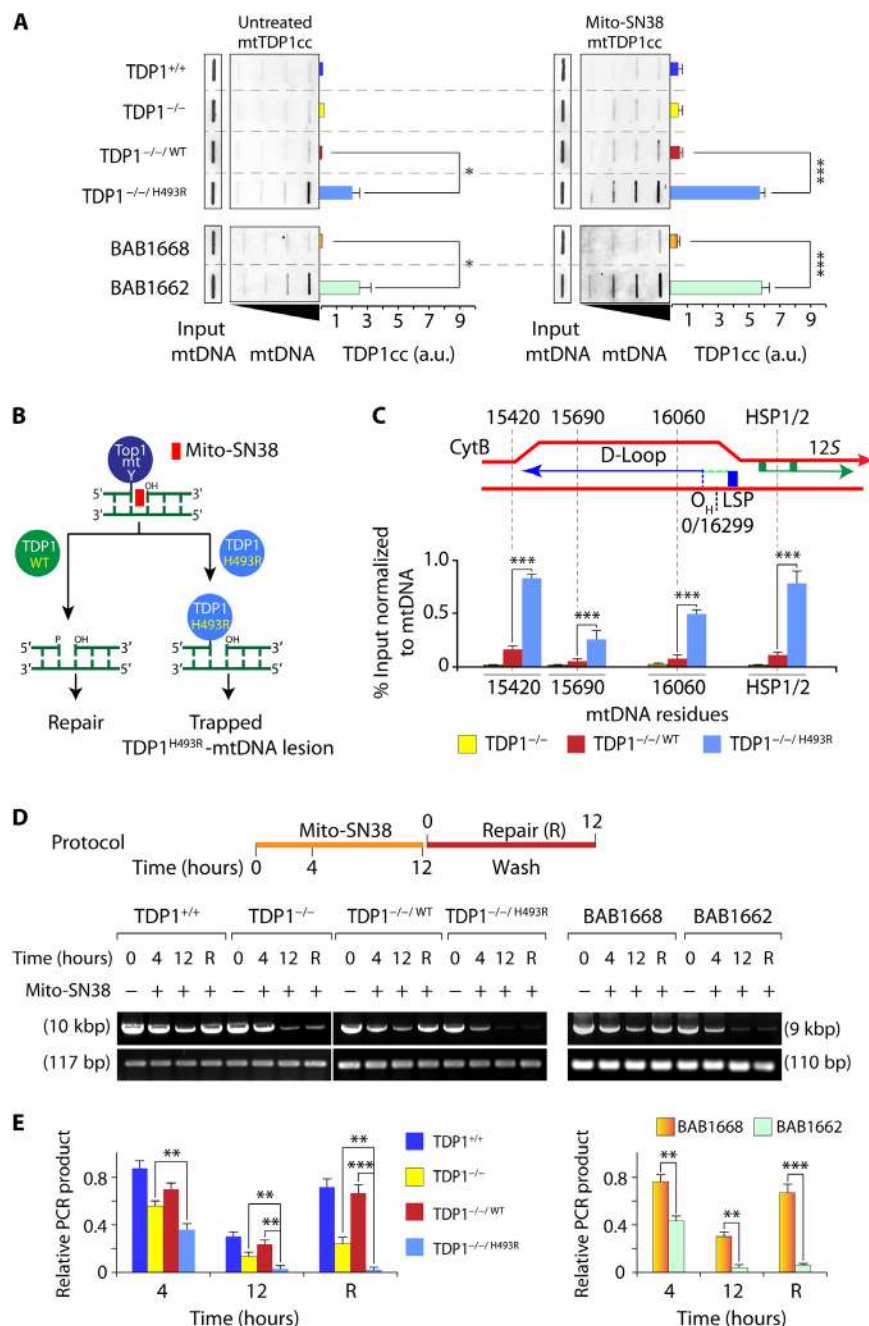


**Fig. 2. Induction of irreversible mtDNA damage through selective trapping of TDP1<sup>H493R</sup>.** (A) Detection of trapped TDP1-mtDNA complexes (mtTDP1cc) by ICE bioassays in the indicated cells following no treatment or treated with mito-SN38 (5  $\mu$ M for 3 hours). MtDNA at increasing concentrations (0.5, 1, 2, and 4  $\mu$ g) was immunoblotted with an anti-TDP1-specific antibody. The mtDNA input was probed with anti-dsDNA antibody. Densitometry analysis of the trapped mtTDP1cc band intensity was quantified and expressed as fold increase relative to mtDNA input (error bars represent means  $\pm$  SEM). Asterisks denote statistically significant difference ( $*P < 0.1$  and  $***P < 0.001$ , *t* test). (B) Catalytically defective SCAN1-TDP1 was hypothesized to be trapped at the Top1mtcc binding sites; this is shown schematically. (C) Detection of TDP1<sup>H493R</sup> trapping sites on mtDNA by chromatin immunoprecipitation (ChIP) followed by mtDNA-specific quantitative polymerase chain reaction (qPCR) analysis. FLAG-TDP1-DNA adducts were immunoprecipitated with anti-FLAG antibody in the indicated cells after treatment with mito-SN38 treatment (5  $\mu$ M for 3 hours), and the putative TDP1-binding site was quantified by qPCR. The mtDNA copy numbers of each cell line were concomitantly measured using primers for the ND2 (mitochondrial) and B2M (nuclear) genes. Enrichment of TDP1-bound mtDNA is expressed as percent input, which is then normalized to the mtDNA copy number of the cell line. Data represent means  $\pm$  SE of independent experiments. Asterisks denote statistically significant differences ( $***P < 0.001$ , *t* test). (D and E) Cells were treated with mito-SN38 for the indicated times. After mito-SN38 removal (R), cells were cultured in drug-free medium for 12 hours (top). Long-range qPCR was used to evaluate mtDNA damage. (D) Induction of mito-SN38-induced mtDNA damage in indicated cell types. Representative images are shown for mtDNA long- and short-fragment PCR after treatment (mito-SN38, 20  $\mu$ M) and drug removal (R) for the indicated time. Mouse and human mtDNA-specific primers were used. (E) Quantification of mtDNA damage using the ratio of the long-fragment versus short-fragment PCR products. Data represent means  $\pm$  SE of independent experiments. Asterisks denote statistically significant difference ( $**P < 0.01$  and  $***P < 0.001$ , *t* test). kbp, kilobase pair; bp, base pair.



technique to analyze the rate of redistribution of mitochondrial matrix-localized mito-YFP (yellow fluorescent protein), ectopically expressed in MEFs expressing TDP1 variants (49). In the absence of mito-SN38, mitochondrial FRAP recovery of TDP1-proficient (TDP1<sup>+/+</sup> and TDP1<sup>-/-WT</sup>) and TDP1<sup>-/-</sup> MEFs was fast (65 to 75% in 60 s), indicating that, under steady-state conditions, there is a rapid and large-scale diffusion of mito-YFP due to the existence of a closely associated mitochondrial network (see Fig. 3A and the quantification in Fig. 3B). However, the mitochondrial fluorescence recovery of TDP1<sup>-/-H493R</sup> MEFs was slower after 30 s of bleaching and only reached a maximum intensity of 55 to 60% in 60 s (Fig. 3B), suggesting a delay in mitochondrial fusion rate. Mito-SN38 pretreatment significantly blocked the mitochondrial FRAP recovery (~10 to 15% in 60 s) in TDP1<sup>-/-H493R</sup> MEFs (Fig. 3, C and D) compared to TDP1<sup>-/-</sup> MEFs. Under similar conditions, catalytically active TDP1 (TDP1<sup>+/+</sup> or TDP1<sup>-/-WT</sup>) rescued (~20 to 25%) the FRAP recovery (Fig. 3, C and D), suggesting the existence of a dispersed mitochondrial network due to increased mitochondrial fission in SCAN1-TDP1-expressing MEFs.

Further evidence for mitochondrial fragmentation in SCAN1-TDP1-harboring cells was seen by live-cell microscopy with the mitochondria-specific dye MitoTracker red. The average length of a mitochondrion was substantially shorter in TDP1<sup>-/-H493R</sup> MEFs (~2.7  $\mu$ m), as compared with TDP1<sup>-/-WT</sup> MEFs (~4.3  $\mu$ m) and TDP1<sup>-/-</sup> MEFs (~3.4  $\mu$ m; Fig. 3, E and F; untreated). Mito-SN38 treatment markedly induced mitochondrial fragmentation in TDP1<sup>-/-H493R</sup> MEFs (~1.2  $\mu$ m) compared to TDP1<sup>-/-</sup> (1.7  $\mu$ m) or TDP1<sup>-/-WT</sup> (2.8  $\mu$ m) MEFs (Fig. 3, E and F; treated) consistent with increased fission rates (Fig. 3, C and D).

To further validate the mitochondrial fragmentation in TDP1<sup>-/-H493R</sup> MEFs, we directly measured the expression of the key proteins associated with mitochondrial fission and fusion like Drp1 (dynamin-related protein 1; mitochondrial fission protein) and Mfn1 (mitofusin 1; mitochondrial fusion protein) (32) in cells expressing TDP1 variants in the presence or absence of mito-SN38 (Fig. 3G). We detected a ~2-fold reduction in Mfn1 expression in TDP1<sup>-/-H493R</sup> MEFs compared to TDP1<sup>-/-WT</sup> MEFs after mito-SN38 treatment (Fig. 3E). In contrast, under similar conditions, the expression of Drp1 was enhanced ~2.5-fold in TDP1<sup>-/-H493R</sup> MEFs compared to TDP1<sup>-/-WT</sup> MEFs, confirming mitochondrial fragmentation (Fig. 3H), which is in agreement with an increased fission rate (Fig. 3, C and D). Similarly, we also detected a mito-SN38-induced increase (~2.5-fold) in Drp1 levels in human SCAN1 cells (BAB1662) compared to their wild-type counterpart (BAB1668) (Fig. 3F), confirming that TDP1<sup>H493R</sup> trapping directs mitochondrial dynamics toward mitochondrial fission.

### TDP1<sup>H493R</sup>-mtDNA lesions impair mitochondrial biogenesis and OXPHOS function

We next tested the impact of TDP1<sup>H493R</sup> trapping on the integrity of the mitochondrial membrane potential ( $\Delta\psi$ m) in cells expressing TDP1 variants by tetramethylrhodamine methyl ester (TMRM) staining and flow cytometry analysis. Figure 4A shows that mito-SN38 treatment caused pronounced depolarization of  $\Delta\psi$ m in TDP1<sup>-/-H493R</sup> MEFs, which were rescued by complementation of wild-type human TDP1 (Fig. 4A). SCAN1 cells treated with mito-SN38 showed a marked reduction (~15-fold) in the mRNA expression of OXPHOS subunits encoded by mtDNA such as ND2, ND5, ND6, CytB, Cox1, Cox2, and ATP8 along the mitochondrial polycistronic heavy- and light-chain transcript (fig. S1C). We also detected a ~3- to 4-fold

depletion of mitochondrial respiratory complex V subunit (nuclear encoded) (fig. S1D) and (~4-fold) reduction in ATP content in SCAN1 cells (fig. S1E). Collectively these data indicate that irreversible mtDNA damage in TDP1<sup>-/-H493R</sup> (Fig. 2D) impaired the assembly of mitochondrial respiratory chain complexes and maintenance of membrane potential (Fig. 4A).

Furthermore, we quantitatively measured mitochondrial mass by staining cells with MitoTracker green using flow cytometry (50). Figure 4B indicates a subtle reduction in the overall mitochondrial volume in TDP1<sup>-/-H493R</sup> MEFs without treatment, while mito-SN38 treatment caused steady reduction in mitochondrial volume in TDP1<sup>-/-H493R</sup> MEFs, which is in keeping with a marked increase of mitochondrial fission rate as obtained from FRAP experiment (Fig. 4B).

Mitobiogenesis is a coordinated process licensing increased production of nuclear and mitochondria-encoded proteins to increase mitochondrial function or to compensate for removal of the damaged mitochondria (32, 51). This prompted us to test the expression of nuclear genes in SCAN1 cells that are solely responsible for maintaining the mitochondrial homeostasis. We detected ~1.5-fold reduction in the mRNA and the protein levels of PGC1 $\alpha$  (peroxisome proliferator-activated receptor gamma coactivator 1- $\alpha$ ), NRF1 (nuclear respiratory factor 1), and TFAM (mitochondrial transcription factor A) after mito-SN38 treatment for 6 hours ( $P < 0.01$ ; Fig. 4, C and D). Prolonged treatment (mito-SN38, 12 hours) resulted in a ~5-fold reduction in protein levels for TFAM, NRF1, and PGC1 $\alpha$  in SCAN1 cells (Fig. 4D).

To investigate the mechanistic link between mitochondrial dysfunction and nuclear gene function essential for the mitochondrial biogenesis and OXPHOS, we tested ROS formation and accumulation of DNA damage in the nucleus by  $\gamma$ H2AX staining (52). TDP1<sup>-/-H493R</sup> MEFs treated with mito-SN38 for 12 hours accumulate (~2.5-fold) increased ROS formation ( $P < 0.01$ ; Fig. 4E and quantitation in Fig. 4F) and ~3-fold increase in nuclear  $\gamma$ H2AX compared to 6-hour treatment ( $P < 0.001$ ; Fig. 4G and quantitation of  $\gamma$ H2AX foci in Fig. 4H). We further confirmed that pretreatment with ROS inhibitor *N*-acetyl-L-cysteine significantly blocked ROS formation ( $P < 0.01$ ; Fig. 4, E and F) and nuclear DNA damage in TDP1<sup>-/-H493R</sup> MEFs ( $P < 0.01$ ; Fig. 4, G and H) after treatment with mito-SN38 for 12 hours. Collectively, we provide evidence that selective trapping of TDP1<sup>H493R</sup> in the mitochondria triggers nuclear DNA damage as a bystander effect through ROS formation.

### Mito-SN38 activates autophagy in SCAN1 cells

Accumulation of damaged mitochondria in cells expressing TDP1<sup>H493R</sup> prompted us to test the mechanism of its removal through autophagy (38, 53, 54). We directly measured steady-state levels of autophagosomes by testing the level of endogenous microtubule-associated protein 1A/1B light chain 3B (LC3-II) lipidation using immunoblotting in cells expressing TDP1 variants after treatment with mito-SN38. Figure 5 (A and B) shows a marked increase (~2-fold) in LC3-II conversion after incubation with sublethal dosage of mito-SN38 in TDP1<sup>-/-H493R</sup> MEFs compared to TDP1<sup>-/-WT</sup> MEFs, which is consistent with human SCAN1 cells showing marked increase in LC3-II conversion compared to their wild-type counterpart after mito-SN38 treatment (Fig. 5, A and B).

To further confirm autophagy activation in cells harboring SCAN1-TDP1, we performed green fluorescent protein (GFP)-LC3 puncta formation assay by using live-cell confocal microscopy (53, 55). Bafilomycin A1 (Baf A1; an autophagy inhibitor) (56) alone increases



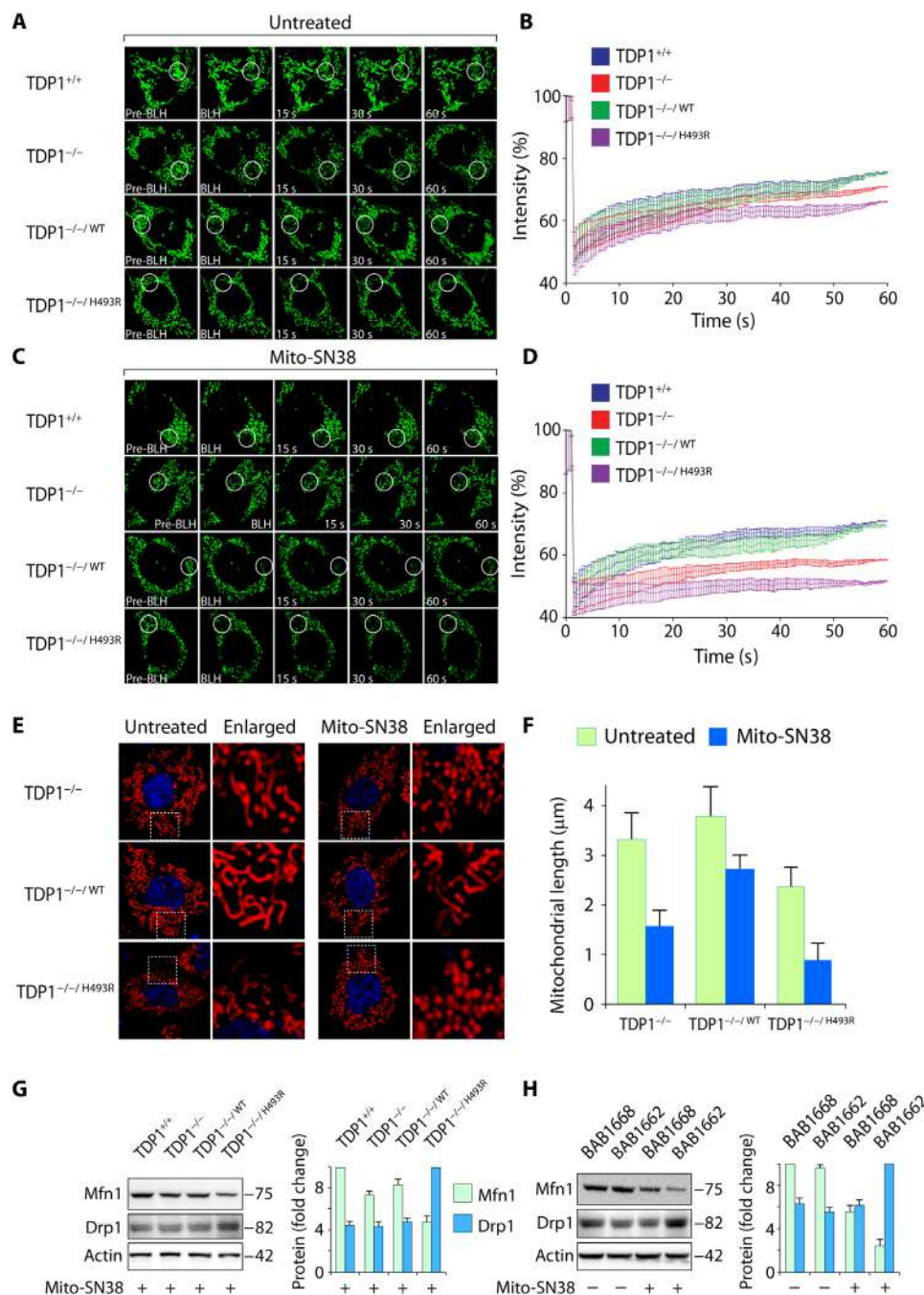


**Fig. 3. TDP1<sup>H493R</sup> trapping promotes mitochondrial fission.** Mitochondrial network dynamics were analyzed in the indicated cells using live-cell microscopy and photobleaching (FRAP analysis) of cells ectopically expressing the mitochondrial targeted fluorescence protein construct (mito-YFP). Cells were either untreated (**A**) or pretreated with mito-SN38 (5 μM for 3 hours) (**C**). A submitochondrial spot indicated by a circle was bleached (BLH) with a 514-nm laser for 30 ms and imaged at regular intervals of 500 ms thereafter. Successive images taken for 60 s after bleaching illustrate the level of return of fluorescence into the bleached areas. (**B** and **D**) Quantitative mitochondrial FRAP data ( $n = 25$ ). Error bars represent means  $\pm$  SEM. (**E** and **F**) Mitochondrial length was measured in the indicated MEFs by staining with MitoTracker red with or without mito-SN38 (5 μM for 3 hours). Nuclei were stained with Hoechst 33342 (blue). The bar graph ( $n = 25$ ) represents means  $\pm$  SEM. (**G** and **H**) Western blot analysis of Mfn1 (mitofusin 1) and Drp1 (dynamin-related protein 1) in total lysates obtained from the indicated cells after treatment with mito-SN38 (5 μM for 6 hours). Actin served as the loading control. Migration of protein molecular weight markers is indicated on the right. Bar graphs represent the fold change in densitometry analysis of Mfn1 and Drp1 normalized to actin (error bars represent means  $\pm$  SEM).

the number of GFP-LC3 puncta in TDP1<sup>-/-</sup>/H493R MEFs that were markedly elevated (~2- to 3-fold) when combined with mito-SN38 ( $P < 0.001$ ; Fig. 5C; see the quantification in Fig. 5D) in contrast to its wild-type counterpart.

To further investigate the role of TDP1<sup>H493R</sup> trapping in neuronal cells, we differentiated human neuroblastoma cells (SH-SY5Y) to neurons (fig. S2A) (34) and then ectopically expressed TDP1<sup>WT</sup> or TDP1<sup>H493R</sup> (fig. S2A). The SH-SY5Y cells were stably selected with

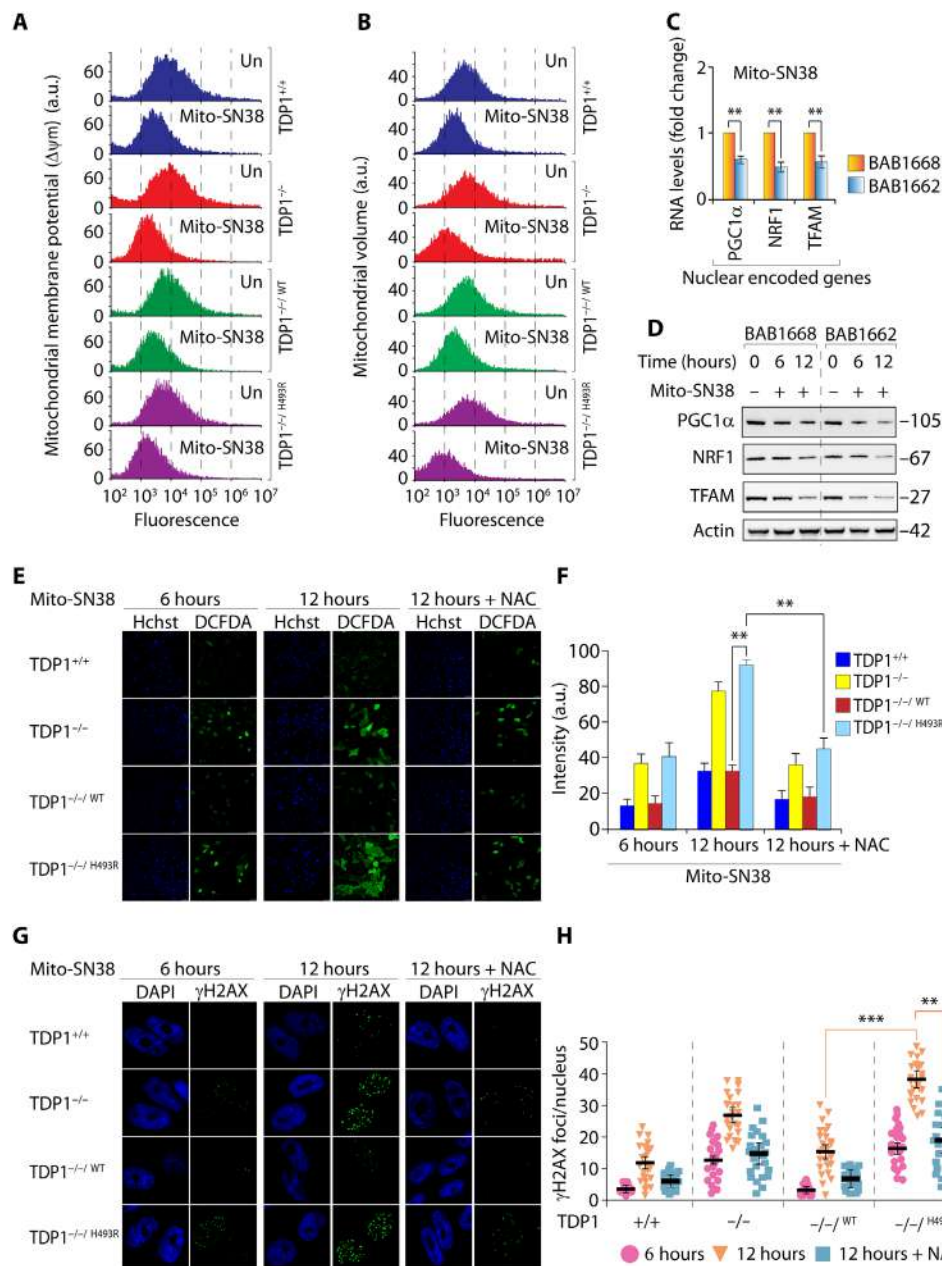


**Fig. 4. TDP1<sup>H493R</sup> trapping promotes mitochondrial dysfunction in SCAN1 cells.** (A) Fluorescence-activated cell sorting (FACS) analysis of mitochondrial membrane potential ( $\Delta\psi_m$ ) using TMRM before or after treatment with mito-SN38 (5  $\mu$ M for 6 hours) in the indicated cells. TMRM fluorescence was plotted against cell numbers (count). Data represent means  $\pm$  SE of independent experiments. (B) FACS analysis of mitochondrial volume in the indicated cells using MitoTracker green before and after treatment with mito-SN38 (5  $\mu$ M for 6 hours). Data represent means  $\pm$  SE of independent experiments. (C) The gene expression profile of nuclear-encoded genes [nuclear respiratory factor 1 (NRF1), peroxisome proliferator-activated receptor gamma coactivator 1- $\alpha$  (PGC1 $\alpha$ ), and mitochondrial transcription factor A (TFAM)] for mitochondrial biogenesis by reverse transcription PCR. Indicated cells were either not treated or treated with mito-SN38 (5  $\mu$ M for 6 hours). Data represent means  $\pm$  SE of three independent experiments. Asterisks denote statistically significant differences (\*\* $P$  < 0.01,  $t$  test). (D) Representative Western blots for nuclear-encoded NRF1, PGC1 $\alpha$ , and TFAM in SCAN1 patient-derived lymphoblastoid cell lines (BAB1662) and their wild-type counterpart (BAB1668) before and after treatment with mito-SN38 (5  $\mu$ M) for the indicated time periods. Actin is shown as the loading control. (E and F) ROS formation was measured by fluorescent dye CM-H<sub>2</sub>DCFDA in live-cell microscopy after treatment with mito-SN38 (5  $\mu$ M) or with pretreatment of *N*-acetyl-L-cysteine (NAC) (10 mM for 2 hours) for the indicated time. The ROS intensity is shown in green, and nuclei were stained with Hoechst 33342 (blue) in the indicated cells. Plots shown on the right represent means  $\pm$  SDs of at least three experiments. Asterisks denote statistically significant difference (\*\* $P$  < 0.01,  $t$  test). (G and H) Representative  $\gamma$ H2AX visualization by immunofluorescence microscopy in MEFs expressing TDP1 variants after treatment with mito-SN38 (5  $\mu$ M) or with pretreatment of NAC (10 mM for 2 hours) for the indicated time. The  $\gamma$ H2AX is shown in green, and nuclei were stained with 4',6-diamidino-2-phenylindole (DAPI) (blue). Scattergrams are shown on the right for at least three experiments; means  $\pm$  SDs are indicated. Asterisks denote statistically significant differences (\*\* $P$  < 0.01 and \*\*\* $P$  < 0.001,  $t$  test).

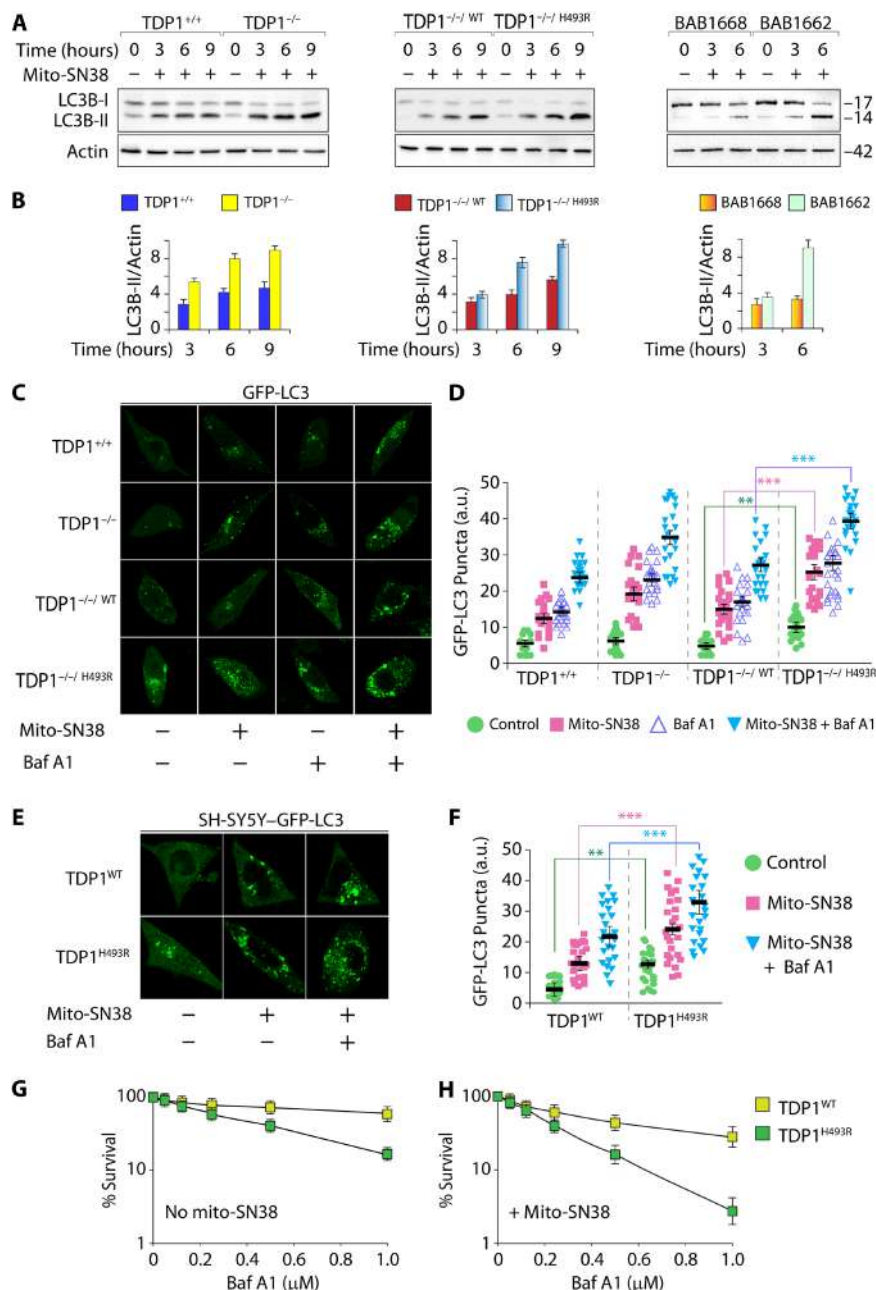


**Fig. 5. SCAN1-TDP1 in mitochondria activates autophagy.** (A) Immunoblotting for LC3-II lipidation with an anti-LC3B-specific antibody with the indicated cell lysates before or after treatment with a sublethal dose of mito-SN38 (2.5 μM) for the indicated time periods. The positions of LC3B-I and LC3B-II are indicated. Actin is shown as the loading control. (B) Plots represent fold increase in LC3B-II band intensity in the indicated cells, normalized to actin (error bars represent means ± SEM). (C) Representative images of GFP-LC3 puncta formation using live-cell confocal microscopy in the indicated cells by ectopically expressing GFP-LC3. The cells were either untreated or treated with mito-SN38 (2.5 μM for 12 hours) or the autophagy inhibitor Baf A1 (200 nM for 4 hours) alone or in combination with Baf A1 (200 nM for 4 hours) + mito-SN38 (2.5 μM for 12 hours). The translocation of GFP-LC3 to phagosome triggers steady-state levels of autophagosomes, as indicated by GFP-LC3 puncta formation. (D) Quantification of GFP-LC3 puncta per cell after the indicated treatment obtained from immunofluorescence confocal microscopy was calculated for 20 to 25 cells (mean ± SEM) from independent experiments. Asterisks denote statistically significant differences (\*\* $P < 0.01$  and \*\*\* $P < 0.001$ ,  $t$  test). (E) Representative images of differentiated neuronal cells derived from human neuroblastoma cells (SH-SY5Y) stably expressing GFP-LC3 were transfected with lentiviral constructs of TDP1<sup>WT</sup> or TDP1<sup>H493R</sup> and were analyzed for GFP-LC3 puncta formation under live-cell confocal microscopy. The cells were either kept untreated or treated with mito-SN38 (2.5 μM for 12 hours) or the autophagy inhibitor Baf A1 (200 nM for 4 hours) alone or in combination with Baf A1 (200 nM for 4 hours) + mito-SN38 (2.5 μM for 12 hours). (F) Quantification of GFP-LC3 puncta per cell after the indicated treatments was obtained from live-cell microscopy calculated for 20 to 25 cells (mean ± SEM) from independent experiments. Asterisks denote statistically significant differences (\*\* $P < 0.01$  and \*\*\* $P < 0.001$ ,  $t$  test). (G and H) Cell survival of differentiated neuronal cells from SH-SY5Y cells expressing TDP1<sup>WT</sup> or TDP1<sup>H493R</sup>. Baf A1-induced cytotoxicity (%) was calculated with respect to the untreated control (G). Combination of mito-SN38 (2.5 μM for 12 hours) + Baf A1 (for the next 24 hours)-induced cytotoxicity (%) was calculated with respect to the untreated control (H). Each point corresponds to the mean ± SD of at least three experiments. Error bars represent SD ( $n = 3$ ).



GFP-LC3, so we tested GFP-LC3 puncta formation in differentiated SH-SY5Y expressing TDP1 variants under live-cell microscopy. We detected notable increase in the basal levels of GFP-LC3 puncta formation in the differentiated SH-SY5Y cells only by expressing TDP1<sup>H493R</sup>, which was significantly increased after treatment with the autophagy inhibitor Baf A1 ( $P < 0.001$ ; Fig. 5E; see the quantification in Fig. 5F) compared to wild-type TDP1 expression. GFP-LC3 puncta were markedly elevated by ~3-fold in the presence of mito-SN38 + Baf A1 in differentiated SH-SY5Y cells expressing TDP1<sup>H493R</sup> compared to wild-type TDP1 ( $P < 0.001$ ; Fig. 5E; see the quantification in Fig. 5F).

To test the functional role of autophagy in the survival of the differentiated neuronal cells expressing TDP1<sup>H493R</sup>, we performed survival assays with the autophagy inhibitor Baf A1 alone or in combination with a sublethal dose of mito-SN38 in the neuronal cells expressing TDP1 variants. We noted that inhibition of autophagy by Baf A1 alone significantly induced cell death in TDP1<sup>H493R</sup>-expressing neuronal cells (Fig. 5G), which was markedly increased in combination with a sublethal dose of mito-SN38 (Fig. 5G; see mito-SN38 + Baf A1) compared to cells expressing the TDP1 wild-type counterpart, suggesting that autophagy rescues mito-SN38-induced mitochondrial toxicity in SCAN1 cells. Collectively, our data provide evidence that TDP1<sup>H493R</sup> trapping promotes the steady-state level of autophagosome formation, and upon inhibition of autophagy, this shifts toward apoptosis.

### Trapping of TDP1<sup>H493R</sup> activates PTEN-induced kinase 1-dependent mitophagy

Elimination of damaged mitochondria occurs through a specialized form of autophagy referred to as mitophagy (32, 33, 53). Thus, for the quantitative assessment of mitophagy in cells expressing TDP1 variants, we used a specific traffic light mitophagy reporter (mito-mRFP-EGFP) construct consisting of a pH-stable red fluorescent protein (RFP) fused to an acidic pH-labile GFP with a mitochondria-targeting signal (36). Localization of autophagic mitochondria inside the lysosome leads to formation of red-only fluorescence against yellow fluorescence for nonautophagic mitochondrial counterparts in cells expressing the mito-mRFP-EGFP construct (Fig. 6A). Without mito-SN38 treatment, we detected significant increases in red-only fluorescence in 30 to 35% of mitochondria in TDP1<sup>-/-H493R</sup> MEFs compared to TDP1-proficient cells expressing the traffic light construct ( $P < 0.01$ ; Fig. 6B), which is in keeping with the significant increase in the number of GFP-LC3 puncta without drug treatment in TDP1<sup>-/-H493R</sup> MEFs (Fig. 5, C and D) or differentiated neuronal cells expressing TDP1<sup>H493R</sup> (Fig. 5, E and F) and related to drug-independent trapping of TDP1<sup>H493R</sup> (Fig. 2A). Mito-SN38 treatment markedly increased mitophagy in TDP1<sup>H493R</sup> MEFs as revealed by more than 80% red-only fluorescence in the mitochondria ( $P < 0.001$ ; Fig. 6C) compared to TDP1<sup>+/+</sup> or TDP1<sup>-/-WT</sup> MEFs. Furthermore, we confirmed that the red-only fluorescent mitochondria in TDP1<sup>H493R</sup> MEFs correspond to mitochondria engulfed by lysosomes, as shown by colocalization with the lysosomal-specific LysoTracker dye (fig. S2C).

The sequential events that promote mitophagy is initiated by mitochondrial depolarization and accumulation of PINK1 (PTEN-induced kinase 1) in the outer mitochondrial membrane of the dysfunctional mitochondria (32, 37). Therefore, we ectopically expressed GFP-PINK1 in cells harboring TDP1 variants and investigated PINK1 accumulation in the mitochondria by costaining the cells with the mitochondrion-specific dye MitoTracker red under live-cell confocal microscopy. Figure 6D shows that 70 to 80% of TDP1<sup>-/-H493R</sup> MEFs

accumulate significantly higher expression of GFP-PINK1 in the mitochondria ( $P < 0.01$ ; see merged image Fig. 6D) within 3 hours of mito-SN38 treatment compared to (20 to 25%) TDP1<sup>+/+</sup> or TDP1<sup>-/-WT</sup> MEFs. Therefore, mitochondrial depolarization in TDP1 defective MEFs (Fig. 4A) activates PINK1-dependent mitophagy. These observations highlight the role of SCAN1-TDP1 trapping in mitochondrial fragmentation, a phenomenon in mitophagy associated with mitochondrial clearance.

### DISCUSSION

To our knowledge, the present study provides the first evidence that mitochondria in cells harboring SCAN1-TDP1 (TDP1<sup>H493R</sup>) are selectively trapped on the mtDNA at Top1mt cleavage sites, are shorter in length, and have increased fission rates. We demonstrate that TDP1<sup>H493R</sup> trapping prevents mitochondrial transcription, energy production, and mitobiogenesis. SCAN1-TDP1 trapping triggers autophagy that allows identification of dysfunctional mitochondria through PINK1 accumulation and their subsequent removal through mitophagy. Our current work offers further evidence that inhibition of autophagy in the neuronal cells expressing TDP1<sup>H493R</sup> is detrimental, suggesting that mitophagy is critical for SCAN1.

MtDNA is essential for cell viability, as it encodes subunits of OXPHOS as well as mitochondrial mRNA and tRNA (30). The mitochondrial genome accumulates topological stress from bidirectional transcription and replication, resolved by recruiting the Top1mt to the regulatory noncoding region of mtDNA (mtNCR) to relax mtDNA supercoiling generated during these processes (46, 48, 57). Accordingly, Top1mt knockout mice accumulate increased negative supercoiling in the mtDNA that impairs mtDNA replication (58, 59), promoting mitochondrial dysfunction (52). A number of things enhance the trapping of Top1mtcc in mitochondria including anticancer drugs like marine alkaloids lamellarin D (47), mitochondria-targeted irinotecan (mito-SN38; Fig. 1), and camptothecin treatment of purified mitochondria (46). Top1cc can also be trapped by endogenous DNA breaks, oxidized bases, nicks, and DNA modifications generated by ROS (6, 60).

MtDNA repair is particularly critical for the mitochondrial genome, as the mtNCR region is mostly prone to genome instability (61), because it is the most exposed region, which harbors the primary replication initiation site and the critical promoter elements both for the heavy and light strands (30). Thus, the ability of TDP1 to resolve 3'-phosphotyrosyl linkages is consistent with the role of the enzyme in protecting cells against cytotoxic Top1-DNA lesions generated both in the nucleus and in mitochondria (Fig. 1) (4, 12, 18, 27). We detected significant trapping of TDP1<sup>H493R</sup> in mitochondria without drug treatment (Fig. 2A), plausibly corresponding to the defective catalytic turnover of SCAN1-TDP1 at endogenous mtDNA lesions (10, 20, 21) or drug-independent Top1mtcc break sites, which were markedly enhanced after mito-SN38 treatment (Fig. 2A). TDP1<sup>H493R</sup> is selectively trapped at mitochondrial nucleotide residues 15420, 15690, and 16060 along the mtNCR (Fig. 2C) at Top1mtcc binding sites (46, 48). SCAN1-TDP1 displays a rapid depletion of mtDNA (~2-fold) and was deficient in recovery of mtDNA even after 12 hours of repair in drug-free medium (Fig. 2, D and E). Subsequently, TDP1<sup>H493R</sup> trapping induces transcriptional collapse of OXPHOS genes and is defective in organelle assembly of oxidative phosphorylation complexes in SCAN1 cells, which results in reduction in the steady-state level of ATP. This is in agreement with the recent



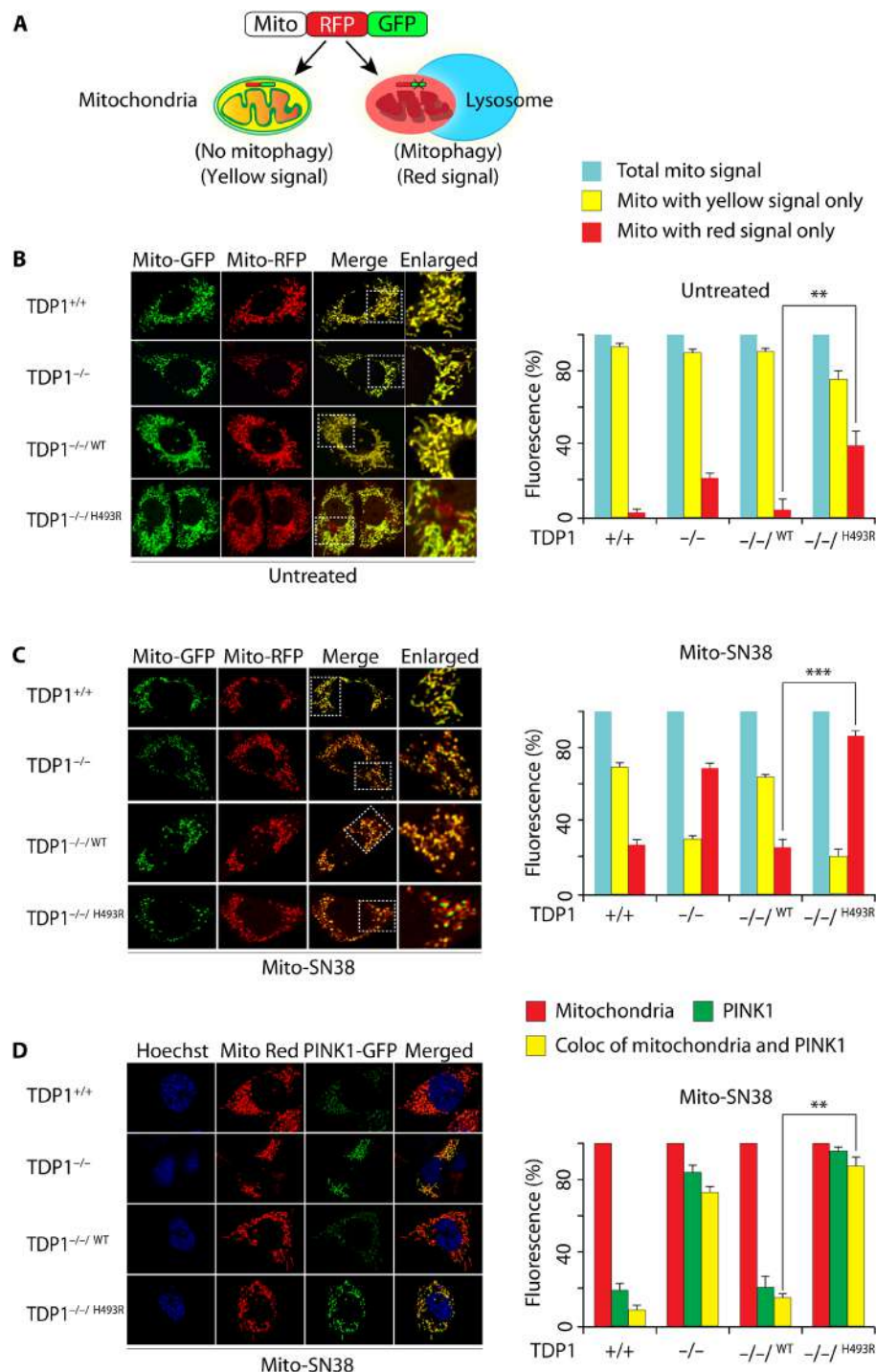


**Fig. 6. TDP1<sup>H493R</sup> trapping in mitochondria activates mitophagy.** (A) Schematic representation for mitophagy monitoring using the dual fluorescence reporter construct p-mito-mRFP-EGFP (pAT016). Lysosomal delivery of the tandem fusion protein mito-mRFP-EGFP along with entire mitochondria results in pH-dependent quenching of green fluorescence resulting in red-only fluorescence for visual analysis of mitophagic flux. (B and C) Representative confocal live images of indicated MEFs ectopically expressing mito-mRFP-EGFP targeting mitochondria. Cells were kept untreated (B) or treated with mito-SN38 (2.5  $\mu$ M for 12 hours) (C) and were analyzed under live-cell microscopy. The yellow fluorescence signals denote no mitophagy (merged image); red-only fluorescence signals denote mitophagy or mitochondria inside lysosomes. The enlarged panel shows higher-magnification image. Quantification of the indicated fluorescence obtained from live-cell confocal microscopy was calculated for 20 to 25 cells (calculated value  $\pm$  SEM) in at least three independent experiments. Asterisks denote statistically significant differences (\*\* $P$  < 0.01 and \*\*\* $P$  < 0.001,  $t$  test). (D) Representative confocal images of live cells for the indicated MEFs showing accumulation of ectopic PTEN-induced kinase 1 (PINK1)-GFP after mito-SN38 (2.5  $\mu$ M for 3 hours) treatment. Mitochondria are labeled with MitoTracker red; the colocalization of PINK1-GFP (green) in the mitochondrial network (red) is indicated in the merged image. Quantification of the indicated fluorescence obtained from live-cell confocal microscopy was calculated for 20 to 25 cells (calculated value  $\pm$  SEM) obtained from independent experiments. Asterisks denote statistically significant differences (\*\* $P$  < 0.01,  $t$  test).

report showing that TDP1 promotes the integrity of electron transport chain (18). Further evidence for dysregulated oxidative phosphorylation across the mitochondrial inner membrane is revealed by depolarization of the membrane potential in TDP1<sup>H493R</sup> harboring MEFs after mito-SN38 treatment (Fig. 4D).

The dynamic equilibrium between mitochondrial fusion and fission preserves the mitochondrial network (32–34, 39). Here, our live-cell imaging shows that cells harboring SCAN1-TDP1 have reduced mitochondrial networks because of an increase in mitochondrial fission rate (Fig. 3C), which results in shortening of mitochondrial length (Fig. 3, E and F) together with the quantitative loss of mitochondrial volume (Fig. 4E). This is further supported by increased levels of mitochondrial fission-associated protein Drp1 in SCAN1 cells (Fig. 3F) and is in agreement with the observation that expression of catalytically active TDP1 rescues the mitochondrial fission-fusion dynamics, mitochondrial length (Fig. 2), and respiratory capacity (Fig. 3) in TDP1<sup>−/−</sup> MEFs.

Fusion and fission dynamically regulate mitochondrial morphology and mitobiogenesis (32, 51), which occurs by division of preexisting organelles in coordination with nuclear encoded proteins and cellular proliferation. In SCAN1 cells, we observed a significant reduction in the transcription (Fig. 4F) and protein level (Fig. 4G) of nuclear encoded mitobiogenesis genes including PGC1 $\alpha$ , NRF1, and TFAM after prolonged treatment with mito-SN38, which is associated with nuclear DNA damage mediated through ROS (Fig. 4, H and I). We provide evidence that trapping of TDP1<sup>H493R</sup> in the mitochondria produces potentially toxic DNA lesions that not only dampens mitochondrial activity but also triggers nuclear DNA damage as a bystander effect through ROS formation (Fig. 4). Maneuvering of fission or fusion improves mitochondrial physiology. Disruption of mitochondrial dynamics is common in severe disorders, including Alzheimer's disease, Parkinson's disease, and Huntington's disease, which show neurodegeneration (32, 33, 38, 39, 42, 43, 54).

Because SCAN1 cells accumulate a fragmented mitochondrial network and disrupted respiratory complexes that fail to manage the cellular energy requirements, they have low levels of ATP. To match the metabolic demand, SCAN1-TDP1-harboring cells increase autophagosomes (Fig. 5) to retain a lower number of fit mitochondria and channel the damaged ones to mitophagy by PINK1 accumulation on the outer mitochondrial membrane of the damaged mitochondria (Fig. 6).

In conclusion, the present study establishes the significance of autophagy to overcome TDP1<sup>H493R</sup>-induced mitochondrial toxicity in neuronal cells (Fig. 5, E to G). Through evolution, cells that are critically dependent on mitochondria for energy production like neurons have acquired useful mechanisms to sequester and eliminate dysfunctional mitochondria for cell survival. It is worth mentioning that caloric restriction and mammalian target of rapamycin inhibition show life span-extending interventions via increased autophagy and mitophagy (62). This supports the argument that mitophagy in the SCAN1 phenotype may play a crucial role in neuroprotection and plausibly is associated with the late onset of neurological disorders as in patients with SCAN1.

## MATERIALS AND METHODS

### Drugs, reagents, and antibodies

Puromycin (P8833), Baf A1 (J61835), polybrene (H9268), irinotecan (I1406), all-*trans*-retinoic acid (R2625), and *N*-acetyl-L-cysteine (A9165) were all purchased from Sigma-Aldrich (USA). Anti-Top1mt-

specific antibody (47, 52) (Top1mt, polyclonal mouse) was a gift from Y. Pommier [Center for Cancer Research, National Cancer Institute, National Institutes of Health (NIH), USA]. Rabbit polyclonal antibodies [TDP1 (Ab4166), PGC1 $\alpha$  (Ab54481), NRF1 (Ab34682), and mtTFAM (Ab47517)] and mouse monoclonal antibodies [COX IV (Ab14744), DRP1 (Ab56788), Mfn1 (Ab57602), and double-stranded DNA (dsDNA) (Ab27156)] were purchased from Abcam (Cambridge, USA). Mouse monoclonal antibodies [FLAG (M2) (F3165)] and rabbit polyclonal antibodies [FLAG (F7425) and LC3B (L7543)] were purchased from Sigma-Aldrich (St. Louis, MO, USA). Mouse monoclonal  $\gamma$ H2AX (05-636) antibody was purchased from Millipore, USA. Rabbit monoclonal GFP (G10362) and anti OXPHOS complex kit (457999) antibodies were purchased from Invitrogen. Mouse monoclonal actin (SC-8432) and secondary antibodies [horseradish peroxidase-conjugated anti-rabbit immunoglobulin G (IgG) or anti-mouse IgG] were purchased from Santa Cruz Biotechnology (Santa Cruz, USA). MitoTracker red (M22426), MitoTracker green (M7514), TMRM (T668), CM-H<sub>2</sub>DCFDA (C6827), and LysoTracker red DND-99 (L7528) were obtained from Molecular Probes.

### Synthesis of mitochondria-targeted nanoparticle containing irinotecan (mito-SN38)

Production of a mitochondria-targeting cationic nanoparticle containing Top1 poison irinotecan (mito-SN38) was described previously (45). Briefly, 6.0 mg of L- $\alpha$ -phosphatidylcholine, 1.0 mg of  $\alpha$ -tocopherylsuccinate-triphenylphosphine conjugate, 1.0 mg of irinotecan, and 0.6 mg of 1,2-distearoyl-*sn*-glycero-3-phosphoethanolamine-*N*-[amino (polyethylene glycol) 2000] were dissolved in 5.0 ml of dichloromethane-methanol mixture. Solvent was evaporated thoroughly to form a thin uniform lipid film. The lipid film was hydrated with 1 ml of water for 1 hour at 60°C. The nanoparticles formed were passed through Sephadex G-25 followed by extrusion through a 200-nm filter. The nanoparticles (mito-SN38) were stored at 4°C for further use.

### Cell culture, plasmids, and generation of stable cell lines

Cells were cultured at 37°C with 5% CO<sub>2</sub> in Dulbecco's minimum essential medium (DMEM) or RPMI containing 10% fetal bovine serum (FBS) (Life Technologies) (12, 15, 27, 28, 63). TDP1<sup>+/+</sup> and TDP1<sup>−/−</sup> primary MEF cells were a gift from C. F. Boerkoel (University of British Columbia, Vancouver, British Columbia, Canada). Lymphoblastoid cell lines homozygous for the TDP1-H493R mutation (BAB1662; SCAN1) and normal individual (BAB1668) were a gift from J. R. Lupski (Departments of Pediatrics and Molecular and Human Genetics, Baylor College of Medicine, Houston, USA). The human embryonic kidney 293T [American Type Culture Collection (ATCC)] and human SH-SY5Y cells (ATCC) were a gift from D. Biswas (Council of Scientific and Industrial Research-Indian Institute of Chemical Biology, Kolkata, India). The cloning of pCMV-Tag2B-FLAG-TDP1 construct was described previously (12, 27, 28). Plasmid MDK124-FLAG-TDP1 was generated by digesting a FLAG-TDP1 fragment from pCMV-Tag2B-FLAG-TDP1 construct using Nhe I and Eco RI restriction sites and cloned into the pMDK124 lentiviral vector. The following point mutation (pMDK124-FLAG-TDP1<sup>H493R</sup>) was generated using the "QuikChange" protocol (Stratagene, La Jolla, CA, USA). All constructs were confirmed by DNA sequencing. The plasmids were then used for lentivirus generation using a standard protocol and were transduced into TDP1<sup>−/−</sup> MEFs using lentivirus particles containing FLAG-TDP1<sup>WT</sup> or FLAG-TDP1<sup>H493R</sup> in the presence of polybrene (5  $\mu$ g/ml) (Sigma-Aldrich) and were subjected

to puromycin selection (4 µg/ml) for 2 weeks. Individual colonies obtained by this method were further amplified and screened for expression of target proteins using Western blotting against epitope tag-specific antibodies.

The pYFP-Mito construct (15, 49) (protein targeted to the mitochondrial matrix) was a gift from R. J. Youle (National Institutes of Neurological Disorders and Stroke, NIH), the traffic light mitophagy reporter construct pAT016 (p-mito-mRFP-EGFP) was a gift from A. Till (University of Bonn, Germany), the pEGFP-LC3 construct was a gift from A. Saha (Presidency University, India), and the pPINK1 C-GFP construct was a gift from P. Mukherjee (Presidency University, India). All plasmid DNA constructs were transfected with Lipofectamine 2000 (Invitrogen) or FuGENE (Roche) according to the manufacturer's protocol.

Human SH-SY5Y cells were grown in DMEM containing 10% FBS and 1% penicillin and streptomycin and were stably selected for pEGFP-LC3 construct with puromycin (10 µg/ml). Differentiation of SH-SY5Y was performed (34) using 10 µM all-*trans*-retinoic acid (Sigma-Aldrich) dissolved in dimethyl sulfoxide for 7 to 10 days with changing retinoic acid-containing media on alternate days. Microscopic images of differentiated SH-SY5Y cells were taken using a Leica TCS SP8 microscope. The lentiviral particles containing FLAG-TDP1<sup>WT</sup> or FLAG-TDP1<sup>H493R</sup> were transduced into differentiated SH-SY5Y cells in the presence of polybrene (5 µg/ml) (Sigma-Aldrich) and incubated for 48 hours for ectopic expression of proteins. Expression of the target proteins was checked by Western blotting using epitope tag-specific antibodies. Cells were treated with different concentrations of mito-SN38 and Baf A1, as indicated.

### Live-cell confocal microscopy and immunocytochemistry

Live-cell imaging was carried out as described previously (12, 27, 63, 64). Briefly, indicated cells were grown on confocal dishes (Genetix Biotech Asia Pvt. Ltd.). All the plasmid DNA were transfected as above and examined by live-cell confocal microscopy, as indicated. Nuclei were stained with Hoechst 33342 (Sigma-Aldrich). Fluorophores were excited using either separately or in combination with ultraviolet (Diode 405), 488-nm (argon), 561-nm (DPSS 561), or 633-nm (HeNe 633) laser lines using a confocal laser scanning microscope (Leica TCS SP8) with 63×/1.4 numerical aperture oil objective equipped with a heated environmental chamber set to 37°C with an optimal CO<sub>2</sub> facility. The percentage of cells displaying the indicated fluorescence was determined using Adobe Photoshop 7.0 from at least 20 to 25 cells expressing individual constructs.

Immunofluorescence staining and confocal microscopy were performed as described previously (12, 27, 28, 63, 64). Briefly, cells were fixed with 4% paraformaldehyde for 20 min at room temperature. Primary antibodies against γH2AX were detected with anti-mouse IgG secondary antibodies labeled with Alexa Fluor 488 (Invitrogen). Cells were mounted in anti-fade solution with 4',6-diamidino-2-phenylindole (Invitrogen) and examined using a laser scanning confocal microscope (Leica TCS SP8). Images were collected and processed using the Leica LAS X software and sized in Adobe Photoshop 7.0. The γH2AX intensity per nucleus was determined using Adobe Photoshop 7.0 by measuring the fluorescence intensities normalized to the number of cell count.

### Measurements of mitochondrial connectivity using FRAP assays

Photobleaching experiments were carried out as described previously (12, 27, 49, 63) to measure mitochondrial connectivity using a confocal

laser scanning microscope (Leica TCS SP8). FRAP analyses were carried out with MEFs stably expressing TDP1 variants and ectopically expressing mitochondrial matrix targeted (pYFP-Mito) with or without mito-SN38. Bleaching of YFP-mito was applied at randomly chosen mitochondrial regions using a 514-nm laser for 30 ms and photographed at intervals of 500 ms thereafter. Successive images taken for 60 s after bleaching illustrated the level of recovery of fluorescence into the bleached areas. Relative fluorescence intensities of the bleached region were corrected for background. To show the FRAP curves, the fluorescence signal measured in a region of interest (ROI) was individually normalized to the pre-bleach signal in the ROI according to the following equation:  $ROI = (I_t - I_{bg}) / (I_0 - I_{bg}) \times 100$ , where  $I_0$  is the intensity in the ROI during pre-bleach,  $I_t$  is the intensity in the ROI at time point  $t$ , and  $I_{bg}$  is the background signal determined in a region outside of the mitochondria.

### Cell extracts and immunoblotting

Preparation of whole cell extracts and immunoblotting were carried out as described previously (12, 27, 63). Briefly, cells were harvested and lysed in a lysis buffer [10 mM tris-HCl (pH 8), 150 mM NaCl, 0.1% SDS, 1% NP-40, and 0.5% Na-deoxycholate supplemented with complete protease inhibitors] (Roche Diagnostics, Indianapolis, IN) and phosphatase inhibitors (Phosphatase Inhibitor Cocktail 1 from Sigma-Aldrich). After thorough mixing and incubation at 4°C for 2 hours, lysates were then centrifuged at 12,000g at 4°C for 20 min. Supernatants were collected and stored in aliquots at -80°C. Immunoblots were carried out following standard procedures, and immunoreactivity was detected using enhanced chemiluminescence reaction (170-5061, Bio-Rad) under ChemiDoc MP System (Bio-Rad).

### Preparation of mitochondria

Mitochondria were prepared as described previously (15). Briefly, cell pellets were suspended in 10 mM NaCl, 1.5 mM CaCl<sub>2</sub>, and 10 mM tris-HCl (pH 7.5) at 25°C for 5 min. Following osmotic shock, cells were homogenized using a glass Dounce homogenizer and mixed with stabilizing buffer [2 M sucrose, 35 mM EDTA, and 50 mM tris-HCl (pH 7.5) at 25°C]. Cell lysates were centrifuged at 750g for 5 min to remove nuclei and cell debris. Mitochondria were spun down from the supernatant at 10,000g for 20 min, washed three times with MT buffer [250 mM sucrose, 10 mM KCl, 1.5 mM MgCl<sub>2</sub>, 1 mM EDTA, 1 mM EGTA, 5 mM dithiothreitol (DTT), and 20 mM Hepes-KOH (pH 7.4) at 25°C], and resuspended in MT buffer. For all experiments, freshly prepared mitochondria were used.

### ICE bioassay

Detection of Top1mt, TDP1, and nuclear Top1-cleavage complexes by ICE bioassay was performed as described previously (47). Briefly, cells ( $5 \times 10^6$ ) expressing TDP1 variants were either untreated or treated with the indicated concentration of drugs. Mitochondria were isolated as described above and lysed by adding lysis buffer [6 M guanidinium thiocyanate, 10 mM tris-HCl (pH 6.5), 20 mM EDTA, 4% Triton X-100, 1% sarosyl, and 1% DTT]. Mitochondrial lysates were mixed with 0.4 ml of 100% ethanol, incubated at -20°C for 5 min, and cleared by centrifugation (12,000g for 10 min). Supernatants were discarded, and pellets were washed two times with 100% ethanol and then dissolved in 0.2 ml of 8 mM NaOH (freshly made) and sonicated for 10 to 20 s at 20% power. For immunodetection, mtDNA at varying concentrations were spotted onto a nitrocellulose membrane (Millipore, USA) using a slot-blot vacuum system (Bio-Rad, USA).



For detection of nuclear Top1cc, whole cells were lysed by adding lysis buffer, cleared by centrifugation, and the pellet was dissolved in 8 mM NaOH and slot-blotted as indicated above. Immunoblotting was carried out with anti-Top1mt (47, 52) or anti-TDP1 (15) and anti-nuclear Top1-specific antibodies. Anti-dsDNA was used for loading control. Immunoblots were visualized using enhanced chemiluminescence reactions on a ChemiDoc MP System.

### Cell survival assays

Cell survival was carried out as described previously (28, 45, 65). Briefly, TDP1<sup>+/+</sup> MEFs, TDP1<sup>-/-</sup> MEFs, and TDP1<sup>-/-</sup> MEF cells stably expressing FLAG-TDP1 variants (TDP<sup>-/-</sup>/WT, TDP<sup>-/-</sup>/H493R, or TDP<sup>+/+/H493R</sup>) or human lymphoblastoid cells (BAB1662 or BAB168) or differentiated SH-SY5Y cells ectopically expressing FLAG-TDP1<sup>WT</sup> or FLAG-TDP1<sup>H493R</sup> ( $1 \times 10^3$ ) cells were seeded in 96-well plates (BD Biosciences, USA). After 24 hours, cells were treated with the indicated drugs and kept for a further 48 hours. Cell survival was then assessed by 3-(4,5-dimethylthiazol-2-yl)-2,5-diphenyltetrazolium bromide (MTT; Sigma-Aldrich, M5655). Plates were analyzed on a Molecular Devices Spectra MaxM2 Microplate Reader at 570 nm. The percent inhibition of viability for each concentration of drugs was calculated with respect to the control. Data represent means  $\pm$  SD for three independent experiments.

### Quantification of mtDNA damage

To compare the levels of mtDNA damage and repair in cells expressing TDP1 variants, cells were treated with mito-SN38 (20  $\mu$ M) for the indicated times or further cultured in drug-free medium to measure repair using mtDNA long-range PCR as described previously (15, 66). We used human and mouse mtDNA sequence-specific primers to amplify a 9- or 10-kbp (kilo-base pair) fragment of mtDNA, respectively. A small 110-bp (for human) or 117-bp (for mouse-specific) mtDNA fragment was also amplified for normalization. PCR reactions were limited to 18 cycles to ensure that the amplification process was still in the exponential phase. The damage index was determined by the ratio LR/SR of long-range PCR product (LR) by the short-range PCR product (SR). The sequences of the primers are listed in table S1.

### ChIP and reverse transcription qPCR

ChIP was performed as described previously (18, 48). Briefly, MEF cells expressing TDP1 variants ( $1 \times 10^7$ ) were treated with mito-SN38 (5  $\mu$ M) for 6 hours followed by fixation with formaldehyde (1.1% final concentration) for 10 min at room temperature, and reactions were stopped by adding 125 mM glycine for 5 min. Cells were then washed with phosphate-buffered saline (PBS), scraped, and lysed in 0.5 ml of ChIP lysis buffer [50 mM Hepes-KOH (pH 7.5), 140 mM NaCl, 1 mM EDTA (pH 8), 1% Triton X-100, 0.1% sodium deoxycholate, 0.1% SDS, and 1 $\times$  protease inhibitor] on ice for 30 min. Lysates were sonicated 10 times for 30 s at 30% power to yield fragments of 200 to 300 bp and cleared by centrifugation at 14,000g for 10 min at 4°C. The supernatant (50  $\mu$ l) was stored at -20°C as input and labeled as “no-IP.” The remainder was diluted fourfold in dilution buffer [50 mM tris-HCl (pH 8), 150 mM NaCl, 2 mM EDTA (pH 8), 1% NP-40, 0.5% sodium deoxycholate, 0.1% SDS, and 1 $\times$  protease inhibitors] and incubated with 10  $\mu$ l of FLAG antibody on a rotating platform overnight at 4°C. The following day, 150  $\mu$ l of A/G PLUS-Agarose beads (Santa Cruz Biotechnology) was added and further incubated on a rotating platform for 2 hours at 4°C. The beads were then washed twice with low-salt wash buffer [0.1% SDS, 1% Triton X-100, 2 mM

EDTA, 20 mM tris-HCl (pH 8), and 150 mM NaCl], twice with high-salt wash buffer [0.1% SDS, 1% Triton X-100, 2 mM EDTA, 20 mM tris-HCl (pH 8), and 500 mM NaCl], followed by one wash with lithium chloride buffer [0.25 M LiCl, 1% NP-40, 1% sodium deoxycholate, 1 mM EDTA, and 10 mM tris-HCl (pH 8)], and twice with TE buffer. The immunoprecipitated complex was then eluted from the beads in 150  $\mu$ l of elution buffer (1% SDS and 100 mM NaHCO<sub>3</sub>). The eluent and the no-IP control samples were then treated with RNase A and proteinase K. The DNA was purified using phenol-chloroform extraction and ethanol precipitation. The pellets were resuspended in 30  $\mu$ l of distilled water.

For qPCR, the no-IP or input and ChIP samples were diluted 1:10; then, 5  $\mu$ l was mixed with 2.5  $\mu$ l of 5  $\mu$ M forward and reverse primers (table S1) with 10  $\mu$ l of 2 $\times$  SYBR Green PCR mix (Applied Biosystems). The PCR mix was aliquoted into reaction volumes (20  $\mu$ l) in triplicate and amplified using an ABI 7500 thermocycler (Applied Biosystems). The PCR reactions were carried out with thermocycling conditions of 95°C for 10 min and then 40 cycles at 90°C for 15 s, 50°C for 15 s, and 72°C for 30 s, with signal acquisition at the end of each cycle. Quantification of chromatin enrichment was calculated by percent input normalized to the mtDNA copy number in the input samples. The sequences of the primers are listed in table S1.

### Quantification of mitochondrial gene transcription by real-time PCR

The total RNA was extracted from indicated cells ( $1 \times 10^6$ ) using TRIzol reagent (15596018, Invitrogen) according to the manufacturer's protocols, which includes deoxyribonuclease (AMPD1; Sigma-Aldrich) treatment for each sample (52). An aliquot of 1  $\mu$ g of RNA was reverse-transcribed using a reverse transcription kit (4368814, Applied Biosystems). Real-time PCR was performed with SYBR Green PCR master mix (A25742, Applied Biosystems) on the ABI 7500 thermocycler (Applied Biosystems). Reaction mixtures contained 5  $\mu$ l of 2 $\times$  SYBR-Green PCR master mix and 2  $\mu$ l of reverse transcriptase-generated cDNA diluted 10-fold in a final volume of 10  $\mu$ l containing primers at 25 nM. The thermocycling conditions were 95°C for 5 min, followed by 40 cycles at 95°C for 50 s, 50°C (variable) for 50 s, and 72°C for 60 s. Relative gene expression was expressed as a ratio of the expression level of the gene of interest to that of  $\beta$ -actin RNA, with values in wild-type cells defined as 100%. The sequences of the primers are listed in table S1.

### Analysis of mitochondrial length

Mitochondrion length was measured as described previously (49). Briefly, MEFs expressing TDP1 variants were incubated with or without mito-SN38, as indicated. Then, cells were stained with MitoTracker red and were subjected to live-cell confocal microscopy (Leica TCS SP8). Individual mitochondrial length analysis was performed using the line measurement property of Leica LAS X software. An average length of ~20 to 25 mitochondria per cell was measured.

### Mitochondrial membrane potential

Determination of  $\Delta\psi$ m was performed using TMRM (200 nM for 30 min at 37°C) (50, 52), which is a positively charged, colorless dye that enters mitochondria in a membrane potential-dependent manner and emits bright red-orange fluorescence that was analyzed by flow cytometry (BD, FACSaria III).



## Determination of mitochondrial mass

Mitochondrial mass was measured by MitoTracker Green FM (Molecular Probes) staining (50, 52). Cells were trypsinized and resuspended in PBS with 200 nM MitoTracker Green FM (30 min at 37°C) in the dark and were analyzed by flow cytometry (BD, FACSAria III).

## ATP determination

ATP level in indicated cells was determined using an ATP determination kit (A22066; Molecular Probes) following the manufacturer's protocol (52).

## Intracellular ROS detection by confocal microscopy

For intracellular ROS detection by live-cell confocal (Leica TCS SP8) microscopy, MEFs expressing TDP1 variants were seeded in confocal dishes and treated with or without mito-SN38 for the indicated time periods and then washed twice with PBS (pH 7.4) and 10  $\mu$ M CM-H<sub>2</sub>DCFDA in PBS was applied to live cells and kept at 37°C for 5 min (28, 45, 65). The CM-H<sub>2</sub>DCFDA diffuses into cells where the free nonfluorescent 2',7'-dichlorodihydrofluorescein in the cytoplasm is oxidized to the green fluorescent moiety, dichlorofluorescein, by intracellular ROS upon excitation with 488-nm argon laser. Nuclei were stained with Hoechst 33342.

## SUPPLEMENTARY MATERIALS

Supplementary material for this article is available at <http://advances.sciencemag.org/cgi/content/full/5/11/eaax9778/DC1>

Fig. S1. Mito-SN38 does not trap nuclear-Top1cc but impairs mitochondrial metabolism through SCAN1-TDP1 trapping in the mitochondria.

Fig. S2. Differentiation of SH-SY5Y cells showing expression of FLAG-TDP1 and lysosomal localization of SCAN1 mitochondria showing mitophagy.

Table S1. List of primers used.

[View/request a protocol for this paper from Bio-protocol.](#)

## REFERENCES AND NOTES

- H. Takashima, C. F. Boerkoel, J. John, G. M. Saifi, M. A. M. Salih, D. Armstrong, Y. Mao, F. A. Quiocho, B. B. Roa, M. Nakagawa, Mutation of *TDP1*, encoding a topoisomerase I-dependent DNA damage repair enzyme, in spinocerebellar ataxia with axonal neuropathy. *Nat. Genet.* **32**, 267–272 (2002).
- S.-W. Yang, A. B. Burgin Jr., B. N. Huizenga, C. A. Robertson, K. C. Yao, H. A. Nash, A eukaryotic enzyme that can disjoin dead-end covalent complexes between DNA and type I topoisomerases. *Proc. Natl. Acad. Sci. U.S.A.* **93**, 11534–11539 (1996).
- A. S. Kawale, L. F. Povirk, Tyrosyl-DNA phosphodiesterases: Rescuing the genome from the risks of relaxation. *Nucleic Acids Res.* **46**, 520–537 (2017).
- Y. Pommier, S.-y. N. Huang, R. Gao, B. B. Das, J. Murai, C. Marchand, Tyrosyl-DNA-phosphodiesterases (tdp1 and tdp2). *DNA Repair* **19**, 114–129 (2014).
- S. F. El-Khamisy, To live or to die: A matter of processing damaged DNA termini in neurons. *EMBO Mol. Med.* **3**, 78–88 (2011).
- Y. Pommier, Y. Sun, S.-y. N. Huang, J. L. Nitiss, Roles of eukaryotic topoisomerases in transcription, replication and genomic stability. *Nat. Rev. Mol. Cell Biol.* **17**, 703–721 (2016).
- S. Katyal, Y. Lee, K. C. Nitiss, S. M. Downing, Y. Li, M. Shimada, J. Zhao, H. R. Russell, J. H. Petrini, J. L. Nitiss, Aberrant topoisomerase-1 DNA lesions are pathogenic in neurodegenerative genome instability syndromes. *Nat. Neurosci.* **17**, 813–821 (2014).
- S. Katyal, S. F. El-Khamisy, H. R. Russell, Y. Li, L. Ju, K. W. Caldecott, P. J. McKinnon, TDP1 facilitates chromosomal single-strand break repair in neurons and is neuroprotective in vivo. *EMBO J.* **26**, 4720–4731 (2007).
- S. F. El-Khamisy, G. M. Saifi, M. Weinfeld, F. Johansson, T. Helleday, J. R. Lupski, K. W. Caldecott, Defective DNA single-strand break repair in spinocerebellar ataxia with axonal neuropathy-1. *Nature* **434**, 108–113 (2005).
- H. Interthal, H. J. Chen, T. E. Kehl-Fie, J. Zotzmann, J. B. Leppard, J. J. Champoux, SCAN1 mutant Tdp1 accumulates the enzyme-DNA intermediate and causes camptothecin hypersensitivity. *EMBO J.* **24**, 2224–2233 (2005).
- K. W. Caldecott, Single-strand break repair and genetic disease. *Nat. Rev. Genet.* **9**, 619–631 (2008).
- B. B. Das, S. Antony, S. Gupta, T. S. Dexheimer, C. E. Redon, S. Garfield, Y. Shiloh, Y. Pommier, Optimal function of the DNA repair enzyme TDP1 requires its phosphorylation by ATM and/or DNA-PK. *EMBO J.* **28**, 3667–3680 (2009).
- R. Hirano, H. Interthal, C. Huang, T. Nakamura, K. Deguchi, K. Choi, M. B. Bhattacharjee, K. Arimura, F. Umehara, S. Izumo, Spinocerebellar ataxia with axonal neuropathy: Consequence of a Tdp1 recessive neomorphic mutation? *EMBO J.* **26**, 4732–4743 (2007).
- A. J. Hawkins, M. A. Subler, K. Akopiants, J. L. Wiley, S. M. Taylor, A. C. Rice, J. J. Windle, K. Valerie, L. F. Povirk, In vitro complementation of Tdp1 deficiency indicates a stabilized enzyme-DNA adduct from tyrosyl but not glycolate lesions as a consequence of the SCAN1 mutation. *DNA Repair* **8**, 654–663 (2009).
- B. B. Das, T. S. Dexheimer, K. Maddali, Y. Pommier, Role of tyrosyl-DNA phosphodiesterase (TDP1) in mitochondria. *Proc. Natl. Acad. Sci. U.S.A.* **107**, 19790–19795 (2010).
- J. Murai, S.-y. N. Huang, B. B. Das, T. S. Dexheimer, S. Takeda, Y. Pommier, Tyrosyl-DNA phosphodiesterase 1 (TDP1) repairs DNA damage induced by topoisomerases I and II and base alkylation in vertebrate cells. *J. Biol. Chem.* **287**, 12848–12857 (2012).
- H. K. Fam, K. Choi, L. Fougner, C. J. Lim, C. F. Boerkoel, Reactive oxygen species stress increases accumulation of tyrosyl-DNA phosphodiesterase 1 within mitochondria. *Sci. Rep.* **8**, 4304 (2018).
- S.-C. Chiang, M. Meagher, N. Kassouf, M. Hafezparast, P. J. McKinnon, R. Haywood, S. F. El-Khamisy, Mitochondrial protein-linked DNA breaks perturb mitochondrial gene transcription and trigger free radical-induced DNA damage. *Sci. Adv.* **3**, e1602506 (2017).
- K. V. Inamdar, J. J. Pouliot, T. Zhou, S. P. Lees-Miller, A. Rasouli-Nia, L. F. Povirk, Conversion of phosphoglycolate to phosphate termini on 3' overhangs of DNA double strand breaks by the human tyrosyl-DNA phosphodiesterase hTdp1. *J. Biol. Chem.* **277**, 27162–27168 (2002).
- H. Interthal, H. J. Chen, J. J. Champoux, Human Tdp1 cleaves a broad spectrum of substrates including phosphoamide linkages. *J. Biol. Chem.* **280**, 36518–36528 (2005).
- T. Zhou, J. W. Lee, H. Tatavarthi, J. R. Lupski, K. Valerie, L. F. Povirk, Deficiency in 3'-phosphoglycolate processing in human cells with a hereditary mutation in tyrosyl-DNA phosphodiesterase (TDP1). *Nucleic Acids Res.* **33**, 289–297 (2005).
- S. B. Hassine, B. Arcangioli, Tdp1 protects against oxidative DNA damage in non-dividing fission yeast. *EMBO J.* **28**, 632–640 (2009).
- W. Zhang, X. Hu, Q. Shen, D. Xing, Mitochondria-specific drug release and reactive oxygen species burst induced by polyprodrug nanoreactors can enhance chemotherapy. *Nat. Commun.* **10**, 1704 (2019).
- S.-y. N. Huang, J. Murai, I. Dalla Rosa, T. S. Dexheimer, A. Naumova, W. H. Gmeiner, Y. Pommier, TDP1 repairs nuclear and mitochondrial DNA damage induced by chain-terminating anticancer and antiviral nucleoside analogs. *Nucleic Acids Res.* **41**, 7793–7803 (2013).
- S.-C. Chiang, J. Carroll, S. F. El-Khamisy, TDP1 serine 81 promotes interaction with DNA ligase III $\alpha$  and facilitates cell survival following DNA damage. *Cell Cycle* **9**, 588–595 (2014).
- J. J. R. Hudson, S.-C. Chiang, O. S. Wells, C. Rookyard, S. F. El-Khamisy, SUMO modification of the neuroprotective protein TDP1 facilitates chromosomal single-strand break repair. *Nat. Commun.* **3**, 733 (2012).
- B. B. Das, S.-y. N. Huang, J. Murai, I. Rehman, J.-C. Amé, S. Sengupta, S. K. Das, P. Majumdar, H. Zhang, D. Biard, PARP1-TDP1 coupling for the repair of topoisomerase I-induced DNA damage. *Nucleic Acids Res.* **42**, 4435–4449 (2014).
- I. Rehman, S. M. Basu, S. K. Das, S. Bhattacharjee, A. Ghosh, Y. Pommier, B. B. Das, PRMT5-mediated arginine methylation of TDP1 for the repair of topoisomerase I covalent complexes. *Nucleic Acids Res.* **46**, 5601–5617 (2018).
- C. Liao, R. Beveridge, J. J. Hudson, J. D. Parker, S.-C. Chiang, S. Ray, M. E. Ashour, I. Sudbery, M. J. Dickman, S. F. El-Khamisy, UCHL3 regulates topoisomerase-induced chromosomal break repair by controlling TDP1 proteostasis. *Cell Rep.* **23**, 3352–3365 (2018).
- D. C. Wallace, A mitochondrial paradigm of metabolic and degenerative diseases, aging, and cancer: A dawn for evolutionary medicine. *Annu. Rev. Genet.* **39**, 359–407 (2005).
- I. J. Holt, Mitochondrial DNA replication and repair: All a flap. *Trends Biochem. Sci.* **34**, 358–365 (2009).
- D. C. Chan, Mitochondria: Dynamic organelles in disease, aging, and development. *Cell* **125**, 1241–1252 (2006).
- R. J. Youle, A. M. Van Der Bliek, Mitochondrial fission, fusion, and stress. *Science* **337**, 1062–1065 (2012).
- H. Chen, M. Vermulst, Y. E. Wang, A. Chomyn, T. A. Prolla, J. M. McCaffery, D. C. Chan, Mitochondrial fusion is required for mtDNA stability in skeletal muscle and tolerance of mtDNA mutations. *Cell* **141**, 280–289 (2010).
- T. Lieber, S. P. Jeedigunta, J. M. Palozzi, R. Lehmann, T. R. Hurd, Mitochondrial fragmentation drives selective removal of deleterious mtDNA in the germline. *Nature* **570**, 380–384 (2019).
- S.-J. Kim, M. Khan, J. Quan, A. Till, S. Subramani, A. Siddiqui, Hepatitis B virus disrupts mitochondrial dynamics: Induces fission and mitophagy to attenuate apoptosis. *PLOS Pathog.* **9**, e1003722 (2013).

37. R. J. Youle, D. P. Narendra, Mechanisms of mitophagy. *Nat. Rev. Mol. Cell Biol.* **12**, 9–14 (2011).
38. D. C. Rubinsztein, C. F. Bento, V. Deretic, Therapeutic targeting of autophagy in neurodegenerative and infectious diseases. *J. Exp. Med.* **212**, 979–990 (2015).
39. E. S. Chocron, E. Munkácsy, A. M. Pickering, Cause or casualty: The role of mitochondrial DNA in aging and age-associated disease. *Biochim. Biophys. Acta Mol. Basis Dis.* **1865**, 285–297 (2019).
40. F. M. Yakes, B. Van Houten, Mitochondrial DNA damage is more extensive and persists longer than nuclear DNA damage in human cells following oxidative stress. *Proc. Natl. Acad. Sci. U.S.A.* **94**, 514–519 (1997).
41. C. Richter, J.-W. Park, B. N. Ames, Normal oxidative damage to mitochondrial and nuclear DNA is extensive. *Proc. Natl. Acad. Sci. U.S.A.* **85**, 6465–6467 (1988).
42. M. Scheibye-Knudsen, E. F. Fang, D. L. Croteau, D. M. Wilson III, V. A. Bohr, Protecting the mitochondrial powerhouse. *Trends Cell Biol.* **25**, 158–170 (2015).
43. N. C. de Souza-Pinto, D. M. Wilson, T. V. Stevensner, V. A. Bohr, Mitochondrial DNA, base excision repair and neurodegeneration. *DNA Repair* **7**, 1098–1109 (2008).
44. Y. Pommier, Drugging topoisomerases: Lessons and challenges. *ACS Chem. Biol.* **8**, 82–95 (2013).
45. A. Mallick, M. M. Kuman, A. Ghosh, B. B. Das, S. Basu, Cerberus nanoparticles: Cotargeting of mitochondrial DNA and mitochondrial topoisomerase I in breast cancer cells. *ACS Appl. Nano Mater.* **1**, 2195–2205 (2018).
46. H. Zhang, Y. Pommier, Mitochondrial topoisomerase I sites in the regulatory D-loop region of mitochondrial DNA. *Biochemistry* **47**, 11196–11203 (2008).
47. S. Khiati, Y. Seol, K. Agama, I. Dalla Rosa, S. Agrawal, H. Zhang, K. Neuman, Y. Pommier, Poisoning of mitochondrial topoisomerase I by lamellarin D. *Mol. Pharmacol.* **86**, 193–199 (2014).
48. I. Dalla Rosa, S.-y. N. Huang, K. Agama, S. Khiati, H. Zhang, Y. Pommier, Mapping topoisomerase sites in mitochondrial DNA with a poisonous mitochondrial topoisomerase I (Top1mt). *J. Biol. Chem.* **289**, 18595–18602 (2014).
49. M. Karbowski, K. L. Norris, M. M. Cleland, S.-Y. Jeong, R. J. Youle, Role of Bax and Bak in mitochondrial morphogenesis. *Nature* **443**, 658–662 (2006).
50. S. Dingley, K. A. Chapman, M. J. Falk, in *Mitochondrial Disorders* (Springer, 2012), pp. 231–239.
51. C. Ploumi, I. Daskalaki, N. Tavernarakis, Mitochondrial biogenesis and clearance: A balancing act. *FEBS J.* **284**, 183–195 (2016).
52. C. Douarre, C. Sourbier, I. Dalla Rosa, B. B. Das, C. E. Redon, H. Zhang, L. Neckers, Y. Pommier, Mitochondrial topoisomerase I is critical for mitochondrial integrity and cellular energy metabolism. *PLOS ONE* **7**, e41094 (2012).
53. I. Galluzzi, E. H. Baehrecke, A. Ballabio, P. Boya, J. M. Bravo-San Pedro, F. Cecconi, A. M. Choi, C. T. Chu, P. Codogno, M. I. Colombo, A. M. Cuervo, J. Debnath, V. Deretic, I. Dikic, E. L. Eskelinen, G. M. Fimia, S. Fulda, D. A. Gewirtz, D. R. Green, M. Hansen, J. W. Harper, M. Jäättelä, T. Johansen, G. Juhasz, A. C. Kimmelman, C. Kraft, N. T. Ktistakis, S. Kumar, B. Levine, C. Lopez-Otin, F. Madeo, S. Martens, J. Martinez, A. Melendez, N. Mizushima, C. Münz, L. O. Murphy, J. M. Penninger, M. Piacentini, F. Reggiori, D. C. Rubinsztein, K. M. Ryan, L. Santambrogio, L. Scorrano, A. K. Simon, H. U. Simon, A. Simonsen, N. Tavernarakis, S. A. Tooze, T. Yoshimori, J. Yuan, Z. Yue, Q. Zhong, G. Kroemer, Molecular definitions of autophagy and related processes. *EMBO J.* **36**, 1811–1836 (2017).
54. P. Boya, F. Reggiori, P. Codogno, Emerging regulation and functions of autophagy. *Nat. Cell Biol.* **15**, 713–720 (2013).
55. N. Mizushima, T. Yoshimori, B. Levine, Methods in mammalian autophagy research. *Cell* **140**, 313–326 (2010).
56. D. C. Rubinsztein, A. M. Cuervo, B. Ravikumar, S. Sarkar, V. I. Korolchuk, S. Kaushik, D. J. Klionsky, In search of an “autophagometer”. *Autophagy* **5**, 585–589 (2009).
57. H. Zhang, J. M. Barceló, B. Lee, G. Kohlhaagen, D. B. Zimonjic, N. C. Popescu, Y. Pommier, Human mitochondrial topoisomerase I. *Proc. Natl. Acad. Sci. U.S.A.* **98**, 10608–10613 (2001).
58. I. Dalla Rosa, H. Zhang, S. Khiati, X. Wu, Y. Pommier, Transcription profiling suggests that mitochondrial topoisomerase IB acts as a topological barrier and regulator of mitochondrial DNA transcription. *J. Biol. Chem.* **292**, 20162–20172 (2017).
59. H. Zhang, Y.-W. Zhang, T. Yasukawa, I. Dalla Rosa, S. Khiati, Y. Pommier, Increased negative supercoiling of mtDNA in *TOP1mt* knockout mice and presence of topoisomerases IIa and IIβ in vertebrate mitochondria. *Nucleic Acids Res.* **42**, 7259–7267 (2014).
60. Y. Pommier, J. M. Barcelo, V. A. Rao, O. Sordet, A. G. Jobson, L. Thibaut, Z. H. Miao, J. A. Seiler, H. Zhang, C. Marchand, K. Agama, J. L. Nitiss, C. Redon, Repair of topoisomerase I-mediated DNA damage. *Prog. Nucleic Acid Res. Mol. Biol.* **81**, 179–229 (2006).
61. O. Rothfuss, T. Gasser, N. Patenge, Analysis of differential DNA damage in the mitochondrial genome employing a semi-long run real-time PCR approach. *Nucleic Acids Res.* **38**, e24 (2009).
62. S. C. Johnson, P. S. Rabinovitch, M. Kaeblerlein, mTOR is a key modulator of ageing and age-related disease. *Nature* **493**, 338–345 (2013).
63. S. K. Das, I. Rehman, A. Ghosh, S. Sengupta, P. Majumdar, B. Jana, B. B. Das, Poly (ADP-ribose) polymers regulate DNA topoisomerase I (Top1) nuclear dynamics and camptothecin sensitivity in living cells. *Nucleic Acids Res.* **44**, 8363–8375 (2016).
64. B. Kundu, S. K. Das, S. Paul Chowdhuri, S. Pal, D. Sarkar, A. Ghosh, A. Mukherjee, D. Bhattacharya, B. B. Das, A. Talukdar, Discovery and mechanistic study of tailor-made quinoline derivatives as topoisomerase 1 poison with potent anticancer activity. *J. Med. Chem.* **62**, 3428–3446 (2019).
65. S. K. Das, A. Ghosh, S. Paul Chowdhuri, N. Halder, I. Rehman, S. Sengupta, K. C. Sahoo, H. Rath, B. B. Das, Neutral porphyrin derivative exerts anticancer activity by targeting cellular topoisomerase I (Top1) and promotes apoptotic cell death without stabilizing Top1-DNA cleavage complexes. *J. Med. Chem.* **61**, 804–817 (2018).
66. S. Khiati, I. Dalla Rosa, C. Sourbier, X. Ma, V. A. Rao, L. M. Neckers, H. Zhang, Y. Pommier, Mitochondrial topoisomerase I (Top1mt) is a novel limiting factor of doxorubicin cardiotoxicity. *Clin. Cancer Res.* **20**, 4873–4881 (2014).

**Acknowledgments:** We thank Y. Pommier of the NCI, NIH, USA, for the reagents and help during the study. We are also thankful to C. Austin of the Institute for Cell and Molecular Biosciences, Newcastle University, UK, for critically reading the manuscript. **Funding:** B.B.D.'s team was supported by a Wellcome Trust/DBT India alliance intermediate fellowship grant (award no. IA/I/13/1/500888), a DST-SERB core research grant (EMR/2017/001652), and the Indian Association for the Cultivation of Science intramural fund. A.G. and S.B. are the recipients of CSIR-NET Senior and Junior Research Fellowship, respectively, in India. A.M. and S.B. thank CSIR-UGC doctoral fellowship and DST-Nanomission [SB/NM/NB-1083/2017 (G)], respectively, for financial support. B.B.D. is a Wellcome Trust/DBT India alliance intermediate fellow. **Author contributions:** A.G., S.B., S.P.C., A.M., I.R., and S.B. performed the experiments. A.G. and B.B.D. designed and analyzed the data and wrote the manuscript. B.B.D. provided supervision. **Competing interests:** The authors declare that they have no competing interests. **Data and materials availability:** All data needed to evaluate the conclusions in the paper are present in the paper and/or the Supplementary Materials. Additional data related to this paper may be requested from the authors.

Submitted 9 May 2019  
 Accepted 17 September 2019  
 Published 6 November 2019  
 10.1126/sciadv.aax9778

**Citation:** A. Ghosh, S. Bhattacharjee, S. P. Chowdhuri, A. Mallick, I. Rehman, S. Basu, B. B. Das, SCAN1-TDP1 trapping on mitochondrial DNA promotes mitochondrial dysfunction and mitophagy. *Sci. Adv.* **5**, eaax9778 (2019).